Submarine weathering in the surficial sediments of climate-sensitive high latitude oceans

Supervisor: Dr. Wei-Li Hong

Student: Nezhla Amiri

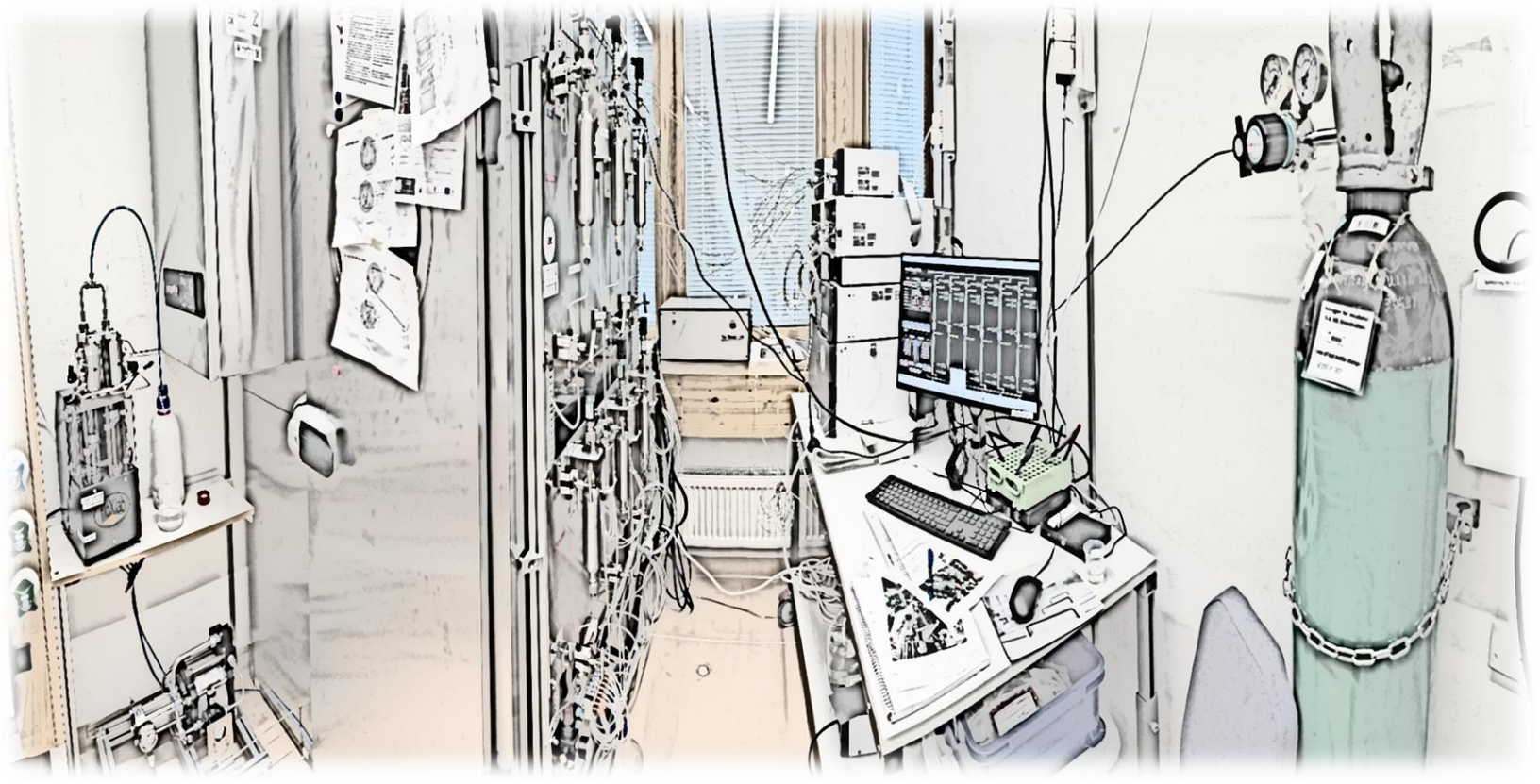

Table of Contents

Table of Tables

Table of Figures

Introduction

Arctic fjord systems are characterized by their dynamic interactions with the ocean, atmosphere, and cryosphere, which play a major role in carbon cycling as well as glacier stability. Increased sea ice loss, warming ocean temperatures, and increased glacial meltwater due to climate change are having an impact on Arctic fjord systems by affecting flow patterns, stratification, and biogeochemical processes within these systems. Thus, Arctic fjords are becoming increasingly valuable for studying how physical factors and carbon dynamics are interrelated in high-latitude systems (Aguilar-Vega et al., 2025).

The Petermann fjord, in northwestern Greenland, is a place of particular interest because it is part of the largest remaining floating ice tongue in Greenland. The fjord has complex circulation due to three main factors: the inflow of warm Atlantic waters, subglacial discharge, and sills/bathymetric constraints, all of which impact how much freshwater is melted from glaciers and how stable those glaciers are. These same three factors also impact the carbonate chemistry and CO_2 exchange processes, as well as the overall carbon cycling processes that occur in the fjord, due to the effects of freshwater inputs, biological activity, and sedimentary processes (Prakash et al., 2025).

The motivation behind this work is that arctic fjords and water bodies in high-latitude regions are more sensitive to climate change than those near the equator. The reason is that cold waters have a higher capacity to dissolve $CO_{2_{(atm)}}$, so like soda, polar oceans absorb more CO_2. This increased CO_2 uptake enhances ocean acidification in these regions, which leads to a greater decrease in seawater pH compared to lower latitudes. So, high-latitude marine environments are particularly sensitive to changes in carbonate chemistry and acidification processes.

Also, field observations from Arctic fjords show strong variations in seawater chemistry, especially in pH and total alkalinity (Gattuso et al., 2023; Fransson et al., 2020; Henson et al., 2023). Measurements from 2019 indicate that Petermann Fjord, along with the Nares Strait and Lincoln Sea, has relatively high alkalinity (2000–2150 $\mu mol\ kg^{-1}$) and stable pH values (8.05–8.25). In contrast, the nearby Sherard Osborn Fjord shows much lower alkalinity (1150–1250 $\mu mol\ kg^{-1}$) and lower pH (7.80–8.00) (Fig. 1). Sherard Osborn Fjord surface water experiences very low salinity (10–15) due to freshwater input and relatively high temperatures (up to 4°C). These conditions reduce buffering capacity and make the system more sensitive to acidification. On the other hand, Petermann Fjord does not show such extreme variations in salinity and temperature, suggesting a more stable marine environment with a stronger ability to resist pH changes (Jakobsson et al., 2019).

This contrast leads to an important question:

Why does Petermann Fjord maintain higher alkalinity and a more stable pH compared to nearby fjords?

High alkalinity means that the system has a strong buffering potential, allowing it to resist acidification. One possible explanation is the interaction between seawater and carbonate-rich sediments. Under acidic conditions, carbonate minerals can dissolve and release bicarbonate into the water, increasing alkalinity and stabilizing pH. However, in natural environments, many processes occur at the same time, making it difficult to isolate the effect of sediments (Lehmann & Bach, 2025; Middelburg et al., 2020; Renforth & Henderson, 2017).

To overcome this, this study uses controlled laboratory experiments to simulate acidification. By gradually lowering pH and monitoring alkalinity and ion chemistry, the role of sediment–water interactions can be directly investigated.

Thus, this study attempts to fill these gaps in knowledge by researching the relationships between physical processes, carbonate chemistry, and sedimentary dynamics in Petermann Fjord through a combination of water column and sediment-based observations in order to gain a better understanding of the factors that control carbon cycling and how these processes will function with continued climate change within a northern Greenland fjord system. Through this approach, it also aims to explain the potentially higher buffering capacity observed in Petermann Fjord and to improve understanding of how Arctic fjords respond to ocean acidification.

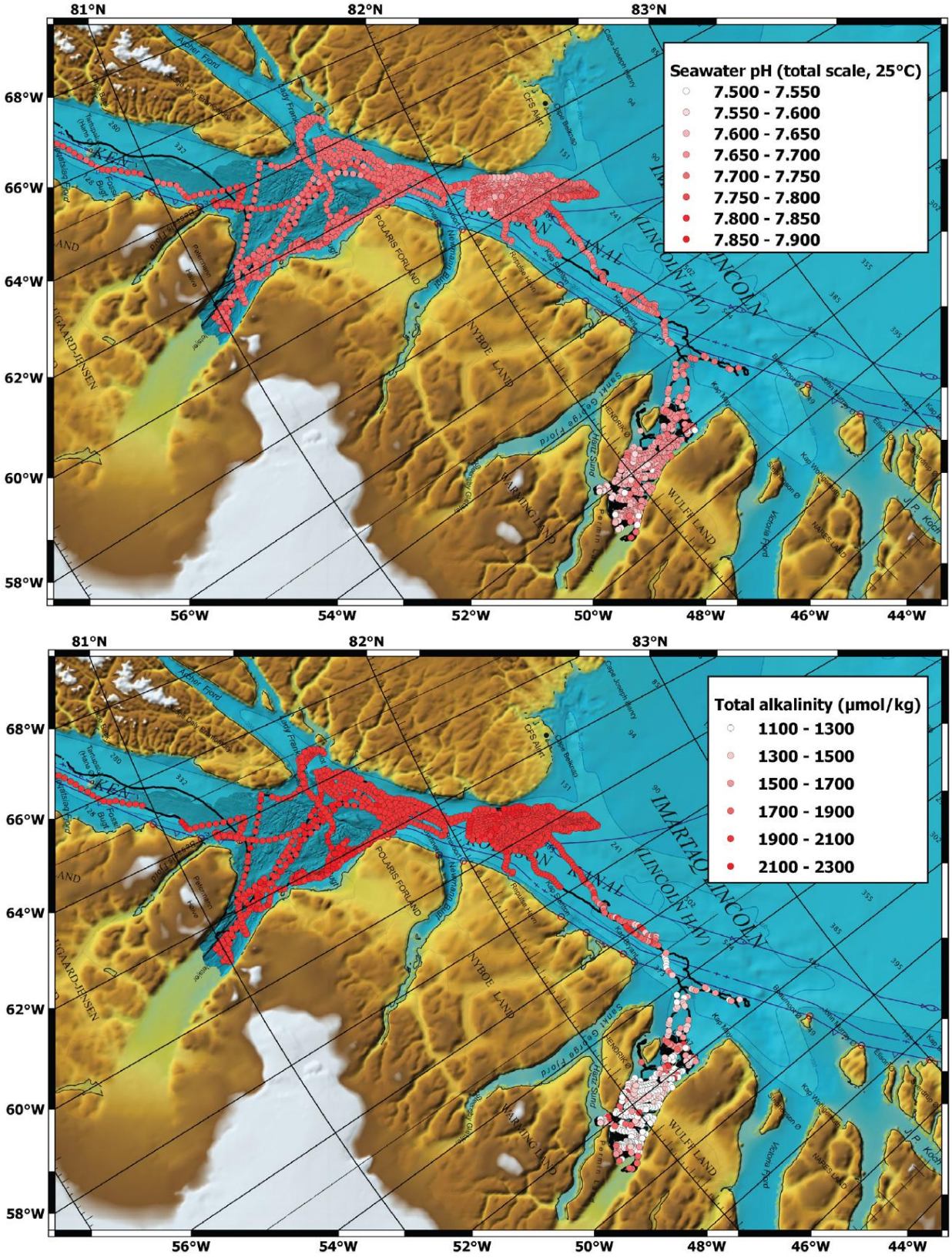

Figure 1. Underway pH and total alkalinity measurements (at constant salinity 35) from the ship's surface intake system; cruise track indicated by black line (Jakobsson et al., 2019)

Literature Review

Greenland fjords provide critical environments to study ocean circulation, ice dynamics, and biogeochemical processes at high-latitudes. In situ observations in Petermann Fjord by Johnson et al. (Johnson et al., 2011) provided a fundamental understanding of the fjord's hydrography. They found that relatively warm Atlantic waters periodically cross the sill at the mouth of the fjord and provide sufficient heat to drive high basal melt rates beneath the ice shelf. Importantly, the studies revealed a complex circulation structure within the fjord with substantial lateral variation in both the in-flow and out-flow of water mass, as well as significant amounts of glacial meltwater at intermediate water depths. A subsequent study by Stranne et al. (Stranne et al., 2021) found that Petermann Fjord is distinctly weakly stratified, primarily because the fjord remains open throughout the year, and thus able to continuously exchange waters with the open ocean. In contrast to most Arctic fjords, which remain locked by sea ice during the summer months, the open nature of Petermann Fjord prevents the formation of a warm surface layer.

Subsequent modeling studies have shown that both ocean forcing and sub-glacial freshwater input are critical to the ice-ocean interaction at such ice shelves. Prakash et al. (Prakash et al., 2025) demonstrated that the sub-glacial discharge promotes enhanced turbulent mixing beneath ice shelf and increases melt rate; with a threshold, sub-glacial discharge has a greater control on ice shelf loss than ocean temperature. Also, Cai et al. (Cai et al., 2017) showed that increasing ocean temperature causes a corresponding increase in basal melt rates, with a significant enhancement by sub-glacial runoff. Gadi et al. (Gadi et al., 2023) specifically highlighted the importance of grounding zone dynamics and processes, wherein ice shelf grounding zone experiences tidally controlled influx of warm seawater into areas where ice is grounded. This results in increased melt rates and enhanced sensitivity of glaciers to ocean warming.

In addition to physical parameters, Arctic fjords also exhibit highly dynamic carbon cycling processes influenced by freshwater, sea ice, and biota. A new study by Aguilar-Vega et al. (Aguilar-Vega et al., 2025) in the Svalbard fjords reveals that sea-ice melt introduces dissolved and particulate organic carbon which is rapidly photo-chemically and microbially processed and rapidly remineralized and converted to CO_2. Another study by Cantoni et al. (Cantoni et al., 2020) shows how glacial freshwater alters seawater concentration and increases atmospheric CO_2 uptake while lowering the carbonate saturation state of surface waters, promoting ocean acidification. Seasonal variations in fjord systems further depend on changes in freshwater input affecting sea-ice carbonate chemistry and its buffering capacity, which in turn is affected by the mineralogy of terrestrial input and sea-ice conditions (Fransson et al., 2020). A study by Legge et al. (Legge et al., 2017) presents

detailed seasonally resolved measurements of Dissolved Inorganic Carbon (DIC) showing that winter mixing and summer biotic uptake are strong controls on DIC concentrations.

Carbon in Greenland fjords is spatially heterogeneous and is strongly regulated by physical forcing. A new study by Akhoudas et al. (Akhoudas et al., 2025) showed that summer CO_2 variability in Petermann Fjord is controlled by a dynamic interplay between stratification, freshwater input and biological uptake, resulting in the fjord acting as a significant summer CO_2 sink mainly regulated by biological processes. The carbon budget of fjords has also been studied through long-term sediment records, showing a strong link between sea ice and fjord dynamics. This link is furthermore supported by studies of past sea ice conditions, showing that the formation of ice arches in Nares Strait controls sea ice extent, productivity and the stability of the Petermann ice tongue, as demonstrated by Detlef et al. (Detlef et al., 2021). However, modern proxy-based studies on Arctic fjords, such as those by Ribeiro et al. (Ribeiro et al., 2017) and Limoges et al. (Limoges et al., 2018), highlight the complex nature of fjord environments and the shortcomings of using proxies to reconstruct past environmental conditions.

Carbonate chemistry and alkalinity generation are key components of Arctic carbon cycling. Lehmann et al. (Lehmann & Bach, 2025) found that small amounts of carbonates can even dominate alkalinity production and affect CO_2 fluxes strongly depending on weathering pathway. However, these carbonate chemistry and alkalinity cycles are significantly modulated by processes associated with glacial processes such as sediment production and sediment delivery to coastal regions. Hogan et al. (Hogan et al., 2020) showed that the sediment flux and erosion in Petermann Fjord are predominantly governed by ice dynamic forcing. However, Wang et al. (Wang et al., 2024) found that enhanced sediment delivery associated with the advance of glacial fronts leads to increased burial of organic carbon on the Greenland margin. Importantly, rapid weathering of deposited glacial sediments was found to be a significant source of ocean alkalinity (Scholz et al., 2025), potentially acting as a negative climate feedback enhancing atmospheric CO_2 uptake.

The geochemical processes associated with the carbonate evolving systems in fjords have been significantly affected by local conditions as shown by work done by Aðalsteinsdóttir et al. (Aðalsteinsdóttir et al., 2025). As an example, water interacting with rocks can produce highly alkaline waters (e.g., Ikaite crystal formation), and therefore the lithological or elemental composition of rocks located in these fjords has the potential to greatly influence the water chemistry of the fjord. Recent scientific observations made by Gattuso and colleagues (Gattuso et al., 2023) showed that even though Arctic fjords experience considerable seasonal variability, they will continue to be long-term sinks of CO_2 within the context of Arctic climate change, however, uncertainties exist concerning the amount of $CaCO_3$ in polar oceans. Henson and colleagues (Henson et al., 2023) speculate

based upon their more extensive, integrated analyses that additional glacial meltwater inputs will contribute further to acidification via processes such as decreasing alkalinity and/or increasing upwelling of CO_2-rich waters. Finally, the method used to measure variability in the carbonate evolving systems has been discussed by Mejía et al. (Mejía et al., 2025) who provide examples of how incorrect selection of proxy methods can introduce errors and biases into the construction of historical ocean conditions, demonstrating the significance of using multiple proxy methods when creating multi-proxy analyses.

Sedimentary processes allow a key look at both carbon cycling and environmental change in sedimentary systems. Early diagenetic processes greatly affect how sediment is composed (changes in sediment composition) and pore water chemistry, frequently obscuring primary signals created during deposition (signals deposited as sediment) (Meinhardt et al., 2016). Several approaches have developed models for determining mechanisms of sedimentary processes through modeling such as MEDUSA (Munhoven, 2021), by including the mechanisms for diffusion, bioturbation and redox reactions. Empirically studied organic matter will differ greatly depending on both source and environmental factors. For example, Karlsson et al. (Karlsson et al., 2015) provide two different examples for degradation pathways produced with marine vs terrestrial organic material. Bridier et al. (Bridier et al., 2019) provide information on organic matter transfer and how quality and transfer of organic materials change seasonally and with freshening of coastal waters. In addition, Kim et al. (2025) show that organic carbon sources exhibit spatial variability throughout open fjord systems that are driven by both glacial melting/run-off and ocean current patterns.

Further research highlights the intricate nature of early diagenetic and biogeochemical phenomena in Arctic sediment. The research of Chen et al. (Chen et al., 2017) illustrated that dissolved organic matter and pore water chemistry are substantially contributed by microbial degradation above sulfate-methane transition zone. Redox-driven reactions further impact sediment biogeochemistry and benthic fluxes as well as trace metal dynamics (Cukrov et al., 2024). At large ecosystem scales, altered plankton community structure may change carbon export efficiency and the biological pump (Sheward et al., 2024), while abrupt permafrost thaw processes may mobilize vast amounts of labile carbon, enhancing its redistribution and degradation across Arctic systems (Grewer, 2017).

Carbon burial efficiency in Arctic fjords is influenced by the interplay of physical forcing, biological processes and sediment dynamics. Knies et al. (Knies et al., 2025) found that deglaciation and reductions in sea ice can initially promote productivity but over time, increasing levels of stratification will lead to decreased levels of nutrient influx and increased rates of remineralisation, resulting in reductions in carbon burial efficiency. Additionally, coupled mineral-carbon processes alter these dynamics since processes such as silicate

weathering and reverse weathering control alkalinity and CO_2 fluxes (Hong et al., 2025) while the production of clays within fjord sediments can serve as a long-term sink for dissolved silica; thus having implications for wider biogeochemical cycling (Dillan et al., 2025).

There have been many studies on how individual components affect the function of Arctic fjord systems. For example, the physical studies (Johnson et al., 2011; Prakash et al., 2025; Cai et al., 2017; Gadi et al., 2023) have looked at factors such as ocean circulation, glacier melt and ice/ocean interaction to help determine what influences glacier stability through the process of basal melting. At the same time, studies that focus on CO_2 cycling in fjords (Aguilar-Vega et al., 2025; Cantoni et al., 2020) have emphasized the role of freshwater from melting glaciers, biology, and seasonal changes as regulating factors for CO_2 dynamics; most of the data is from fjords that are not located in Greenland. The sedimentological studies (Meinhardt et al., 2016; Hong et al., 2025) have focused on how mineral reactions, early diagenetic processes, and alkalinity contribute to constraining the chemistry of pore water and regulating CO_2 cycling.

Most of these processes have been studied separately and there is very little understanding as to how they work together as one integrated system. Of particular concern is the combined effect that changing ocean circulation, increasing meltwater flow into fjords, and sediment deposition has on the CO_2 and alkalinity chemistry of the seawater in Valby Fjord. Furthermore, because early diagenetic processes and minerals that weather quickly regulate the alkalinity and buffering capacity of seawater, these types of processes have seldom been incorporated into this observational work on fjords. This lack of integration has led to considerable uncertainty about how Arctic fjord systems will respond to the consequences of the changing climate.

The present study addresses this gap with laboratory experiments designed to evaluate sediment/water interactions, the release of ions from the sediments to the seawater, and how sediment stored ions regulate seawater chemistry and alkalinity as those sediment stores are affected by changing environmental conditions.

Case Study Location

GEOEO2024 Expedition: The North of **G**reenland **E**arth–**O**cean–**E**cosystem **O**bservatory Expedition

The GEOEO2024 expedition was carried out onboard the Swedish icebreaker *Oden* between August 6 and September 17, 2024 (Fig. 2). The expedition started and ended at Pituffik Space Base in northwest Greenland. Its main goal was to study the marine

environment of the northern Greenland Ice Sheet, including previously unexplored areas such as Victoria Fjord and the outlet of the Ostenfeld Glacier.

The Greenland Ice Sheet is currently the largest contributor to global sea-level rise. The northern part alone contains ice equivalent to about 93cm of global sea level. Therefore, understanding its behavior is important for predicting future climate and ocean changes.

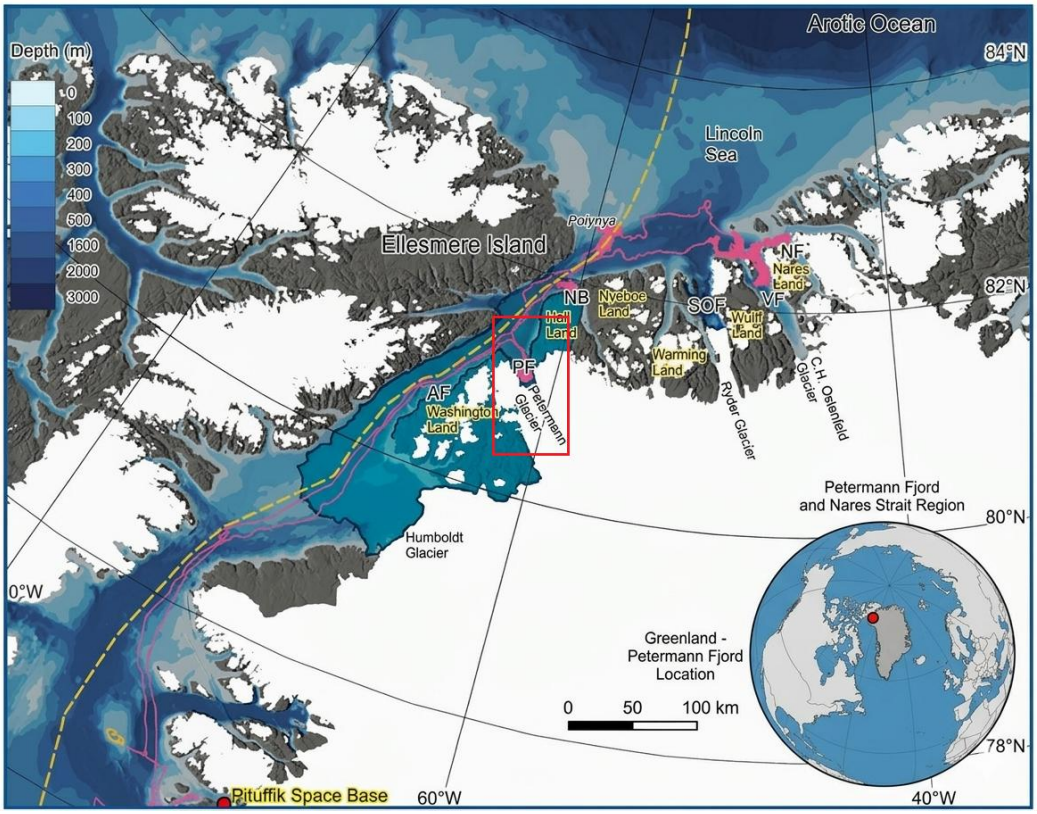

Figure 2. Expedition track between 7 August and 17 September; AF: Aleqatsiaq Fjord, NB: Newman Bugt, PF: Petermann Fjord, SOF: Sherard Osborn Fjord, VF: Victoria Fjord (Jakobsson et al., 2019)

This thesis focuses specifically on Petermann Fjord, where sediment multi-core (MC) samples were collected during the expedition (Fig. 3). Three MCs were sampled from this region:

1. GE24-34-MC3 & MC4
    a. GE24-34-MC3 was used for pore water and carbonate analysis
2. GE24-37-MC1
3. GE24-38-MC1

The focus of this study is on core GE24-38-MC1, which was used for the incubation experiment.

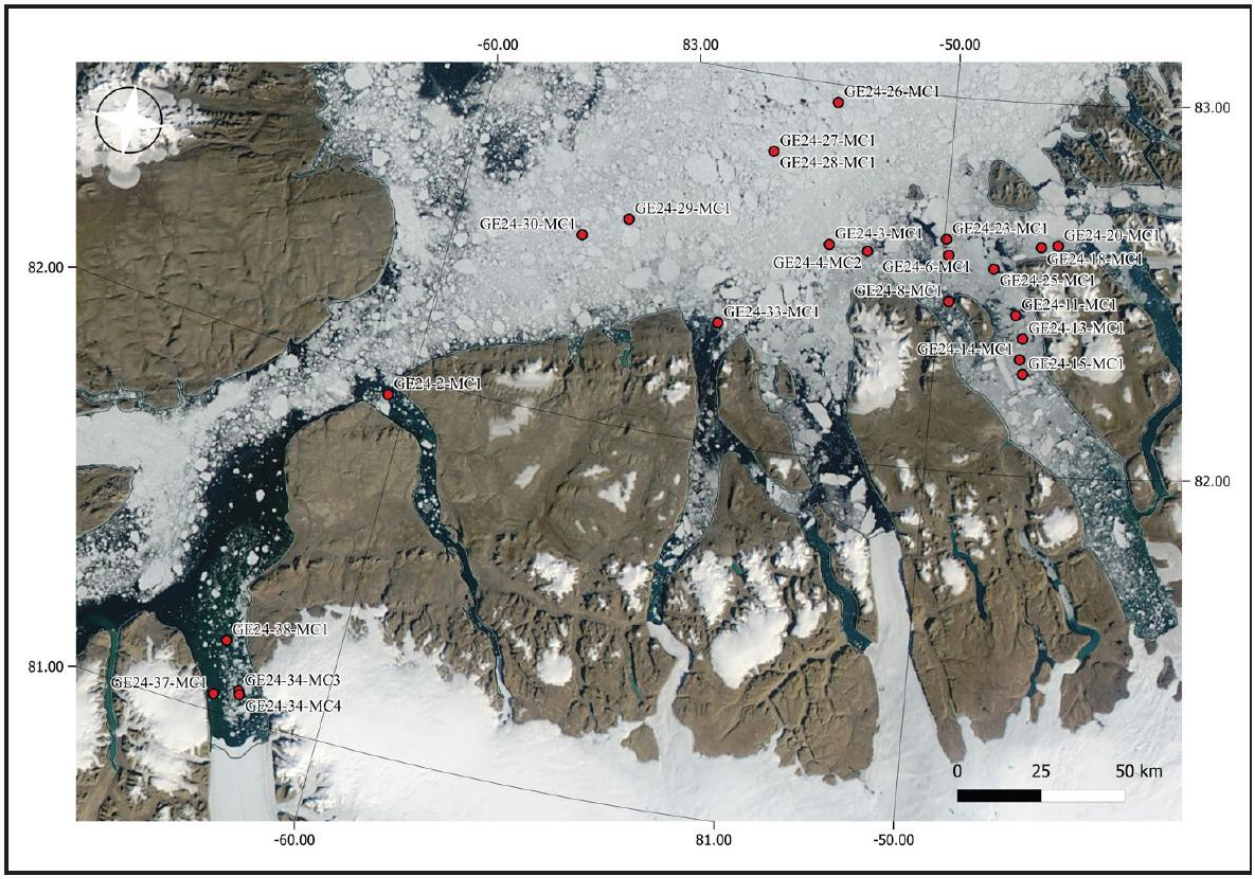

Figure 3. Locations of multi-core stations with porewater sampling (GEOEO Shipboard Scientific Party, 2024)

Incubation System and Method

A laboratory incubation system (Figs. 4 & 5) was developed to enable automated sampling and continuous monitoring of early diagenetic reactions in seafloor sediments under controlled in-situ pressure and temperature conditions. The system integrates a customized flow-through incubator (*Vinci Technologies*) with two automated fluid samplers (*Shimadzu Corporation*), enabling long-term experiments with minimal manual intervention.

The experimental setup operates within a temperature range from approximately 4 °C to room temperature and can sustain pressures up to 250 bar, thereby reproducing environmental conditions relevant to seafloor environments. Fluid circulation is driven by a dual-cylinder positive-displacement pump that delivers modified seawater through the system at controlled flow rates ranging from 10^{-4} to 5 $mL\,min^{-1}$. The dual-cylinder configuration ensures pulse-free fluid injection, which is critical for maintaining stable geochemical conditions during long incubation experiments.

The flow system consists of six independent flow-through cell assemblies (referred to as *incubators* in the thesis). Each assembly contains two 25 cm long Hastelloy tubes (inner diameter: 2.54 cm; referred to as *sandpacks/positions* in the thesis) connected to a visual cell equipped with a sapphire glass window, allowing measurements of in-situ pH values through the near infrared technology. The pressure inside each flow-through cell assembly is regulated by back-pressure regulators (BPRs), enabling independent pressure control for each experimental unit.

To maintain stable experimental temperatures, the entire flow-through incubator is installed inside a refrigerator. The cabinet also provides a dark environment, which is necessary because the pH sensor used in the system is sensitive to light exposure.

Downstream of the sandpacks, twelve fluid sampling ports are installed and connected to the automated sampling units. Each sampler is equipped with two two-position valves and one six-position valve, which manage the sequential collection of samples from the ports, dilution of the collected fluid, and rinsing of the sampling lines. Valve switching and fluid injection are synchronized with the incubator flow system to ensure proper circulation and accurate sample collection.

Fluid samples collected by the automated samplers are subsequently analyzed using *dual-column ion chromatography (IC)* for the determination of major cations and anions. In addition to chemical analysis, a pH sensor is installed in the visual cell in between the two Hastelloy tubes, allowing continuous monitoring of these parameters during the incubation experiments.

The automated sampling system is designed for unattended operation. A complete sampling cycle requires 17.10 minutes per sample, and a full daily sequence of 12 samples takes about 3.5 hours. Sampling can be initiated either locally in the laboratory or remotely via a programmed control script, which executes the sampling sequence automatically without human intervention. However, after the sampling cycle is completed, laboratory personnel must manually retrieve the samples, close the sample vial lids, weigh the samples, and store them in a refrigerator for preservation prior to analysis.

To simulate realistic laboratory conditions, the pressure was maintained at 102 bar and the temperature at approximately 5–8 $°C$. Of the 12 sandpacks prepared, six were selected for sampling: four containing sediment slurry and two containing only seawater, which served as control sandpacks.

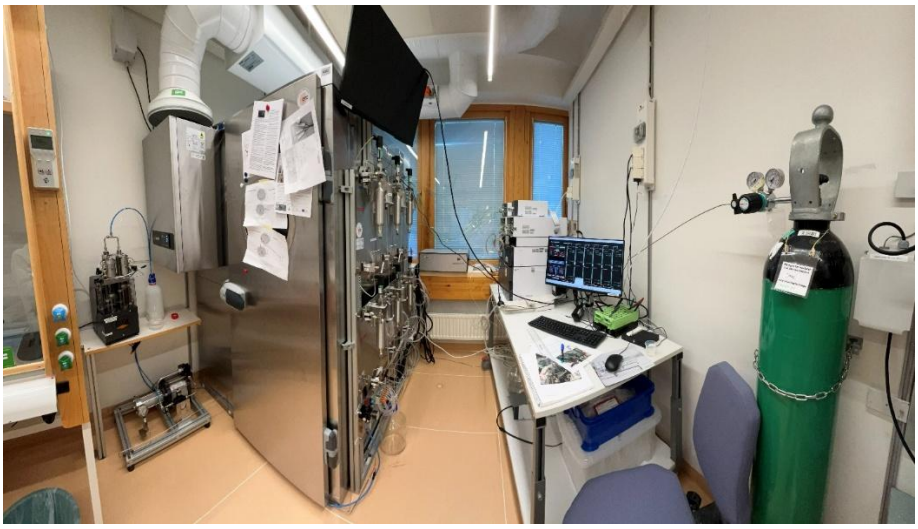

Figure 4. Schematic overview of the incubation system setup

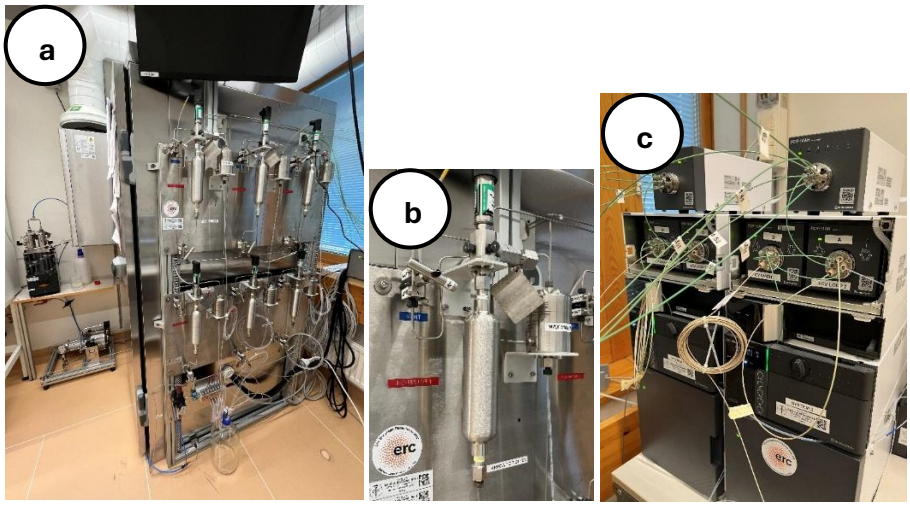

Figure 5. Incubation system setup: (a) dual-piston syringe pump, refrigerator, and backup pressure cylinders; (b) close-up of backup pressure cylinder; (c) fraction collector for automated sampling

System Preparation, Operational Considerations, and Hastelloy Sandpack Assembly

Proper preparation of the flow-through cells is necessary to ensure reliable, leak-free operation. When cleaning or assembling the cylindrical metal sandpack holders, a small amount of high-vacuum grease (DOW Corning) must be applied to the black washer located beneath the filter. This improves sealing performance and prevents leakage during high-pressure operation. Nitrogen gas (N_2) was used to pressurize the back-pressure regulators (BPRs) and switch on/off the various valves within the system.

The Hastelloy sandpack consists of a cylindrical column with an inner diameter of 25.4 mm (1 inch) and a nominal sample length of 25 cm (250 mm) (Fig. 6). This design provides a

controlled environment for packing the sample and conducting flow experiments under well-defined conditions.

One end cap is placed at each end of the sandpack. The end cap is held into the sandpack and tightened onto the sample by a tightening cap. This system allows the user to compress the sample by tightening the tightening cap (6mm free range per cap). As a result, the effective sample length can be varied between a maximum of 250 mm and a minimum of 238 mm.

A Hastelloy sintered metal disc filter is installed at both ends of the sandpack. Each filter has a diameter of 20 mm and a thickness of 5 mm. The filter is held inside a filter holder, which simplifies both assembly and disassembly. The filter holder is screwed inside the end cap, ensuring a secure and stable positioning of the filter within the system. The mesh size of the filter is not fixed in advance but is determined experimentally. Several mesh sizes below 1 µm are tested prior to operation to identify the most suitable option that prevents particle loss while maintaining good flow and minimizing clogging.

In addition, each end cap is equipped with a PT100 temperature probe, which is inserted and held inside the end cap structure. One probe is installed per end cap, allowing temperature measurements at both ends of the sandpack. This setup enables monitoring of temperature conditions along the system during experiments and helps identify any temperature variations that may affect the results.

Overall, the assembly of the Hastelloy sandpack involves installing the filters into their holders, screwing the holders into the end caps, positioning the end caps at both ends of the packed column, inserting the temperature probes, and tightening the caps to achieve the desired level of compression and sealing. This configuration ensures a stable, adjustable, and well-monitored system for experimental use.

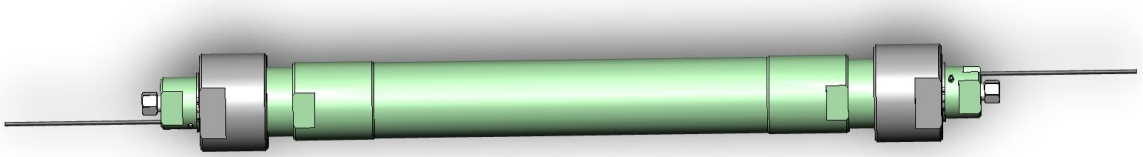

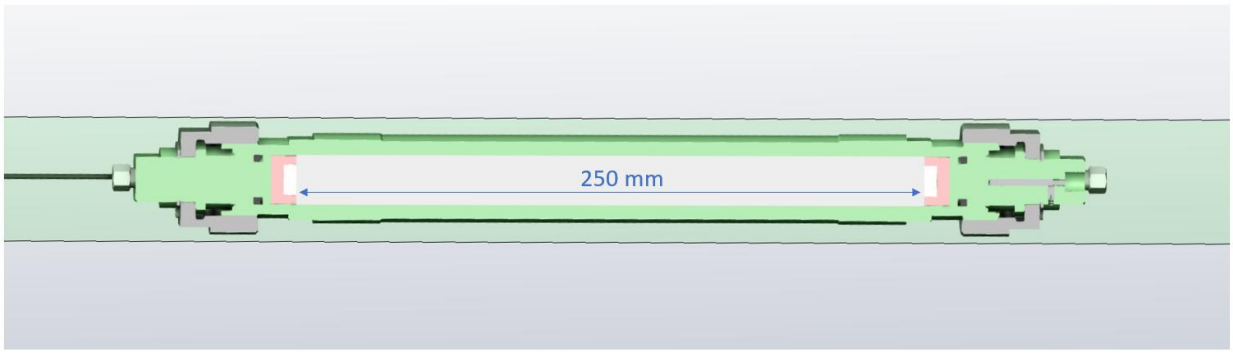
250 mm

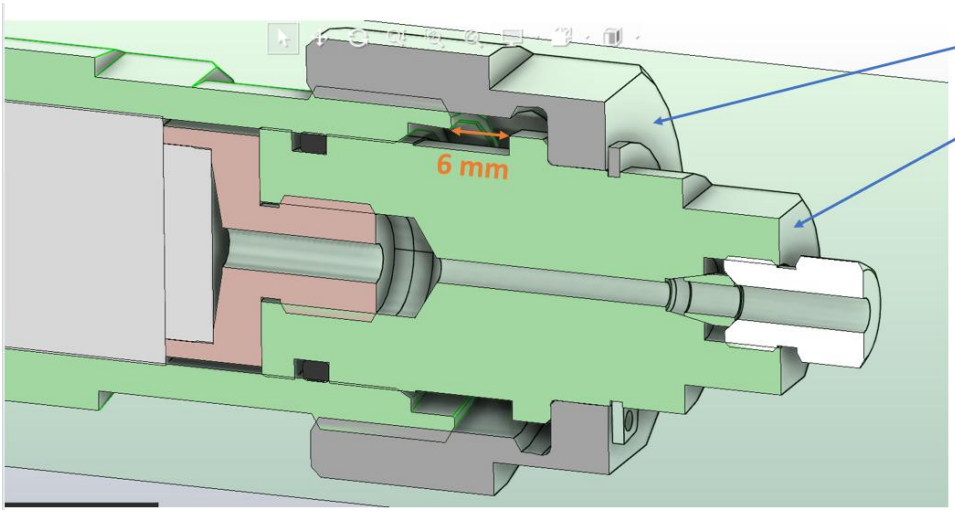
6 mm
Tightening Cap
End Cap

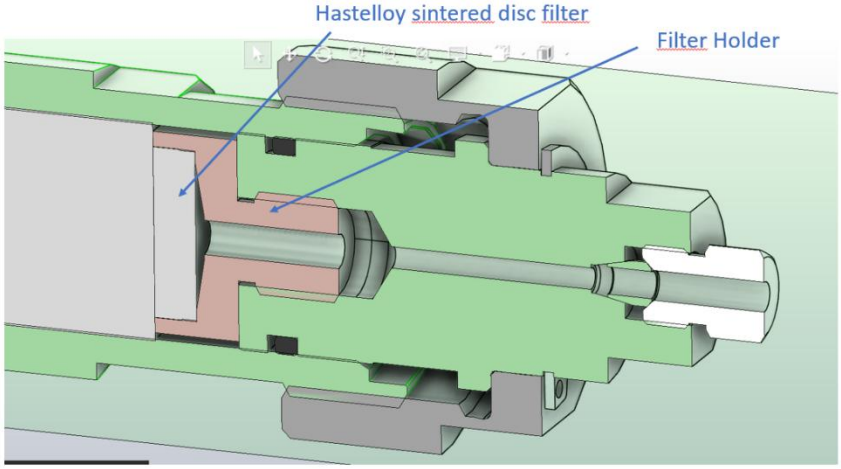
Hastelloy sintered disc filter
Filter Holder

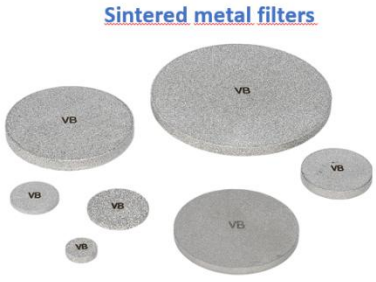
Sintered metal filters
VB

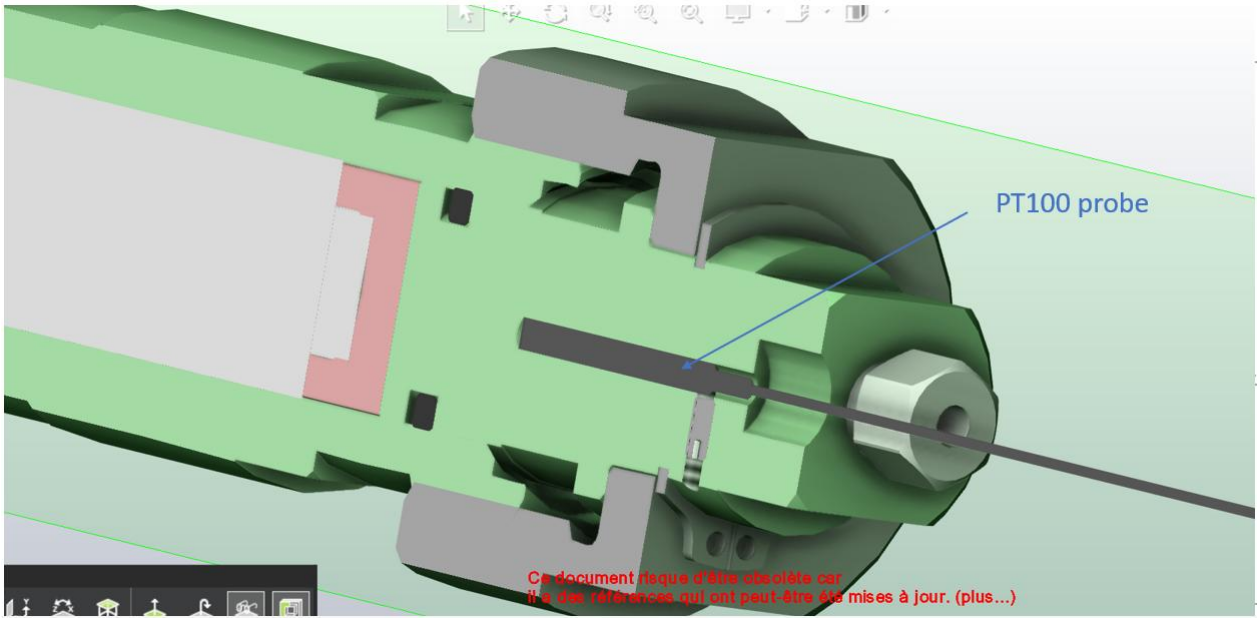

Figure 6. Hastelloy Sandpack Assembly

Initial Pressurization of the Back-Pressure Regulators (BPRs) to the Desired Pressure

When operating the incubation system for the first time, the following startup sequence must be performed to raise the pressure of the back-pressure regulators if the desired pressure is over 50 bar:

1. Open the valve of the BPR mounted on the chamber wall.
2. Open the gas supply from the N_2 tank that has a constant output pressure of 50 bar.
3. Open the valve of the gas booster and adjust the piston volume inside the gas booster to reach a pressure higher than 50 bar (i.e., the output pressure of the N_2 tank).
4. Watch the pressure of BPR until it reaches the desired value.
5. Switch off the valve between the gas booster and BPR once it reaches the desired pressure.
6. Close the cylinder valve.
7. Close the gas supply from the N_2 tank.
8. Close the valve of the gas booster.

9. Vent the BPR by opening the three-way vent valve if the pressure is higher than the desired value.

Daily Incubation Sampling Procedure

To initiate the daily automated sampling sequence:

1. Open the *LabSolutions* software.
2. Select Instrument 1.
3. Create a new batch folder, open it within the *LabSolutions* interface, and save the batch file.
4. Verify in the *Vinci* control software that the pump is running and that the pressure in all sandpacks is maintained at 102 bar, which is the pressure at the water depth of 1020 m for core MC-38.
5. Start the batch run to begin the automated sampling process.

Fig. 7 illustrates the schematic configuration of the sample collection and dilution process used in the automated system. This diagram includes all 6 incubators, while in this experiment, only incubators 1 to 3 were operated, which are connected to one of the fraction collectors (FCV1).

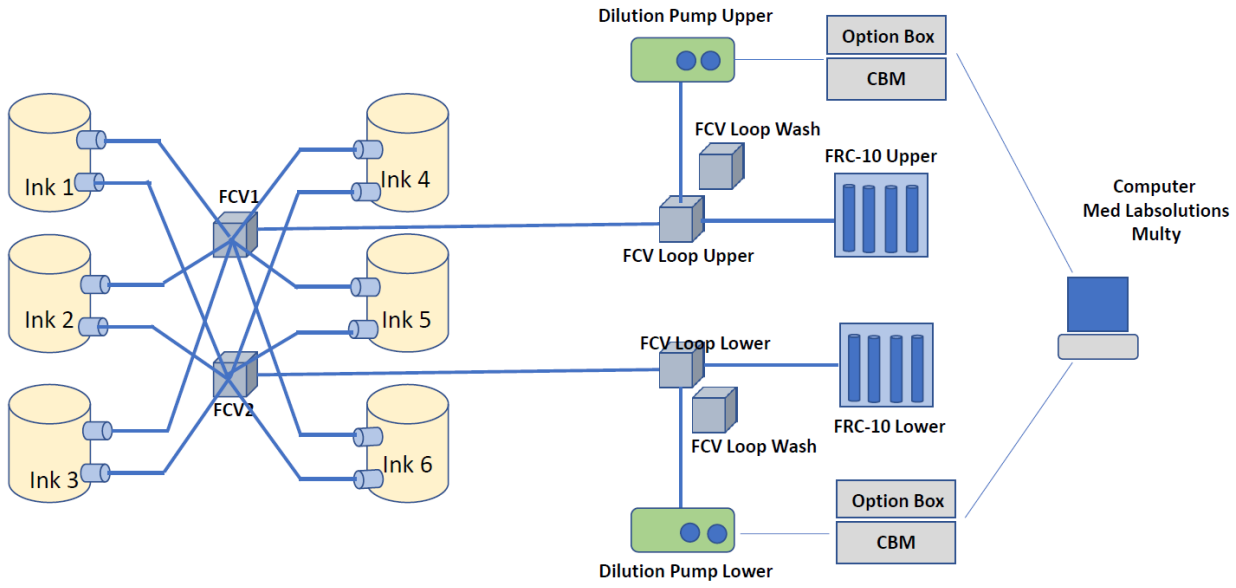

Figure 7. Schematic diagram of the sample dilution process

Monitoring the Incubation System

The incubation system was monitored using the *VINCI Software*, which displays a schematic overview of the experimental setup.

The software interface provides real-time information (Fig. 8), including:

- Sandpack configuration
- Flow-through cells
- Temperature and pressure within each sandpack
- Back pressure values
- Pump status
- Cylinder pressure, etc.

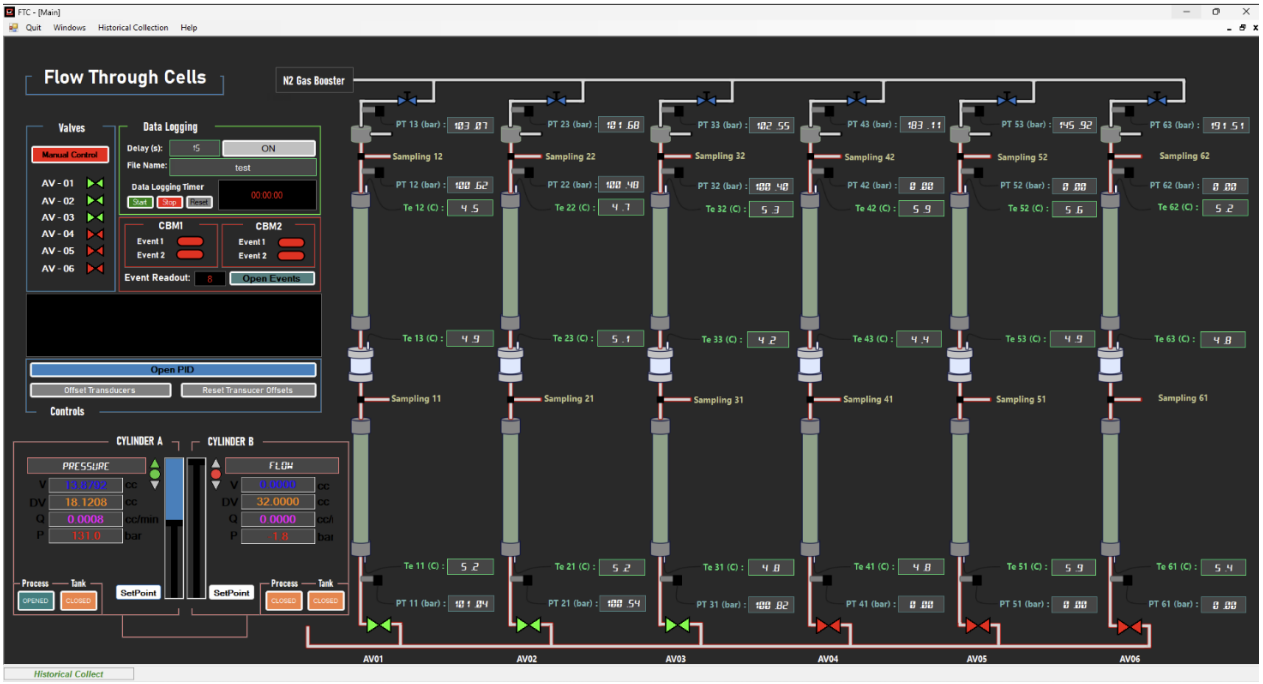

Figure 8. VINCI software interface showing incubation system layout

Automated Sampling Procedure

Automated sampling is controlled through a computer-based interface. We have made a small modification within the sampling procedure to circumvent an issue of communication between the Shimadzu *LabSolution* software and the fraction collector. A custom-made routine "Auto-clicker" was made to detect the window "Start Data Acquisition" and click the "yes" button on the window.

To initialize the automated data acquisition system:

1. Navigate to the desktop of the control computer.
2. Open the *Auto-Clicker* application.
3. Locate the command labeled *"Start Data Acquisition."*
4. After configuring the necessary settings, select *"Start Monitoring"* in the window titled *"Auto Enter Key for Selected Window."*

This initialization step only needs to be performed once and does not require repetition prior to each daily sampling cycle.

Thus, after this, before each daily sampling cycle began, a pop-up confirmation window appeared in the control software indicating that the automated sampling script was active (Fig. 9). Once automatically confirmed, the system proceeded with the programmed sampling sequence.

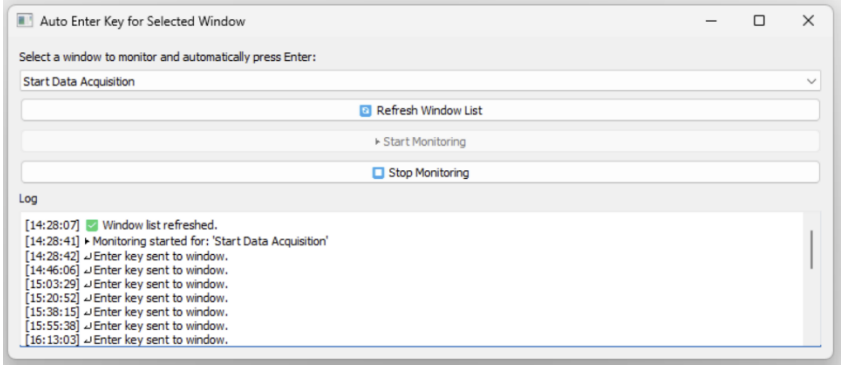

Figure 9. Remote sampling script activation window

Trial Incubation Experiments (Silica Gel Test)

Prior to initiating the main incubation experiments, a series of trial incubation experiments was conducted to evaluate the operational stability and performance of the flow-through incubation system. These preliminary tests used silica gel as a synthetic porous medium to simulate sediment within the sandpacks and allowed assessment of fluid flow behavior, sampling procedures, tracer transport, pressure stability, and analytical performance.

Preparation of the Incubators and Silica Gel Medium

Before the experiment began, both the upper and lower sandpacks were depressurized so that the incubators could be removed from the refrigerator cabinet. The internal

components were then rinsed thoroughly with Milli-Q water to eliminate any residual solutes. After cleaning, the sandpacks were filled with laboratory-prepared silica gel, which served as an artificial sediment matrix. The silica gel powder has a density of 2 g/cm^3 and a particle size of 63µm.

Initially, only Incubator 2 was filled with the silica gel mixture, and sampling was started from both sandpacks associated with that incubator. During the first sampling runs, an experimental error in the preparation procedure was identified and corrected. Subsequently, the remaining sandpacks were filled with a newly prepared silica gel mixture following the corrected protocol.

Silica Gel Preparation and Porosity Determination

The experimental design required preparing silica gel with a known porosity and volume corresponding to the internal capacity of the incubator sandpacks. Each incubator has an internal volume of approximately 126.68 mL. Because each incubator contains two sandpacks, approximately 260 mL of silica gel mixture was required per incubator.

To prepare the silica gel mixture, 1 L of X1000 diluted IAPSO seawater standard was first produced by mixing 1 g of IAPSO standard seawater with 999 g of MQ water, yielding a final mass of 1000.55 g. From this solution, 219.85 g was combined with 112.43 g of silica powder (SiO_2), resulting in a total mass of 332.28 g. The silica gel powder has a density of 2 g/cm^3, while seawater (IAPSO) has a density is 1030 kg/m^3 $= 1.03$ g/cm^3.

The porosity of the prepared mixture was calculated as:

$$\phi = \frac{V_{void}}{V_{total}}$$

$$\phi = \frac{213.45}{269.67} = 0.792 \approx 79.2\%$$

Thus, the silica gel mixture had an approximate porosity of 79%.

To correct this issue, the columns were flushed with MQ water to remove the background chloride originating from the IAPSO solution. After flushing, the tracer solution containing chloride (eg, NaCl, KCl, or a mixture of both) could be introduced into the system to initiate the BTC experiment.

Breakthrough Curve (BTC) Experimental Design

Chloride (Cl^-) was selected as a conservative tracer to monitor solute transport through the silica gel column and evaluate flow behavior within the incubators.

The BTC experiment required collecting 26 samples over a total duration of 260 minutes. This sampling duration corresponds to the combined volume of the two sandpacks (130 mL each), assuming a constant flow rate of 1 mL min^{-1}.

Samples were collected every 10 minutes, yielding 26 samples (260 ÷ 10). In practice, 28 samples were collected in total; however, the first and last samples were discarded to flush residual liquid present in the *PEEK tubing coils*, ensuring that only representative samples from the sandpacks were analyzed.

The 10-minute sampling interval was chosen because the fraction collector must deposit each sample into a specific vial position. At the time of the experiment, the system could not perform fully automated sequential sampling into predefined vial positions. As a result, individual sampling runs had to be manually initiated every 10 minutes. Automation of batch sampling was planned for later experiments once the automatic sampling system was implemented.

Flow Rate and Sampling Volume Tests

During the trial experiments, the stability of the pressure within the sandpacks was also monitored. Pressure fluctuations in the background when no sample was taken were generally within ±10 bar. Initially, the flow rate was set to 1 mL min^{-1}, but it was later reduced to 0.2 mL min^{-1} to better simulate experimental conditions and extend residence time within the sandpacks.

Measurements showed that the sample volume collected (~1.7 mL) remained nearly constant despite the reduction in flow rate. This behavior reflects principles similar to Darcy-type flow, where the pressure gradient rather than absolute flow rate primarily governs the sampling mechanism. Consequently, the system maintained the target sampling volume without requiring extensive recalibration.

Preparing Additional Silica Gel Columns

After the IAPSO solution had been completely flushed from the system, additional silica gel mixtures were prepared for Incubators 1 and 3, this time using MQ water instead of IAPSO to avoid background chloride contamination.

To produce sufficient material for two incubators, the proportions of the previous mixture were doubled. Consequently, 439.7 g of MQ water (density = 1 g/cm^3) was mixed with 224.86 g of silica powder (SiO_2), yielding a total mass of 664.56 g and a porosity identical to the previous preparation:

$$\phi = \frac{439.7}{552.13} = 0.796 \approx 79.6\%$$

Before filling in the incubators, 10 mL of the MQ solution used in the mixture was collected with a syringe, filtered, and added to an ion chromatography (IC) run to verify background solute concentrations.

Ion Chromatography (IC) Analysis

All collected samples were analyzed using dual-channel ion chromatography (IC-dual). Multiple analytical batches were performed to process the samples and calibration standards (Table 1). The analytical sequences included standard solutions, MQ blank, IAPSO control standard, and samples collected from the sandpacks.

Batch No.	Date	Batch
1	26-May	First set of standards (1 rep of levels A & C=14), 1 IAPSO X1000 (2 rep), SP3 (1-14) (2 rep), second set of standards (levels A & C=14) (1 rep)
2	2-Jun	First set of standards (1 rep of levels A & C=14), 1 IAPSO X1000 (2 rep), Clean Room MQ (2 rep), Silica Gel MQ (2 rep), SP3 (15-31) (2 rep), SP4 (1-16) (2 rep), second set of standards (levels A & C=14) (1 rep)
3	10-Jun	First set of standards (1 rep of levels A & C=14), 1 IAPSO X1000 (2 rep), Silica Gel MQ (2 rep), SP4 (1-16) (2 rep), second set of standards (levels A & C=14) (1 rep)

Table 1. List of silica gel test sample batches analyzed by ion chromatography (IC); levels A&C = levels of anion and cation standard; SP3&4 = sandpack 3 and 4.

Incubation Experiment

Cleaning Procedures Prior to Main Experiments

After completion of the silica gel test, all grease-containing components of the incubator system, particularly the filters and sealing elements, were thoroughly cleaned to prevent contamination in subsequent experiments. Cleaning was performed under a fume hood using *Isopropanol (IPA)* as an organic solvent. The solvent was applied to laboratory tissues and used to wipe the surfaces of the relevant components.

This cleaning step was essential before beginning the thesis incubation experiments involving natural sediment samples, where contamination could significantly affect geochemical measurements.

Sandpack Filling and Experimental Setup

For the incubation experiment, six sandpacks from three incubators (of twelve available sandpacks) were used. Two incubators were filled with sediment slurries from Petermann's fjord to provide replicate experimental conditions, while the third incubator served as a control containing only seawater. The use of replicates allowed for improved reliability and comparison of experimental results.

The configuration of the incubators was as follows (Fig. 10):

1. **Incubator 1:** Both the upper and lower sandpacks were filled with a mixture of sediment collected from different depths and undiluted IAPSO standard seawater. The visual observation cell was also filled with undiluted IAPSO solution.
2. **Incubator 2:** Both sandpacks contained the same sediment–IAPSO mixture, while the visual cell (equipped with the pH sensor) was filled with undiluted IAPSO solution.
3. **Incubator 3 (Control):** Both sandpacks contained only IAPSO seawater, and the visual cell was also filled with undiluted IAPSO.

To achieve the target porosity of 0.79, each sediment-filled sandpack required a mixture containing 99.375 g of freeze-dried sediment and 95 mL of IAPSO seawater. The particle density of the sediment was assumed to be 2.5 g cm^{-3}. After filling the sandpacks, a small portion of the remaining mixture was filtered and analyzed to determine the system's initial geochemical composition.

Figure 10. Configuration of sandpacks (brown for sediment-containing SP & blue for control SP), pH sensor (orange), and flow direction (blue arrows) in the Vinci software interface

Reason for Using IAPSO Instead of the Actual Seawater from the Site

The main limitation of using the collected seawater from the study site is the restricted volume available, which is approximately 1.5 L. This limited amount may not be sufficient for extended incubation experiments. As an alternative, IAPSO standard seawater can be used, for which approximately 10L was available in the laboratory. Unlike the collected seawater,

the use of IAPSO is not restricted by sample volume and therefore provides greater flexibility for extended experiments or repeated runs.

Leakage Checking Before Starting the Experiment

Before initiating the incubation scenario, the incubator system was pressurized and left running over the weekend to allow sufficient time to detect any potential leaks in the system. This precaution ensured that the setup was stable before starting the automated sampling sequence.

After the weekend, the incubators were inspected for leakage. A leak was detected in the lower sandpack of Incubator 3 (control sandpack), and the issue was investigated further to identify the cause. In addition, the pressure in the visual cell of Incubator 1 appeared to be unstable and showed a slight decline. The system was monitored further to determine whether the pressure would stabilize.

Initial Pressure Set-up in the Incubators

For the experiment, the pressure in all sandpacks was set to 102 bar, corresponding to the approximate hydrostatic pressure at the depth represented by the studied environment.

Experimental Scenarios and Acidification

The incubation experiment was conducted in several stages to evaluate the geochemical response of the sediment–water system under progressively more acidic conditions. Three main phases were implemented:

1. Background sampling (initial conditions)
    - Seawater pH: 8.3
    - Experiment start date: 24 October 2025
    - No chemical modification was applied to the inlet solution.
2. First acidification scenario
    - Target pH: 7.4
    - Scenario start date: 27 November 2025
3. Second acidification scenario
    - Target pH: 6.0
    - Scenario start date: 16 February 2026

Because approximately 1.5 L of acidified solution was required for the first acidification scenario, the inlet solution was prepared gradually in three batches of 0.5 L as the supply decreased.

The seawater used in the experiment was IAPSO standard seawater, which was acidified using double-distilled high grade 37% *Hydrochloric acid (HCl)*. Hydrochloric acid was selected because chloride ions are relatively inert in seawater systems, minimizing interference with the geochemical reactions being studied. pH of the IAPSO was adjusted by slowing adding HCl into the flask, while measuring pH simultaneously.

Preparation of Acidified IAPSO Solution

First Acidification Scenario (pH 7.4)

The initial pH of 7.4 was selected to simulate moderately acidified marine conditions, representing a transitional state between natural seawater (≈8.1–8.3) and more extreme acidification scenarios. This intermediate value allows the system to respond progressively, enabling clearer observation of buffering processes, carbonate dissolution kinetics, and the evolution of alkalinity under controlled acidification.

Acidification was performed incrementally to carefully monitor pH changes. First, 100mL of IAPSO was poured into a plastic beaker, and its pH was measured. Concentrated HCl was then added dropwise, with each drop corresponding to approximately $1 \mu L$. After each addition, the pH was measured. To maintain a controlled dilution series, 100mL of additional IAPSO was added at each step (Table 2). This stepwise approach allowed accurate tracking of the pH evolution as the solution volume increased.

In total, 1.5 liters of acidified IAPSO seawater (pH = 7.4) were prepared, produced in three separate batches of 0.5 liters each (Tables 2, 3, and 4).

No.	IAPSO volume (ml)	pH		Drops of acid used	Note
		Before adding HCl	After adding HCl		
1	100	8.088	7.260	3	Adding 100ml IAPSO each time
2	200	7.741	7.283	4	
3	300	7.648	7.546	1	
4	400	7.719	7.483	3	
5	500	7.662	**7.410**	5	
	Total			16 drops, each 1ul	

Table 2. Acid volumes used in the preparation of the first 0.5 L of acidified IAPSO solution (pH 7.4)

No.	IAPSO volume (ml)	pH		Drops of acid used	Note
		Before adding HCl	After adding HCl		
1	100	8.102	7.794	2	Adding 100ml IAPSO each time
2	200	_	7.380	3	
3	300	_	7.485	3	
4	400	_	7.371	5	
5	500	_	**7.445**	2	
	Total			15 drops, each 1ul	

Table 3. Acid volumes used in the preparation of the second 0.5 L of acidified IAPSO solution (pH 7.4)

No.	IAPSO volume (ml)	pH		Drops of acid used	Note
		Before adding HCl	After adding HCl		
1	100	8.099	6.42	1(=10ul)	Adding 100ml IAPSO each time, Temp= 21.2 ℃
2	200	_	6.72	1(=3ul)	
3	300	_	7.12	0	
4	400	_	7.38	0	
5	500	_	**7.404**	1(=3ul)	
	Total			16 drops	

Table 4. Acid volumes used in the preparation of the third 0.5 L of acidified IAPSO solution (pH 7.4)

Introducing the Acidified Solution into the Incubation System

To introduce the acidified IAPSO into the system, the following procedure was followed:

1. The valves were closed, and the pump was stopped.
2. The inlet container located outside the incubation refrigerator was rinsed with a small amount of the prepared acidified solution.
3. The container was then filled with the acidified IAPSO.
4. The valves were reopened, and the pump was restarted.

Sampling began the following day (27 November 2025) after the new inlet conditions were stabilized.

Second Acidification Scenario (pH 6)

On 16 February 2026, the inlet solution was further acidified to pH 6 to simulate more extreme acidification conditions (Table 5).

No.	IAPSO volume (ml)	pH		Drops of acid used	Note
		Before adding HCl	After adding HCl		
1	420	8.18	6.98	10(=5ul each drop)	Adding 100ml IAPSO each time, Temp= 21.2 ℃
2	500	_	6.060	2	
3	600	_	6.000	4	
	Total			16 drops=80ul acid	

Table 5. Acid volumes used in the preparation of the second acidification scenario (pH 6.0)

Sampling Methodology

The sampling strategy was designed to obtain daily geochemical measurements of the outlet water from the incubation system. The plan involved sampling six consecutive days per week. Each day, six samples were collected from different sampling ports corresponding to the six sandpacks in the incubation system. Therefore, a total of 36 samples per week were analyzed.

Vials were prepared in advance. On Fridays, additional vials were placed in the rack to enable remote sampling on Sundays.

Samples were subsequently diluted X1000 prior to analysis using *ion chromatography (IC)*.

Sample Weighing and Evaporation Control

Before sampling, empty vials (without caps) were weighed using a precision balance (accuracy 0.000X g). After sample collection, the vials were weighed again to determine the exact volume of collected liquid. This procedure allowed evaluation of variations in sample volume caused by the fraction collector dilution process or unstable pressure conditions.

To minimize evaporation, all samples were stored in a refrigerator immediately after collection. Also, Sampling was avoided on Saturdays to minimize evaporation effects. But samples collected on Sundays remained overnight in the fraction collector, which sometimes resulted in slightly lower measured weights due to evaporation.

Adjustments to Sampling Frequency

Based on previous observations, ion concentrations measured on Sundays and Tuesdays were consistently higher than on other days.

The elevated Sunday values could be explained by accumulation during Saturday, when no sampling occurred. However, the reason for the elevated Tuesday concentrations remained unclear.

To investigate this phenomenon, the sampling strategy was modified for several batches:

- Some batches were diluted X500 instead of X1000 to evaluate the effect of dilution on measured concentrations.
- For certain batches (11–13), the sampling schedule was changed from daily sampling to sampling every other day.

These adjustments were implemented to determine whether sampling frequency influenced measured ion concentrations.

Sampling Order

Sampling followed a fixed sequence to maintain consistency:

1. Sandpack 2 — Sampling port 12
2. Sandpack 1 — Sampling port 11
3. Sandpack 4 — Sampling port 22
4. Sandpack 3 — Sampling port 21
5. Sandpack 6 — Sampling port 32
6. Sandpack 5 — Sampling port 31

LabSolutions Sampling Software

Sampling was performed using the *LabSolutions* software by creating a *Realtime Batch* for each sampling day (Fig. 11).

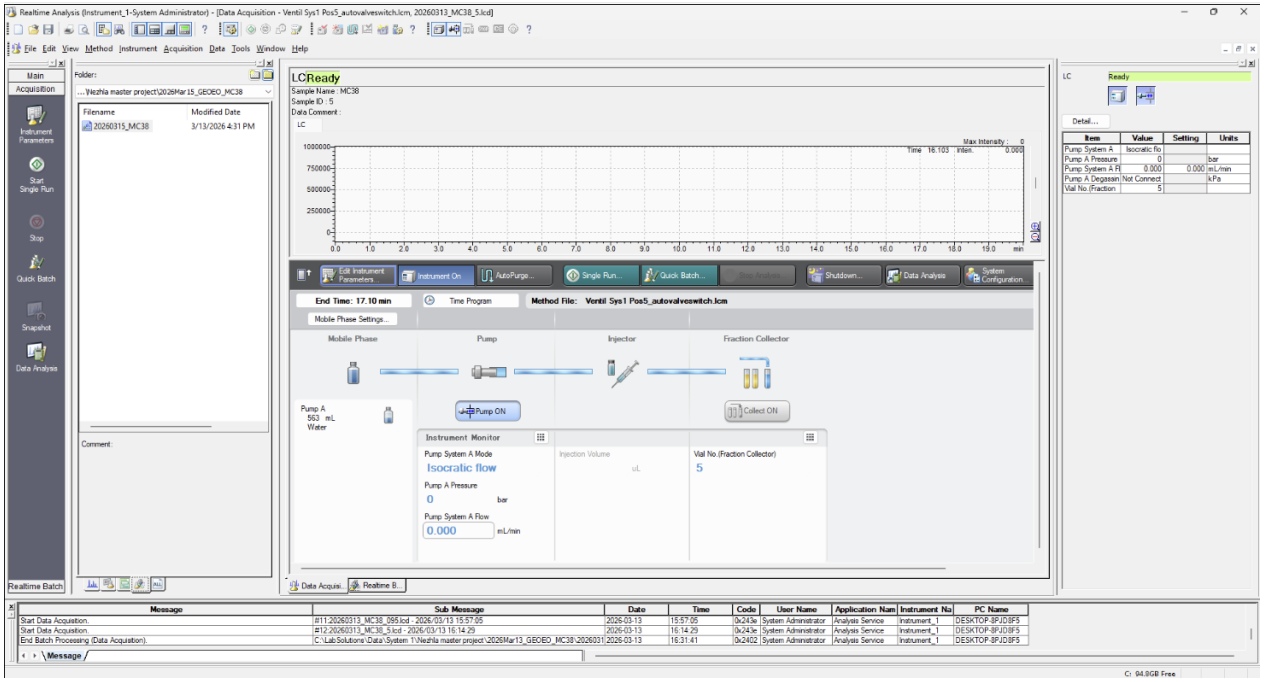

Figure 11. LabSolutions software interface

When the sampling sequence begins, the software displays the active batch and current sampling progress (Fig. 12). Each sampling round (from each port) takes 17.10 minutes.

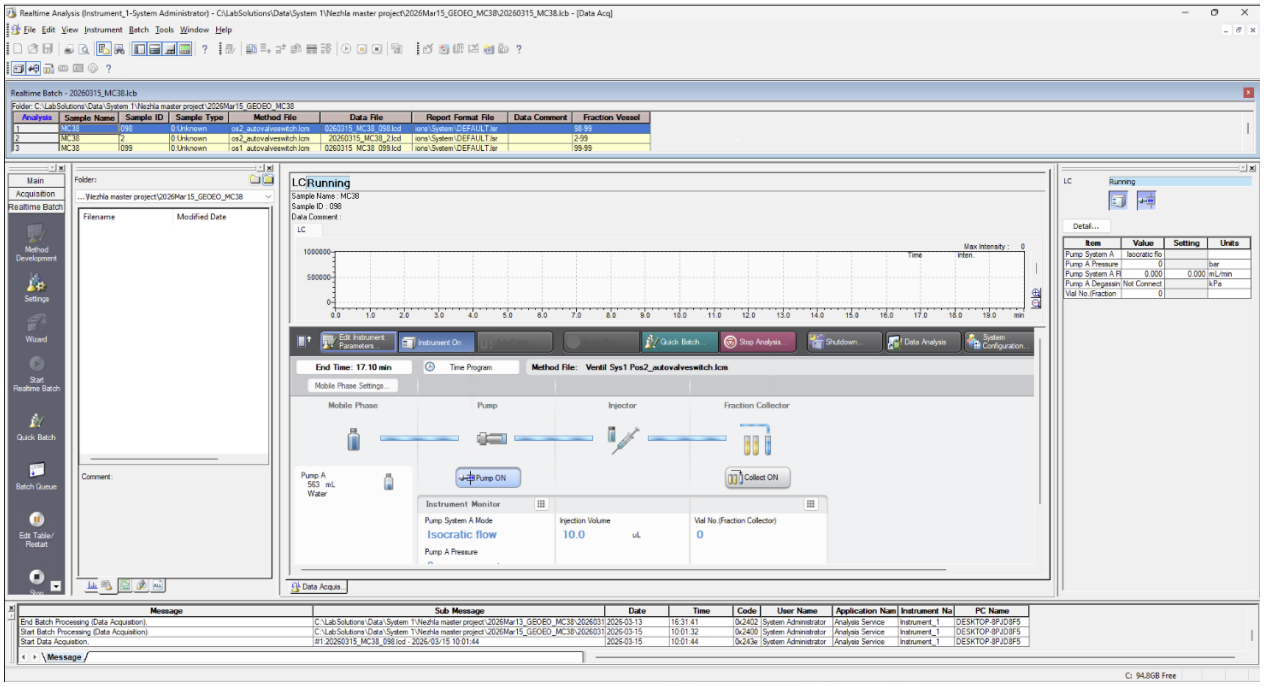

Figure 12. Active batch sampling interface

Because the first sample collected from each port contains residual liquid from the sampling loop, it was discarded. Therefore, the sampling batch included 12 sampling rows, where the first replicate of each sample was directed to waste (Fig. 13).

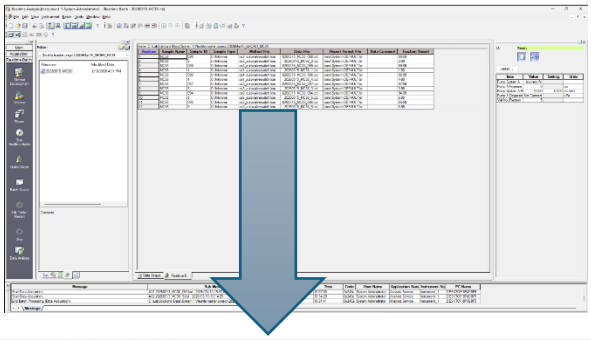

Folder: C:\LabSolutions\Data\System 1\Nezhla master project\2026Mar15_GEOEO_MC38

Analysis	Sample Name	Sample ID	Sample Type	Method File	Data File	Report Format File	Data Comment	Fraction Vessel
1	MC38	098	0:Unknown	os2_autovalveswitch.lcm	0260315_MC38_098.lcd	ions\System\DEFAULT.lsr		98-99
2	MC38	2	0:Unknown	os2_autovalveswitch.lcm	20260315_MC38_2.lcd	ions\System\DEFAULT.lsr		2-99
3	MC38	099	0:Unknown	os1_autovalveswitch.lcm	0260315_MC38_099.lcd	ions\System\DEFAULT.lsr		99-99
4	MC38	1	0:Unknown	os1_autovalveswitch.lcm	20260315_MC38_1.lcd	ions\System\DEFAULT.lsr		1-99
5	MC38	096	0:Unknown	os4_autovalveswitch.lcm	0260315_MC38_096.lcd	ions\System\DEFAULT.lsr		96-99
6	MC38	4	0:Unknown	os4_autovalveswitch.lcm	20260315_MC38_4.lcd	ions\System\DEFAULT.lsr		4-99
7	MC38	097	0:Unknown	os3_autovalveswitch.lcm	0260315_MC38_097.lcd	ions\System\DEFAULT.lsr		97-99
8	MC38	3	0:Unknown	os3_autovalveswitch.lcm	20260315_MC38_3.lcd	ions\System\DEFAULT.lsr		3-99
9	MC38	094	0:Unknown	os6_autovalveswitch.lcm	0260315_MC38_094.lcd	ions\System\DEFAULT.lsr		94-99
10	MC38	6	0:Unknown	os6_autovalveswitch.lcm	20260315_MC38_6.lcd	ions\System\DEFAULT.lsr		6-99
11	MC38	095	0:Unknown	os5_autovalveswitch.lcm	0260315_MC38_095.lcd	ions\System\DEFAULT.lsr		95-99
12	MC38	5	0:Unknown	os5_autovalveswitch.lcm	20260315_MC38_5.lcd	ions\System\DEFAULT.lsr		5-99

Figure 13. Incubator sampling batch configuration

Dual-Column Ion Chromatography (IC) Analysis

Ion concentrations in the incubation samples were measured using a *dual-column ion chromatography (IC)* system, which allows simultaneous analysis of anions and cations (Fig. 14). The analytical workflow consisted of several stages, including sample dilution, batch preparation, system preparation, calibration, chromatographic analysis, and post-run data processing.

Figure 14. Dual-column ion chromatography (IC) system

IC Flow Chart

The dual-column IC system operates through continuous circulation of eluents and sample through multiple components.

Fig. 15 illustrates a dual-channel ion chromatography (IC) system that measures anions and cations from the same sample at the same time. After the sample is injected by the autosampler, it is carried by two separate eluent streams controlled by two pumps: one for anions and one for cations. The flow is split into two independent channels, allowing simultaneous analysis.

In the anion channel, the sample passes through a pre-column, separation column, and suppressor before reaching a conductivity detector. In the cation channel, the sample goes through a cation column and is directly detected by a separate conductivity cell. Both signals are recorded separately, and the remaining flow from both channels is directed to waste.

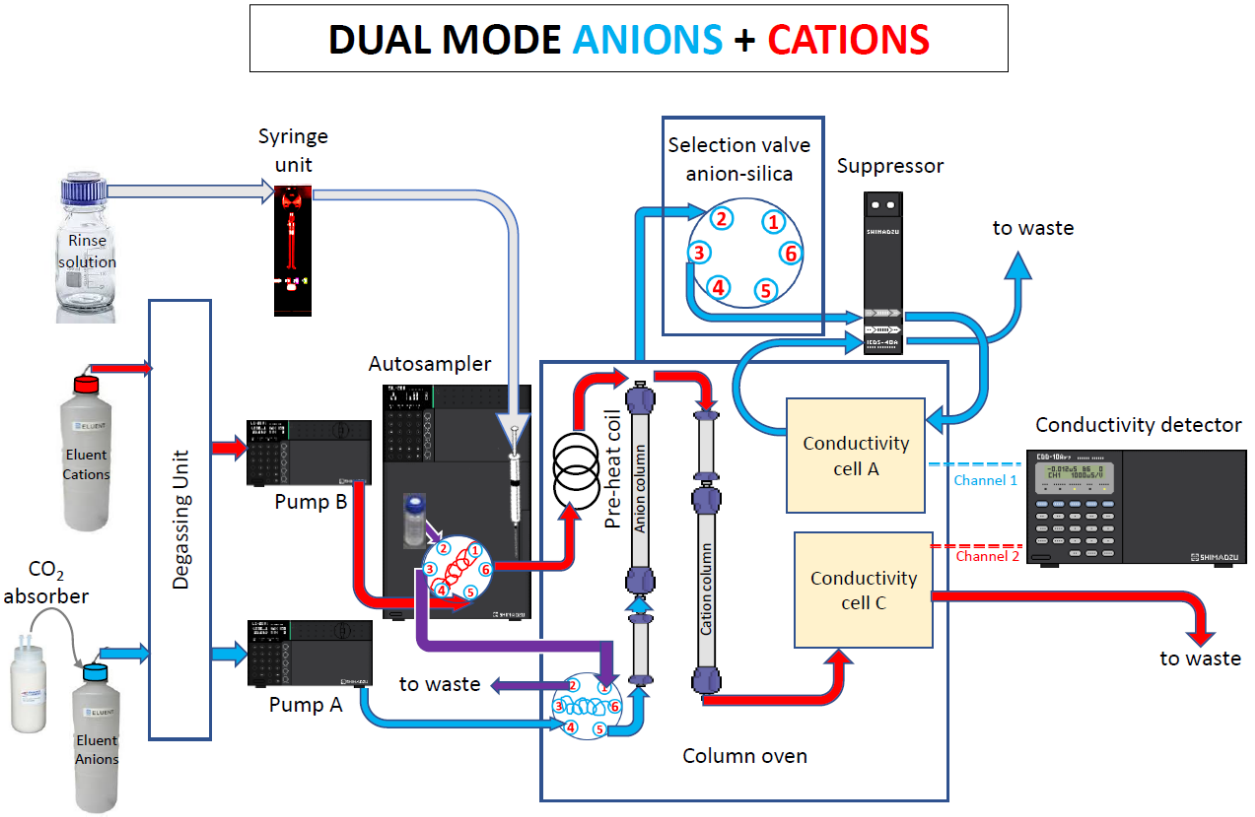

Figure 15. Flow diagram of the dual-column IC system

IC System Preparation

Before starting sample analysis, the IC system must be properly prepared and stabilized.

System Startup Procedure

1. Fill the eluent bottles with diluted eluents
2. Fill the autosampler rinse bottle with fresh MQ water
3. Wake the instrument by pressing the sleep button.
4. Press the purge button on both pumps:
    - Pump A (anion channel)
    - Pump B (cation channel)
5. Reset the eluent volume level in the software
6. Close the purge valve after purging.
7. Turn on the column oven in the *RealtimeAnalysis* software and set it to ~40 $°C$.
8. Check that the suppressor is on
9. Activate the pumps in the software

During operation, the system pressure should stabilize at:

- Pump A (anion channel): 50–52 bar
- Pump B (cation channel): 35–37 bar

Finally, the autosampler is purged, and the system is allowed to stabilize for at least one hour before running samples.

Detailed information about how to start the IC (checklist before running) is provided in the *Supplementary Materials*.

Sample Dilution and Batch Preparation

Prior to IC analysis, all incubation samples were diluted X1000 using MQ water to ensure that ion concentrations fell within the calibration range of the instrument.

Sample Dilution Procedure

Each diluted sample was prepared in a 50mL Falcon tube according to the following ratio:

$$\text{Dilution factor (D.F.)} = \frac{Stock\ concentration}{Final\ Concentration} = \frac{Total\ Weight\ (gr)}{Sample\ or\ Std\ (gr)}$$

$$\text{D.F.} = \frac{50\ mL}{0.05\ mL} = 1000$$

After dilution, the solutions were transferred into IC vials and placed in the autosampler rack.

IC Batch Structure

The maximum capacity of a single IC batch is 41 sample injections, including replicates. Each analytical batch contained the following sequence (Fig. 16):

1. First set of 14 standard levels
    - 8 levels of IV-59 anion standard
    - 6 levels of MU-4 cation standard
2. control standard (IAPSO X1000)
3. 36 incubation samples
    - Each 10 samples, 2 replicates
4. Second set of 14 standard levels
    - 8 levels of IV-59 anion standard
    - 6 levels of MU-4 cation standard

To monitor analytical precision, replicate measurements were incorporated into the batch design. Although each vial could theoretically be analyzed twice, only one replicate per sample was typically measured due to limited eluent availability. However, duplicate analyses were performed every 10 samples to estimate measurement reproducibility.

Detailed information about setting up a *Quick Batch* in the IC is provided in the *Supplementary Materials*.

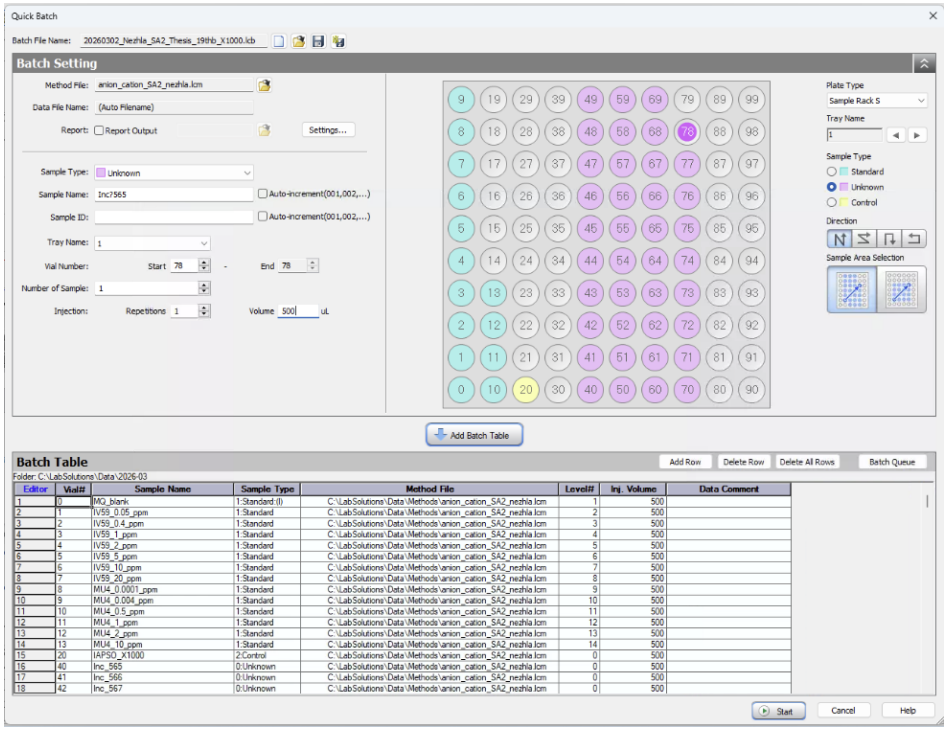

Figure 16. Example IC batch layout in Quick Batch interface (incubation batch setup)

Calibration Standards and Control Standard Preparation

Two certified standards were selected for calibration (Table 6). Fresh anion and cation standard solutions were prepared monthly to maintain stable peak shapes and ensure reliable calibration curves. In addition, the control standard used was the IAPSO standard seawater, an artificial seawater standard.

STD name	Analyte	Concentration (ppm, µg/mL, mg/kg, mg/L, or equivalent units)	Volume (ml)	Matrix
IV-stock-59	Br, Cl, F, NO_3, NO_2, PO_4, SO_4	1000	125	H_2O
CRM-MU-4	Ca, Mg, K, Na	1000	100	2% HNO_3

STD name	Analyte	Concentration (ppm, µg/mL, mg/kg, mg/L, or equivalent units)	Volume (ml)	Matrix
IAPSO	Multi-elements in natural water	Variable, see certificate		Seawater

Table 6. Characteristics of IC calibration standards (IV-stock-59 and CRM-MU-4) and control standard (IAPSO)

Calibration Standards Preparation

Calibration solutions were prepared through serial dilution from the stock standards to produce multiple concentration levels.

Fourteen calibration levels were generated:

- 8 levels for anions
- 6 levels for cations

As shown in Table 7, these levels covered a wide concentration range to ensure accurate calibration across expected sample concentrations.

Level No.	Level Initials	Level	Final conc. (ppm)	Stock used (ppm)	D.F.	Std (gr)	Tot. Weight (g)
14	C14	MU4_10_ppm	10	MU-4 (1000 ppm)	×100	0.5	50
13	C13	MU4_2_ppm	2	MU-4 (1000 ppm)	×500	0.1	50
12	C12	MU4_1_ppm	1	MU-4 (1000 ppm)	×1000	0.05	50
11	C11	MU4_0.5_ppm	0.5	MU-4 (1000 ppm)	×2000	0.025	50
10	C10	MU4_0.004_ppm	0.004	C13 (2 ppm)	×500 (250,000)	5	50
9	C9	MU4_0.0001_ppm	0.0001	C12 (1 ppm)	×10000 (10,000,000)	5	50
Level No.	Level Initials	Level	Final conc. (ppm)	Stock used (ppm)	D.F.	Std (gr)	Tot. Weight (g)
8	A8	MU4_10_ppm	20	IV-59 (1000 ppm)	×50	1	50
7	A7	IV59_10_ppm	10	IV-59 (1000 ppm)	×100	0.5	50
6	A6	IV59_5_ppm	5	IV-59 (1000 ppm)	×200	0.25	50
5	A5	IV59_2_ppm	2	IV-59 (1000 ppm)	×500	0.1	50
4	A4	IV59_1_ppm	1	IV-59 (1000 ppm)	×1000	0.05	50
3	A3	IV59_0.4_ppm	0.4	A5 (2 ppm)	×5 (2500)	10	50
2	A2	IV59_0.05_ppm	0.05	A4 (1 ppm)	×20 (20000)	2.5	50
1	A1	MQ_blank	0	MQ Blank	-	0	50

Table 7. Dilution scheme for calibration standards prepared from CRM-MU-4 and IV-stock-59 (1000 ppm)

Each time a new series of standards is prepared, the corresponding concentrations must be updated in the IC post-run calibration method to ensure accurate calibration. This process is carried out using Excel, where the correct dilution factors and resulting ion concentrations for the newly prepared standards are calculated. The calculated true concentrations, derived from the dilution scheme, are then entered into the post-run method to generate an accurate calibration curve for the batch analysis.

Control Standard Preparation

A diluted seawater control standard (IAPSO X1000) was prepared monthly and included in each batch to check measurement consistency. The standard was diluted step by step, as shown in Table 8.

No.	Name of the Std prepared	Type of std. (ppm)	Must be D.F.	Std (ml)	MQ (ml)	Tot. Vol. (ml)
1	IAPSO X1	Pure IAPSO std.	X1	5	0	5
2	IAPSO X10	(1): Pure IAPSO std.	X10	5	45	50
3	IAPSO X100	(2): IAPSO X10	X100	5	45	50
4	IAPSO X1000	(3): IAPSO X100	X1000	5	45	50

Table 8. Serial dilution scheme for preparation of the IAPSO (X1000) control standard

Eluent Preparation

Separate eluents were used for anion and cation analyses. Each eluent preparation was typically sufficient for about four full batch runs on the IC.

Cation Eluent

The cation eluent consisted of oxalic acid solution.

Preparation steps:

1. Weigh 2.2508 g of oxalic acid.
2. Dissolve in MQ water.
3. Adjust the final volume to 1000mL.

This produces a 0.5mM oxalic acid solution. The solution was mixed using a magnetic stirrer without heating.

Anion Eluent

The anion eluent consisted of a carbonate–bicarbonate buffer solution.

Preparation steps:

1. Weigh 10.08 g sodium bicarbonate ($NaHCO_3$)
2. Weigh 0.64 g of sodium carbonate (Na_2CO_3)
3. Add MQ water to reach 1000mL
4. Heat the solution to 80 °C while stirring to ensure complete dissolution

For IC analysis, the concentrated solutions were filtered, stored in the refrigerator, and diluted before each run. The dilution was prepared in 2L bottles by mixing 200mL of the concentrate with 1800mL of Milli-Q water. Fig. 17 shows the eluent containers used for refrigerated storage.

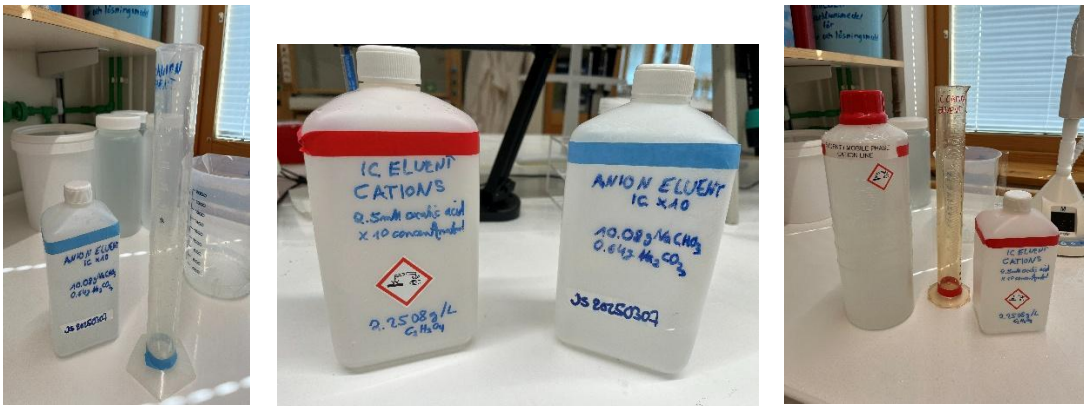

Figure 17. IC cation (red) and anion (blue) eluent containers for storage and preparation

IC System Capacity and Eluent Consumption

The IC system has specific operational limitations that determine batch size and eluent usage:

- Each run requires approximately 22 minutes
- Each run includes 3 minutes of pretreatment
- Total time per replication: 25 minutes
- Each replicate consumes approximately 25mL of eluent because eluent flow is 1 mL/min

Therefore:

- A complete batch can analyze 80 replicates without stabilization
- With stabilization steps included, 78 replicates can be analyzed
- Each eluent reservoir contains 2000mL, with 100mL always left to cover the intake probes

IC Analytical Method and Post-Run Calibration

All IC analyses were performed using the analytical method *anion_cation_SA2_nezhla*. The SA2 column was used for both anion and cation measurements within the dual-column IC system. The main operating parameters included a flow rate of 1 $mL\ min^{-1}$ and a total run time of approximately 25 minutes per injection, including the pretreatment stage. Ammonium (NH_4^+) and lithium (Li^+) were excluded from the quantification method because these ions are not included in the CRM-MU-4 cation calibration standard used in this study.

After completion of each analytical batch, the chromatographic data were processed using a post-run calibration procedure. This procedure ensured accurate identification of ion peaks and the generation of calibration curves for quantitative analysis. The calibration process began by selecting a representative anion standard level from the IV-59 standard series, which in most cases was the 2ppm level. The chromatographic peaks were assigned, and the corresponding retention times were copied from the lower-left table of the software interface to the quantification table in the lower-right panel. The method was then saved as a quantification method, labeled with the date (for example, *20250630_quant*).

Subsequently, a suitable cation standard level from the MU-4 standard series was selected. The previously saved quantification method was loaded, the cation peaks were assigned, and their corresponding retention times were transferred to the quantification

table in the same manner. The method was then saved again so that the quantification file contained retention times for both anions and cations. This updated method was then used to complete the calibration procedure for the entire batch.

Once the batch had been processed, calibration curves were generated individually for each ion. For cations, a linear regression model was applied, whereas anions were calibrated using a quadratic regression model. As a result, calibration for each batch involved two regression steps: linear regression for cations and quadratic regression for anions.

In IC, each ion is characterized by a specific retention time, which allows it to be identified within the chromatogram. However, if the sample dilution factor is not appropriate, the resulting chromatographic peaks may become too large and overlap with neighboring peaks. This can complicate peak identification and negatively affect calibration accuracy. In such cases; the batch may need to be rerun using a corrected dilution factor. If only a limited number of samples are affected, it may still be possible to resolve the issue by adjusting the retention time window used for peak identification.

This adjustment involves comparing the retention time of the ion in the calibration standard used for the batch with the retention times observed in the problematic sample chromatogram. The retention time closest to the standard value is selected as the correct peak for that ion. Once the appropriate peak has been identified, the calibration procedure can be repeated to obtain reliable ion concentrations. Selecting the retention time closest to the calibration standard is important because choosing a value that deviates significantly from the standard could cause incorrect peak assignments in other samples, preventing the software from exporting valid concentration values. A typical anion chromatogram, showing the retention times and order of anion peaks, is presented in Fig. 18.

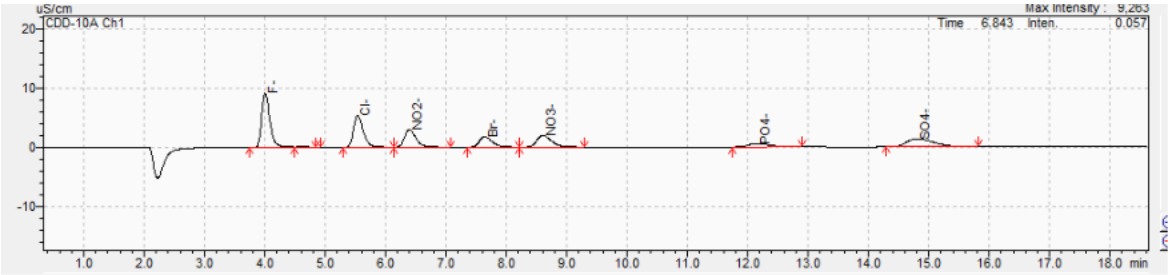

Figure 18. Representative anion chromatogram showing peak order and retention times

Detailed information about the post-run calibration is provided in the *Supplementary Materials*.

Evaluation of IC Data Accuracy

The reliability of IC measurements was assessed using three approaches:

- **Sample replicates** within each batch
- **Control standard (IAPSO X1000)** included in every batch
- **Blank samples** to detect contamination or background signals

These quality control measures ensured the accuracy and reproducibility of the ion concentration data obtained from the incubation experiment.

Other Analytical Methods

pH Sensor Calibration

The pH measurements in this study were carried out using a PICO-pH module (*PyroScience*), which is an optical pH sensor system based on fluorescence measurements rather than a conventional glass electrode. The system consists of three main parts: (1) a pH-sensitive sensor spot containing a fluorescent dye, (2) an optical fiber or rod that transfers light signals, and (3) the PICO-pH readout module that processes the signal.

The sensor works by illuminating the pH-sensitive dye with red light (620 nm). In response, the dye emits near-infrared fluorescence (760 nm), and the intensity and lifetime of this emitted light change depending on the proton concentration (H^+) in the surrounding solution. The optical signal is transmitted through the optical fiber to the PICO-pH module, where it is converted into a pH value after calibration.

One advantage of this system is that the measurements can be performed contactlessly through transparent vessel walls, making it highly suitable for sealed or high-pressure experimental setups. The module also includes connections for an external Pt100 temperature sensor, allowing automatic temperature compensation during measurements. In addition, the instrument contains internal sensors for monitoring temperature, pressure, and humidity within the module.

Calibration of the pH sensor was performed during the trial phase using a two-point calibration method recommended for optical pH sensors. Unlike conventional glass electrodes, which are calibrated with several buffer solutions, the optical sensor was calibrated using two reference conditions: one highly acidic solution (approximately pH 2) and one highly basic solution (approximately pH 10–11). These two calibration points force the fluorescent indicator dye into its fully protonated and fully deprotonated states, defining the complete response range of the sensor. The instrument then uses the fluorescence response from these reference points to generate a calibration curve and convert the measured optical signal into pH values during the experiments.

Buffer solutions with different pH values were prepared according to the experimental protocol (Buffer Reference Center, 2026). Before measuring the pH of these solutions, the laboratory pH meter was calibrated using three commercial standard buffers with pH values of 4.01, 7.00, and 9.21 (Fig. 19). To reproduce the experimental temperature conditions, the sensor probe and buffer solutions were placed in the refrigerator and allowed to equilibrate to approximately 4 $°C$. Once the probe temperature reached 4 $°C$, calibration measurements were performed sequentially using the three buffer solutions (pH 2, 4, and 7). Because buffer pH values depend on temperature, the target calibration values were adjusted according to the temperature-dependent correction provided in the buffer documentation. The adjusted calibration values used at approximately 5 $°C$ are shown in Table 9.

pH	Buffer pH (25 °C)	Temperature correction	Adjusted pH at ~5 °C
2	2.00	+0.01	2.01
4	4.01	-0.01	4.00
7	7.00	+0.09	7.09

Table 9. Temperature-adjusted pH calibration values at 5 °C

Once calibrated, the pH of the prepared solutions was measured:

- 0.12 M HCl solution, produced by dissolving 1 mL of concentrated HCl in 99 mL of Atlantic IAPSO seawater
- 0.105 M NaOH solution, produced by dissolving 4.2147 g NaOH powder in 1 L of MQ water

The prepared solutions were sequentially introduced into the sensor system inside the incubator to perform calibration. The calibration procedure was completed successfully, and the sensor showed stable readings under the experimental temperature conditions.

For the incubation experiment, an acidic HCl solution was prepared by adding two drops of 37% HCl (approximately 2 X 100µL) to the undiluted IAPSO solution within the visual cell. This adjustment established the desired acidic starting conditions by lowering the pH to approximately 2. The solution was then offset by one calibration point. The resulting HCl solution had a measured pH of 2.78 at 21.4 °C.

Figure 19. Calibration of the pH meter and measurement of prepared solution pH

Total Alkalinity (TA) Measurements

The total alkalinity of some samples was determined using an auto-titrator system operated with the *Tiamo software*, which enables automated, sequential measurements (Fig. 20). The system provides outputs for three key parameters: pH, volume of added HCl (mL HCl 4/5), and alkalinity (Alk_45, mmol L^{-1}).

Prior to sample analysis, the instrument was calibrated using pH buffer solutions (pH 4 and pH 7). To ensure that no residual acid remained in the probe from previous runs, three IAPSO X50 control solutions (0.6 mL IAPSO + 29.4 mL MQ) were measured before starting the calibration. In addition, IAPSO control measurements were included at the beginning, middle, and end of each batch for each sandpack to monitor analytical stability. Two additional reference solutions (Borate X50 and X200) were also analyzed as part of the quality control procedure, as borate serves as an alkalinity standard.

All samples and IAPSO control solutions were pre-diluted (X50) one day prior to analysis and stored in a refrigerator. This step was essential to prevent particle settling, which could negatively affect measurement accuracy if samples were left at room temperature overnight. Before analysis, the samples were removed from the refrigerator and allowed to equilibrate to room temperature for a few hours.

The auto-titrator has a total capacity of 24 positions per run (Fig. 20), allocated as follows:

- Three positions for MQ rinse solutions (positions 22-24)
- Two positions for pH buffer calibration (pH 4 and 7) (positions 1 and 2)

- Nineteen positions for IAPSO controls and samples (positions 3-21)

For TA, 32 samples per sandpack (Total = 192) were measured. Sample dilution aimed at a final volume of 30 mL, while minimizing sample consumption. Among the tested dilution factors, X50 dilution (0.6 mL sample + 29.4 mL MQ) was selected as optimal, as it provided reliable results with minimal sample usage. Table 10 summarizes the tested dilution schemes.

Solution Composition	D.F.	
0.5mL IAPSO + 29.5mL MQ	X60	
0.6mL IAPSO + 29.4mL MQ	X50	The best
0.75mL IAPSO + 29.25mL MQ	X40	
1 mL IAPSO + 29 mL MQ	X30	
1.5mL IAPSO + 28.5mL MQ	X20	
3mL IAPSO + 27mL MQ	X10	

Table 10. Evaluated dilution schemes for auto-titrator alkalinity measurements of incubation samples

Figure 20. Auto-titrator device and sample setup

Sediment Preparation and Analysis

Freeze-Drying and Homogenization

In order to choose which multi-core from Petermann fjord to incubate (MC-37, MC-38, and MC-34), sediments from all stations were freeze-dried and homogenized to be analyzed for their carbon content.

For this purpose, I used the Peterman Fjord wet core sediments kept in the fridge (Fig. 21). Wet sediment samples were first placed in plastic bags and weighed (eg, 58.35 g excluding the bag). The samples were then frozen in a freezer before being transferred to the

freeze-dryer, as freezing is necessary to allow sublimation of ice under vacuum conditions (Fig. 22).

Following freeze-drying, the sediments were gently homogenized by hand rather than mechanically ground, to preserve particle structure while ensuring adequate mixing. Each bag of sediment was then weighed, and specific amounts were taken from each depth interval to prepare a representative mixture.

Figure 21. Sediment from core MC-38 used for incubation experiments

Figure 22. Freeze-drying of sediment samples

Carbonate Content Analysis and Sediment Selection

To determine which sediment samples should be used for the incubation experiment, carbonate and total organic carbon (TOC) measurements were performed on sediments from three coring stations (MC-34, MC-37, and MC-38). These cores were collected from different locations in the study area (Fig. 3).

The purpose of this analysis was to determine whether a mixed sediment sample representing the Petermann Fjord could be prepared. If all cores showed similar carbonate

levels, sediments from all cores would be combined. However, if only one core contained elevated carbonate concentrations, that core would be used exclusively.

The results indicated that Core MC-38 was the most suitable source. Therefore, sediments from all depths of MC-38 were mixed to create a representative sample for the experiment.

Because each sandpack can contain approximately 130 mL, filling four sandpacks required a total sediment mixture volume of 520 mL. To ensure that the experimental material represented the vertical variability of the core, sediments from different depth intervals were combined proportionally according to the available material at each depth. The final mixture contained a total of 397.5 g of sediment, distributed across the different depth intervals as summarized in Table 11.

No.	Depth (cm)		Sed. Weight (gr)	Weight to mix
	From	To		
1	0	1	7.65	7.5
2	1	2	11.14	7.5
3	2	3	10.19	7.5
4	3	4	8.8	7.5
5	4	5	7.98	7.5
6	5	10	51.74	37.5
7	10	15	49.71	37.5
8	15	20	47.04	37.5
9	20	25	49.7	37.5
10	25	30	51.38	37.5
11	30	35	57.26	37.5
12	35	40	131.47	37.5
13	40	45	78	37.5
14	45	50	77.83	37.5
15	50	53	38.64	22.5
	Total Weight:		678.5	397.5
	Unit:		gr	Gr

Table 11. Sediment mass distribution by depth used to prepare a representative mixture of core MC-38 for the incubation experiment

Scanning Electron Microscopy (SEM) Analysis

Sample Preparation

Sediment samples were also examined using *Scanning Electron Microscopy (SEM)* to investigate grain morphology and surface characteristics. Prior to analysis, sediment thin sections were coated with a thin conductive layer of gold, typically approximately 10nm thick, to prevent charging during electron beam exposure.

Two types of samples were prepared for SEM analysis:

1. Sediment thin sections, mounted on plates.
2. Loose sediment grains, placed on black carbon tape and subsequently gold-coated.

Imaging Conditions

SEM imaging was performed using several detector configurations:

1. Backscattered Electron Detector (BSD)
2. Secondary Electron Detector (SED)
3. Combined BSD–SED imaging

A specialized topography imaging mode was also used to enhance surface relief features of the sediment particles.

One potential issue during SEM imaging is *electron charging*, which occurs when electrons accumulate on poorly conductive sample surfaces. Charging can produce excessively bright or distorted images. To mitigate this effect, the vacuum level in the chamber can be slightly reduced, allowing increased moisture in the chamber atmosphere. However, this approach represents a compromise, as higher moisture levels may also reduce image clarity.

Samples Investigated

Eight samples were selected for SEM observation. These included both terrestrial (T) (Fig. 23) and water column (W) materials:

- T16
- T18
- T19
- T20
- T23
- Fjord sediments
- W78
- Sea ice sample
- Dust in ice

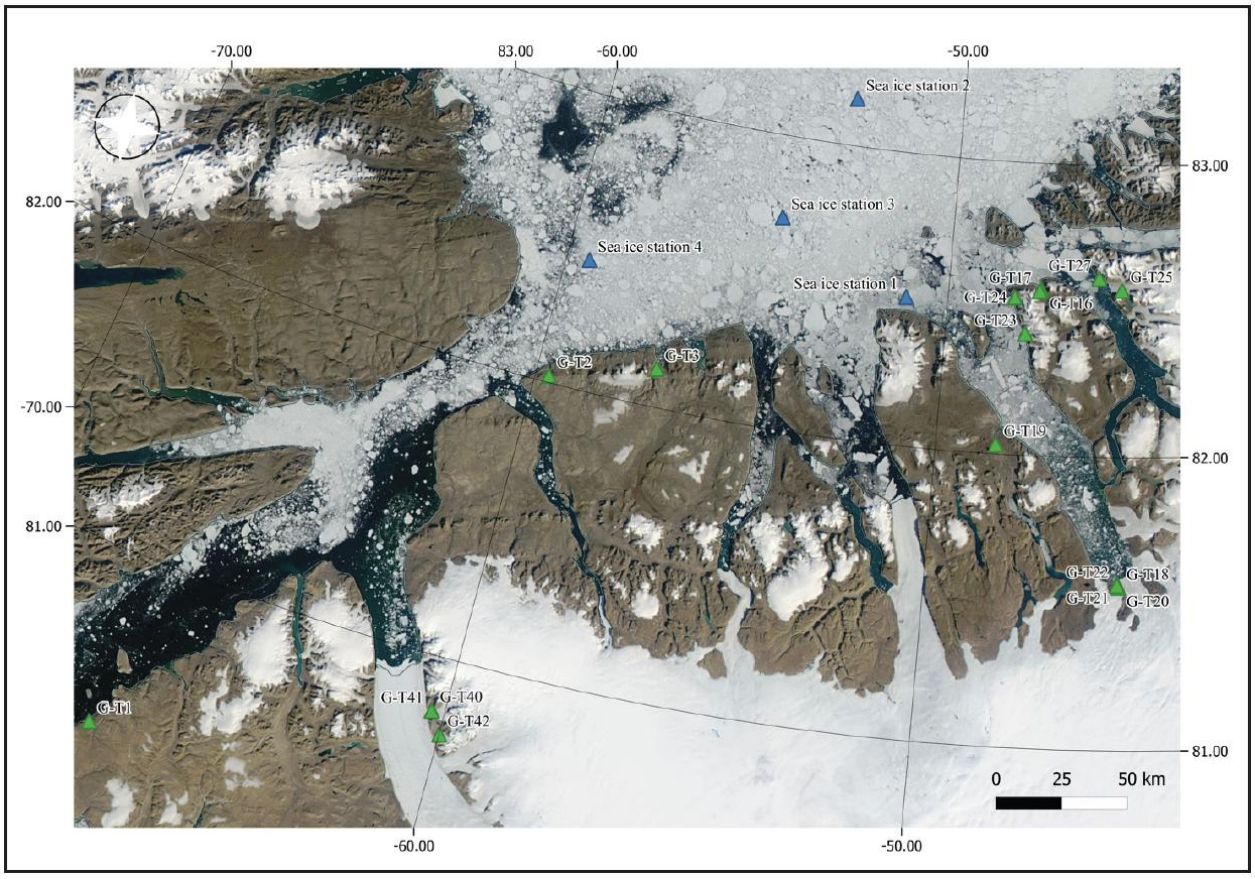

Figure 23. Locations of terrestrial and sea ice sampling stations (GEOEO Shipboard Scientific Party, 2024)

Post-Experiment Sediment Processing and Pore Water Extraction

Following the completion of the experiment, two plexiglass columns were prepared with the intention of collecting undisturbed sediment cores. However, upon opening the first sandpack, the sediment was observed to be highly water-saturated and lacked sufficient structural integrity for intact core sampling. Consequently, the original plan was modified. The sediment was carefully extruded from the sandpack and transferred directly into Falcon tubes. During this process, sediment was gradually pushed out from one end of the sandpack and collected from the opposite end. Samples were collected in Falcon tubes, labeled, and weighed. The top and bottom orientations of each sample were marked on the tubes to preserve core directionality. Porewater samples were extracted using rhizones (Fig. 24). Table 12 provides all information about the collected samples. All materials used during sediment handling and sampling were acid-washed to minimize contamination.

The high water content observed, particularly in sample SP1_3, suggested uneven sediment packing within the sandpack, possibly due to preferential flow paths or fractures that allowed water accumulation.

Date	Sandpack	Sample ID	Description / Treatment
26-Mar-26	Sandpack 1	SP1_1	Pore water extracted using rhizon (IC analysis); sed iment freeze-dried
		SP1_2	Pore water extracted using rhizon (IC analysis); sediment freeze-dried
		SP1_3	Rhizon extraction not feasible due to high water content; overlying water collected, filtered, and transferred into two 15 mL acid-washed Falcon tubes for IC analysis; sediment freeze-dried
		SP1_4	Sediment freeze-dried (no pore water extraction)
27-Mar-26	Sandpack 2	SP2_0	Overlying water collected upon opening; filtered and analyzed by IC
		SP2_1	Pore water extracted using rhizon (IC analysis); sediment freeze-dried
		SP2_2	Pore water extracted using rhizon (IC analysis); sediment freeze-dried
31-Mar-26	Sandpack 4	SP4_1	Freeze-dried sediment
		SP4_2	Freeze-dried sediment
		SP4_3	Pore water extracted using rhizon (IC analysis); sediment freeze-dried
	Sandpack 5	SP5	Water sample collected in 50 mL Falcon tube (IC analysis)
	Sandpack 6	SP6	Water sample collected in 50 mL Falcon tube (IC analysis)
2-Apr-26	Sandpack 3	SP3_1	Sediment freeze-dried (additional sampling)
		SP3_2	Pore water extracted using rhizon (IC analysis); sediment freeze-dried

Table 12. Summary of samples collected from each sandpack and their subsequent processing

Figure 24. Post-experiment sediment processing: porewater extraction

Results & Discussion

Trial Incubation Experiments (Silica Gel Test) Results

Post-Run Analytical Issues

During the post-run IC analysis of the silica gel samples, calibration problems were encountered due to the very high ion concentrations in the samples (mainly Na, Cl, and SO4). These concentrations exceeded the calibration range of the standards, causing significant

deviations in retention times. The excessively large peaks indicated that higher sample dilution factor was necessary before performing IC analysis.

For anions, the peaks for chloride and sulfate were significantly larger than those of the calibration standards (eg, the 1 ppm IV59 standard) and the control solution (IAPSO X1000) (Figs. 25 & 26). For cations, the sodium peak exceeded the highest calibration standard (20 ppm CRM-MU4) and, in some cases, overlapped with the retention time of potassium (K^+), leading to misidentification of peaks. These issues demonstrated the importance of applying an appropriate sample dilution factor prior to analysis.

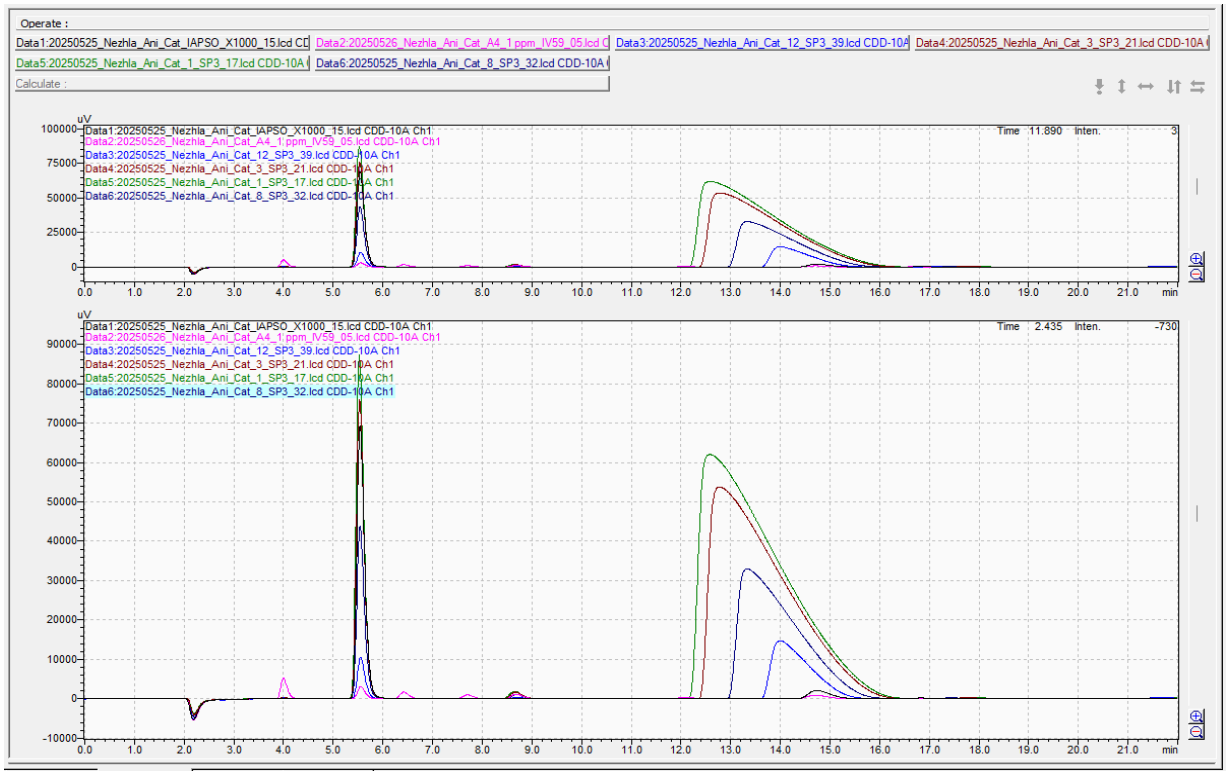

Figure 25. Anion peaks (Cl^- and SO_4^{2-}) in the samples are significantly larger than in the calibration standard (1 ppm_IV59) and control (IAPSO X1000)

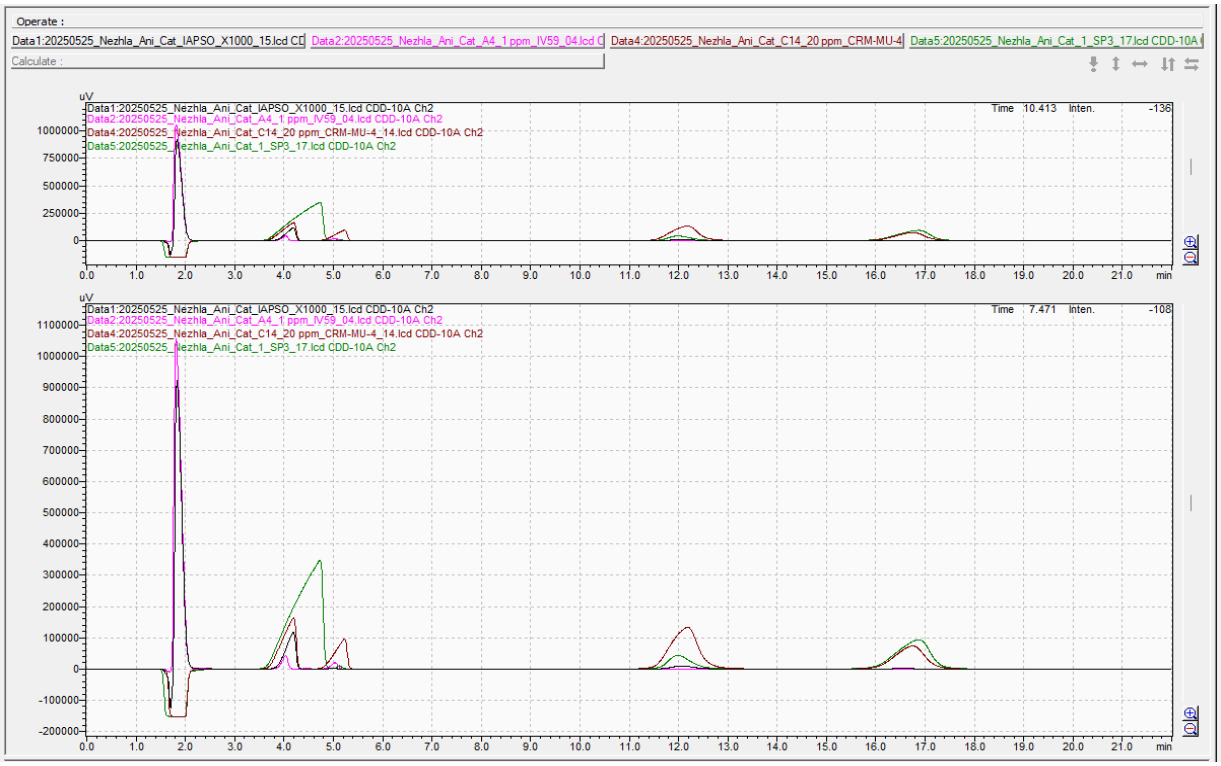

Figure 26. Comparison of Na^+ peak magnitude relative to calibration standards, illustrating excess of calibration range and analytical potential interference

Fig.26 illustrates the magnitude of the sodium (Na^+) peaks observed in the samples compared with the highest concentration level of the cation standard (20 ppm CRM-MU4) and the control standard IAPSOX1000. The Na^+ peak in the samples is approximately twice the area of the 20ppm standard, indicating that the sodium concentration exceeds the instrument's calibration range. When the Na^+ peak becomes excessively large, it may broaden or shift into the retention time window typically associated with potassium (K^+). As a result, the system may incorrectly identify part of the Na^+ signal as a K^+ peak, leading to inaccurate quantification and erroneous analytical results. This issue clearly demonstrates the importance of applying an appropriate dilution factor prior to IC analysis.

Calibration Curve Evaluation

During the calibration process, the anions, particularly chloride (Cl^-), exhibited a quadratic calibration relationship rather than a linear one. Recalibration confirmed that a quadratic regression model provided a significantly better fit for the chloride calibration points compared with a linear model.

In contrast, the calibration curves for cations remained linear across the measured concentration range, indicating that linear regression was appropriate for quantifying these analytes.

Overall, the results demonstrate that quadratic regression is more suitable for anion calibration, especially for chloride, whereas linear regression adequately describes the response of cations. Fig. 27 below illustrates the differences between the linear and quadratic calibration fits for Cl.

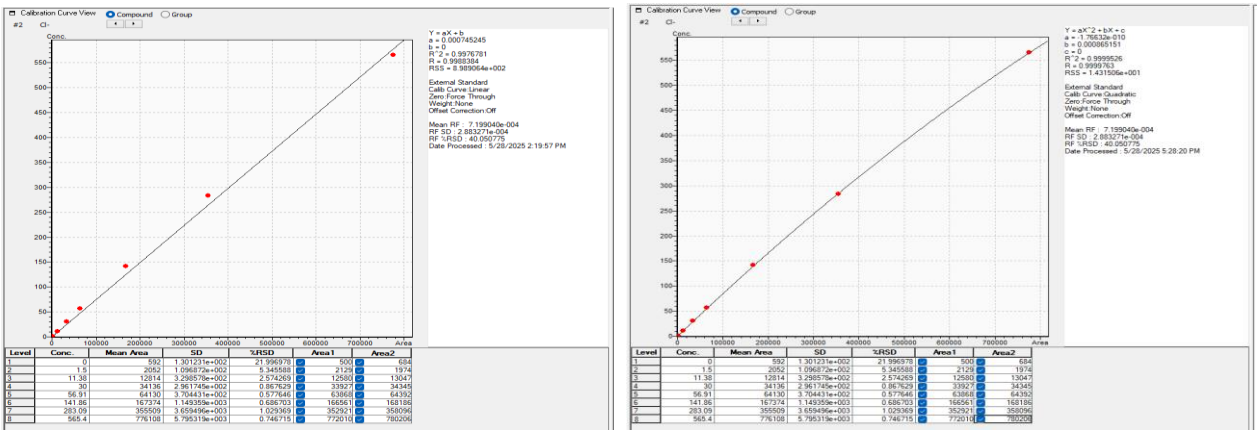

Figure 27. Calibration curve for Cl^- using linear and quadratic fitting

Breakthrough Curve (BTC) Results

Each sampling event collected approximately 1.7 mL of fluid, while the fraction collector introduced an additional volume of Milli-Q water into the sample vials, resulting in slight dilution of the collected samples prior to IC analysis. Although, in principle, the measured concentrations should be corrected using a dilution factor, this was not applied in the final calculations due to the non-constant nature of dilution over time. Variations in sample mass suggest that fluctuations in pressure influenced flow rates and led to inconsistent amounts of water entering the vials. While the dilution factor could potentially be estimated (backcalculated) using chloride (Cl^-) as a conservative tracer (using the formula below), this approach was not pursued here and would require further methodological validation.

$$back\ calculation: [Element]_{IAPSO} + [Element]_{CaCO_3} = \frac{[Element]_{spl}}{DF} = \frac{[Element]_{spl}}{[Cl]_{spl}} \times [Cl]_{IAPSO}$$

Chloride concentrations measured in samples from Incubator 2 (Sandpacks 3 & 4) were used to construct the BTC curves. The resulting concentration profiles showed the gradual displacement of the tracer solution and the flushing behavior of the silica gel column.

Table 13 presents the sampling details for the silica gel test, including the dates, exact times, and the calibrated chloride (Cl) concentrations for SP3 and SP4.

No.	Date	Time of starting sampling							
		Incubator 2							
		Sandpack 3				Sandpack 4			
		No.	sample name	linear Cl Conc. (µmol)	Quadratic Cl Conc. (µmol)	No.	sample name	Linear Cl conc. (µmol)	Quadratic Cl Conc. (µmol)
0		0	IAPSO X1000 blank	570	558				
1	20-May	1	11:36:41	722	672				
3		2	12:03:09	719	671				
5		3	13:33:12	625	601				
7		4	13:57:18	541	535				
9		5	14:23:20	500	501				
11		6	14:44:47	484	488				
13		7	15:08:05	455	462				
15		8	15:29:57	356	373				
17		9	15:49:31	247	267				
19		10	16:08:32	173	191				
21		11	16:27:22	112	126				
23		12	16:46:40	87	98				
25		13	17:06:07	65	74				
27		14	17:26:00	47	54				
29		15	17:45:21	40	46				
31	21-May	16	10:44:09	13	16	16	10:34:43	10	11
33		17	11:38:13	27	31	17	11:25:31	482	485
35		18	12:20:59	48	55	18	12:11:32	434	444
38		19	13:23:16	44	51	19	13:13:52	307	326
40		20	14:04:09	45	52	20	13:54:42	247	267
42		21	14:49:17	28	32	21	14:36:37	234	255
44		22	15:34:35	46	53	22	15:25:12	246	267
47		23	16:37:39	54	62	23	16:28:15	322	342
50		24	17:39:13	73	83	24	17:29:51	432	443
52	22-May	25	14:57:11	70	80	25	14:47:47	458	466
53	23-May	26	12:03:51	63	72	26	11:54:27	407	420
55		27	12:49:06	34	39	27	12:39:42	179	198
57		28	13:40:53	26	30	28	13:31:28	139	155
59		29	14:19:23	23	27	29	14:09:04	114	128
61		30	14:56:56	29	34	30	14:47:33	103	116
63		31	15:34:32	17	20	31	15:25:09	90	102
			31						16
		47 samples in total							

Table 13. Sampling scheme for the silica gel test experiment

Fig. 28 shows the Cl concentrations in the two sandpacks, SP3 and SP4. Both sandpacks follow a similar overall pattern, including the same rises and drops. However, Cl concentrations in SP4 (the upper sandpack) are generally higher than in SP3 (the lower one), with more pronounced fluctuations.

This difference may be due to the sampling sequence: SP4 is sampled first, which could result in higher measured Cl concentrations, while SP3 is sampled afterwards and shows lower values.

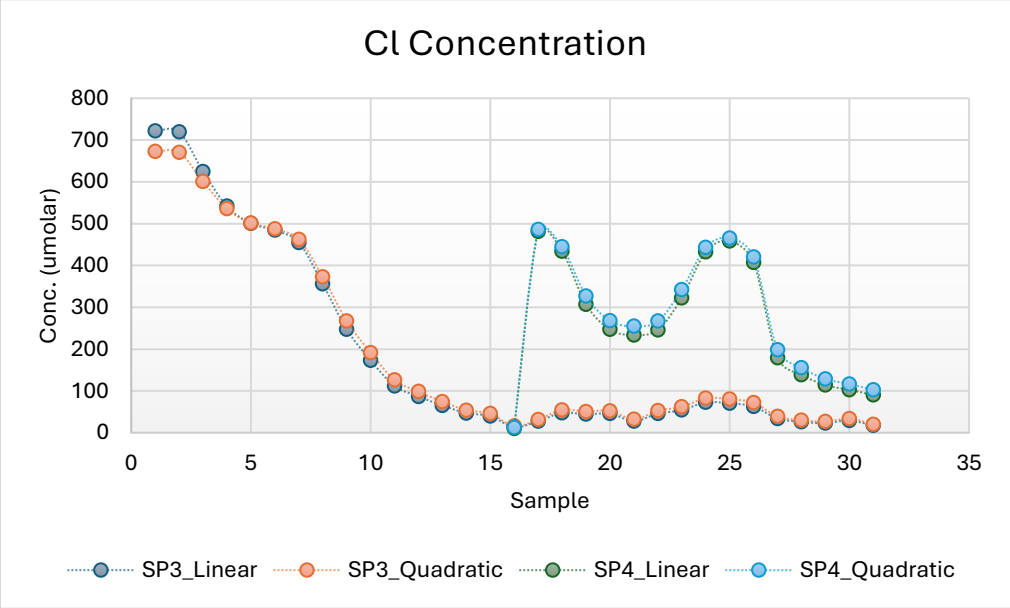

Figure 28. Incubator stability test results (BTC)

Incubator Stability Results

The silica gel test experiment ran for approximately four days, during which the silica gel mixture containing X1000 diluted IAPSO seawater was flushed with deionized MQ water for approximately 17 hours. Sampling was performed from all three incubators.

As observed in Fig. 29, the results showed that the silica gel initially released elevated concentrations of Na^+ and SO_4^{2-} (with Mg^{2+} also present), which decreased over time but remained detectable after prolonged flushing. In contrast, Cl^- and Br^- were primarily derived from the IAPSO solution, with Br^- being almost completely removed after ~3 hours. Elevated Ca^{2+} and K^+ concentrations were also observed in the effluent, exceeding levels in both the silica gel and IAPSO solution, indicating additional sources or release mechanisms within the system. The horizontal dashed lines indicate the solute concentrations of the X1000 diluted IAPSO, while the vertical dashed lines mark the times at which fluid flow was paused.

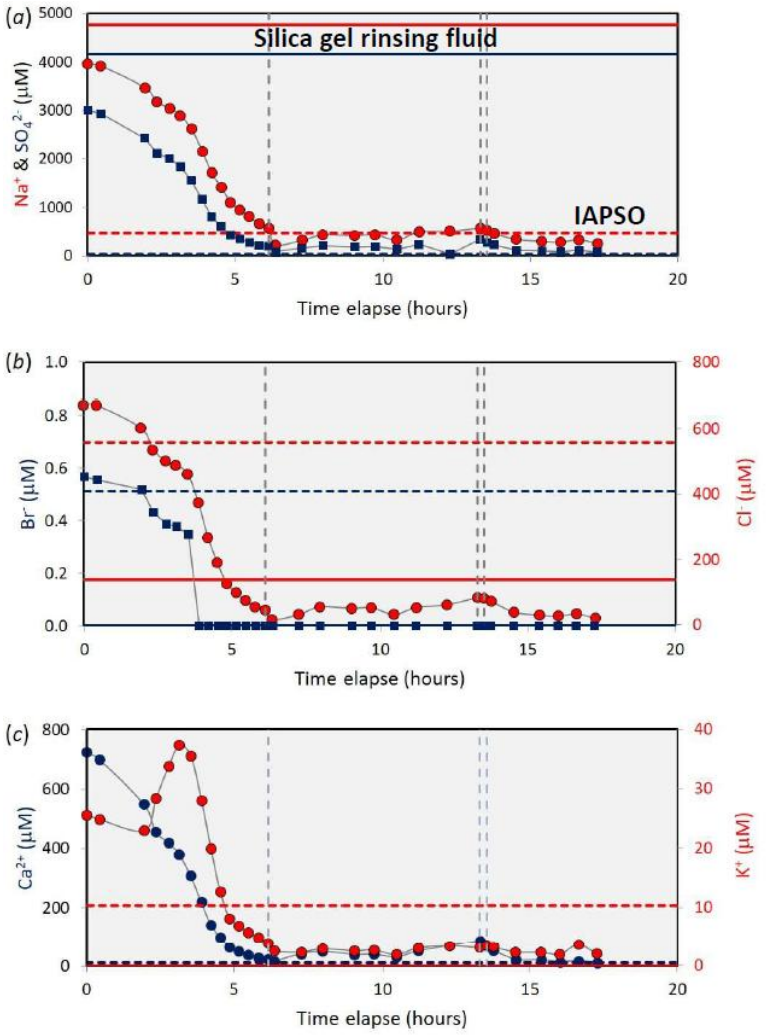

Figure 29. Results of a 4-day flushing experiment with silica gel mixture and diluted IAPSO solution, showing ion behavior during flushing

pH Sensor Stability

A separate 2.5-day stability test was conducted to evaluate the performance of the pH sensor during continuous operation. The results indicated good stability of the sensor signal over the duration of the experiment, confirming that the sensor could reliably monitor pH during long-term incubations (Fig. 30).

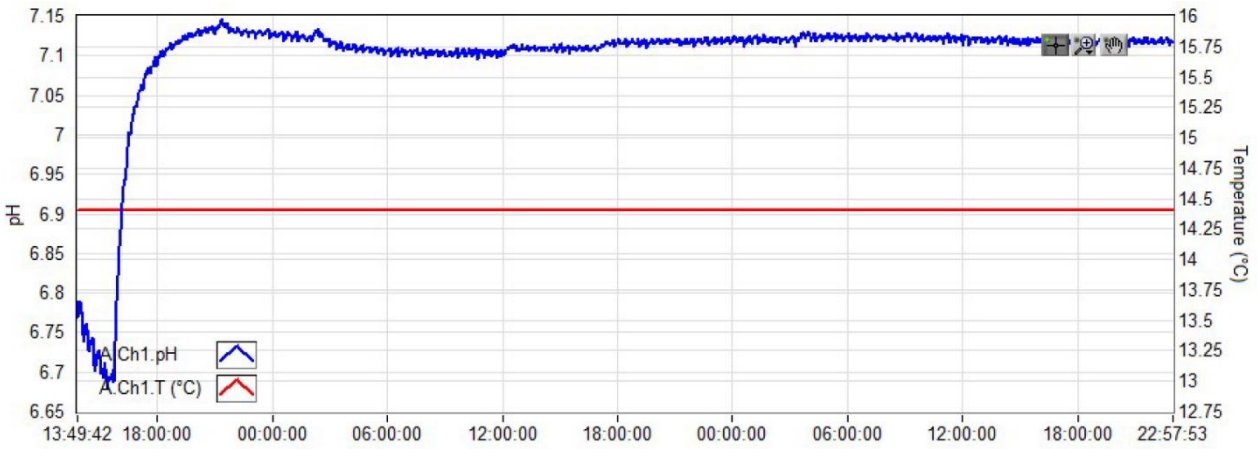

Figure 30. pH sensor stability test over 2.5 days

Incubation Results

Six samples were collected daily from the incubation system over a 145-day period, from 24 October 2025 to 17 March 2026, yielding a total of 654 samples (22 batches). But anion/cation IC results are reported only up to the end of batch 19, corresponding to a total of 576 samples collected by 27 February.

Sample Weights

To monitor sampling consistency and quantify the actual collected volumes, all sampling vials were weighed prior to sampling each day and reweighed after sample collection. This procedure allowed accurate tracking of the volume of diluted sample dispensed into each vial, providing a basis for evaluating variability between sampling positions and incorporating these differences into data interpretation and hypothesis development.

Fig. 31 illustrates the variation in sample weights over the 145 days. Notably, lower weight values correspond to samples collected on Sundays and weighed on Mondays, reflecting increased evaporation due to extended residence time in the fraction collector. On average, each sample had a volume of approximately 1.7mL.

A slight decreasing trend in sample weight is observed over time (indicated by the linear trend line), which may be attributed to gradual pressure loss within the sandpacks towards the end of the experiment. A gap around day ~50 corresponds to a four-day interruption in sampling caused by maintenance and replacement of a broken pump component, while the pump itself remained in operation throughout the experiment. Additionally, the absence of low-weight (Sunday) data points between days 67 and 89 reflects a temporary shift to a

reduced sampling frequency (three days per week), during which Sunday sampling was excluded.

Sample weights were also plotted against Cl concentration; however, no clear correlation was observed, possibly indicating that additional factors, such as pressure, play a significant role. The figure is not included here.

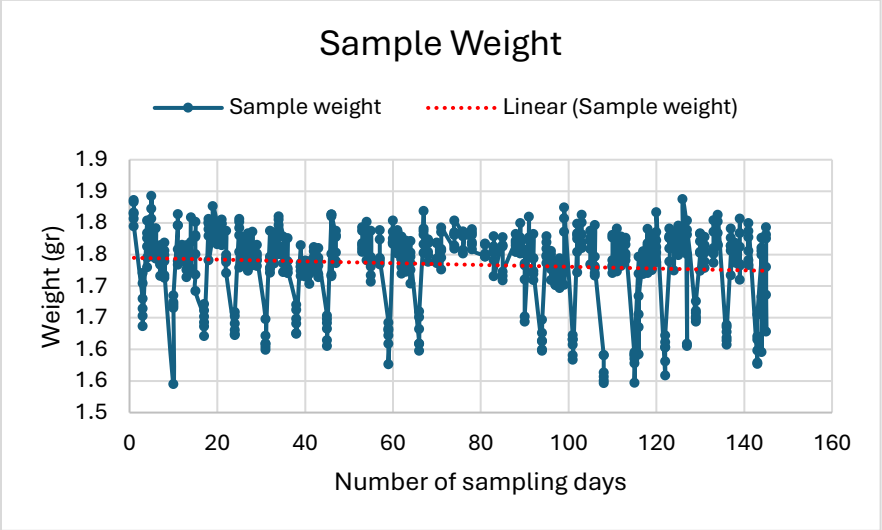

Figure 31. Sample weight changes over the experimental period

During each sampling cycle, 1.7 mL of sample was dispensed into the incubation vial over a total period of 17.10 minutes. The sampling valve switched on at 0.1 min and switched off at 14.4 min, changing from position 1 (sampling sequence) to position 0 (loop-wash sequence directed to waste). Therefore, the valve remained open for 14.3 minutes, representing the effective sampling period during which water from the incubation system was collected.

The amount of water discharged to waste during this interval was measured as 1.33 g, which is the same as the undiluted sample collected prior to dilution by the fraction collector. Dividing this value by the 14.3 min sampling duration yields a flow rate of approximately 0.093 mL/min.

$$Flowrate = \frac{1.33}{14.3} = 0.093\ ml/min$$

The difference between the total collected sample volume (1.7 mL) and the measured water going to waste (1.33 mL) corresponds to approximately 0.37 mL, which is the amount of MQ dispensed in the sample by the fraction collector. Consequently, the dilution accounted for approximately 21.8% of the total collected sample volume.

$$Sample\ dilution = \frac{0.37}{1.7} \times 100 = 21.8\%$$

Sample Weight by Sampling Position

Fig. 32 presents the variation in sample weights for each individual sandpack over the course of the experiment. Consistent with the overall trend, most positions exhibit only minor decreases in sample weight over time. However, the reduction appears to be slightly more pronounced in sediment-containing sandpacks, suggesting that these systems may have been more sensitive to small fluctuations in pressure conditions.

Overall, the observed trends highlight the importance of maintaining stable pressure conditions and consistent sampling protocols to ensure reliable and comparable results across the duration of long-term incubation experiments.

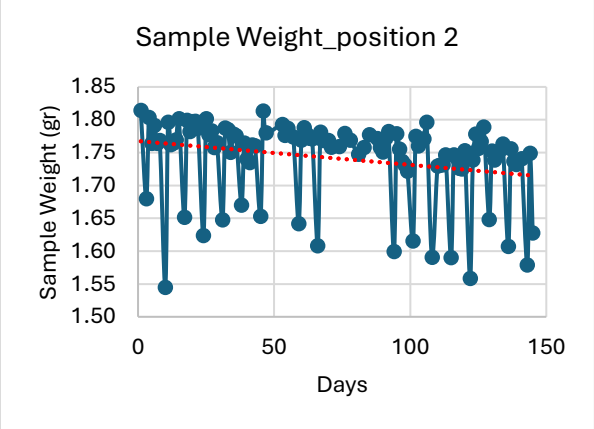

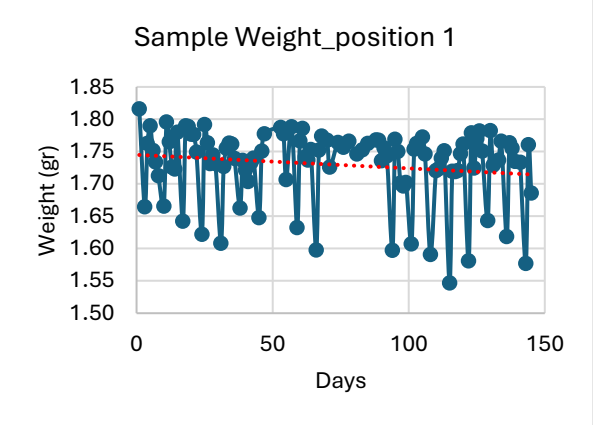

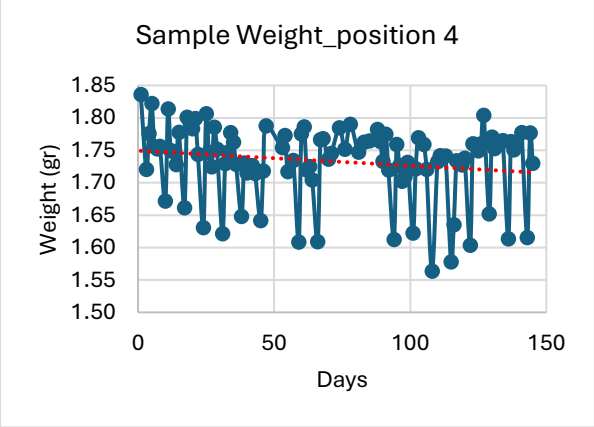

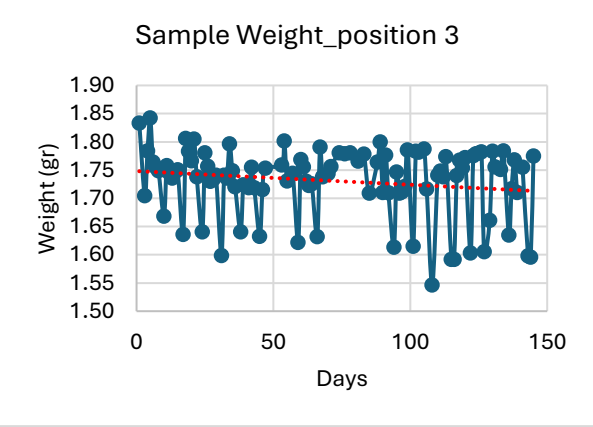

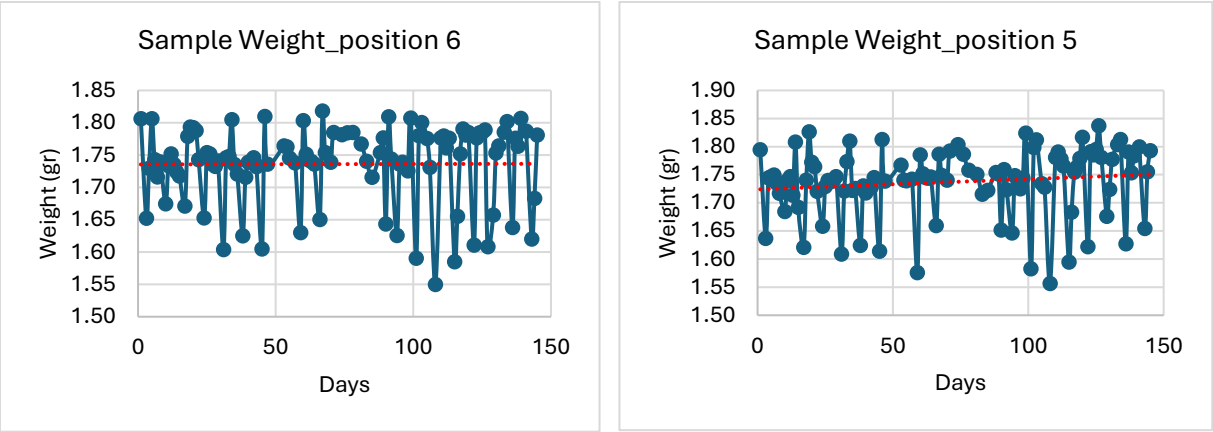

Figure 32. Sample weight variations by position over the experimental period

Incubation Parameters (Pressure, Flow, and Temperature)

Pressure (P)

Fig. 33 presents the pressure data recorded by the incubation system throughout the experimental period. Pump pressures are represented by P1A_P and P1B_P, corresponding to cylinders A and B, respectively (Fig. 5a). Pressure within the individual sandpacks is monitored by sensors (Fig. 8): PT_11_Value (Sandpack 1), PT_12_Value (Sandpack 2), PT_21_Value (Sandpack 3), PT_22_Value (Sandpack 4), PT_31_Value (Sandpack 5), and PT_32_Value (Sandpack 6).

Cylinder B ceased functioning in mid-December. As a result, cylinder A was manually refilled on a daily basis for the remaining period of the experiment. Despite this limitation, cylinder A maintained a relatively stable pressure throughout the experiment, with slightly decreasing pressure from February to March in the sandpacks due to a calibration issue with cylinder A. Therefore, manual adjustment of cylinder A pressure was done. Pressure was restored to approximately 102 bar.

Pressure fluctuations were more pronounced in the upper sandpacks, likely due to sediment accumulation and partial clogging within the sediment matrix. The sediment acted as a filter barrier, reducing permeability and restricting fluid flow, which made pressure transmission and replenishment through these sections more difficult. As a result, localized pressure drops and more variable pressure signals were observed in the upper sandpacks.

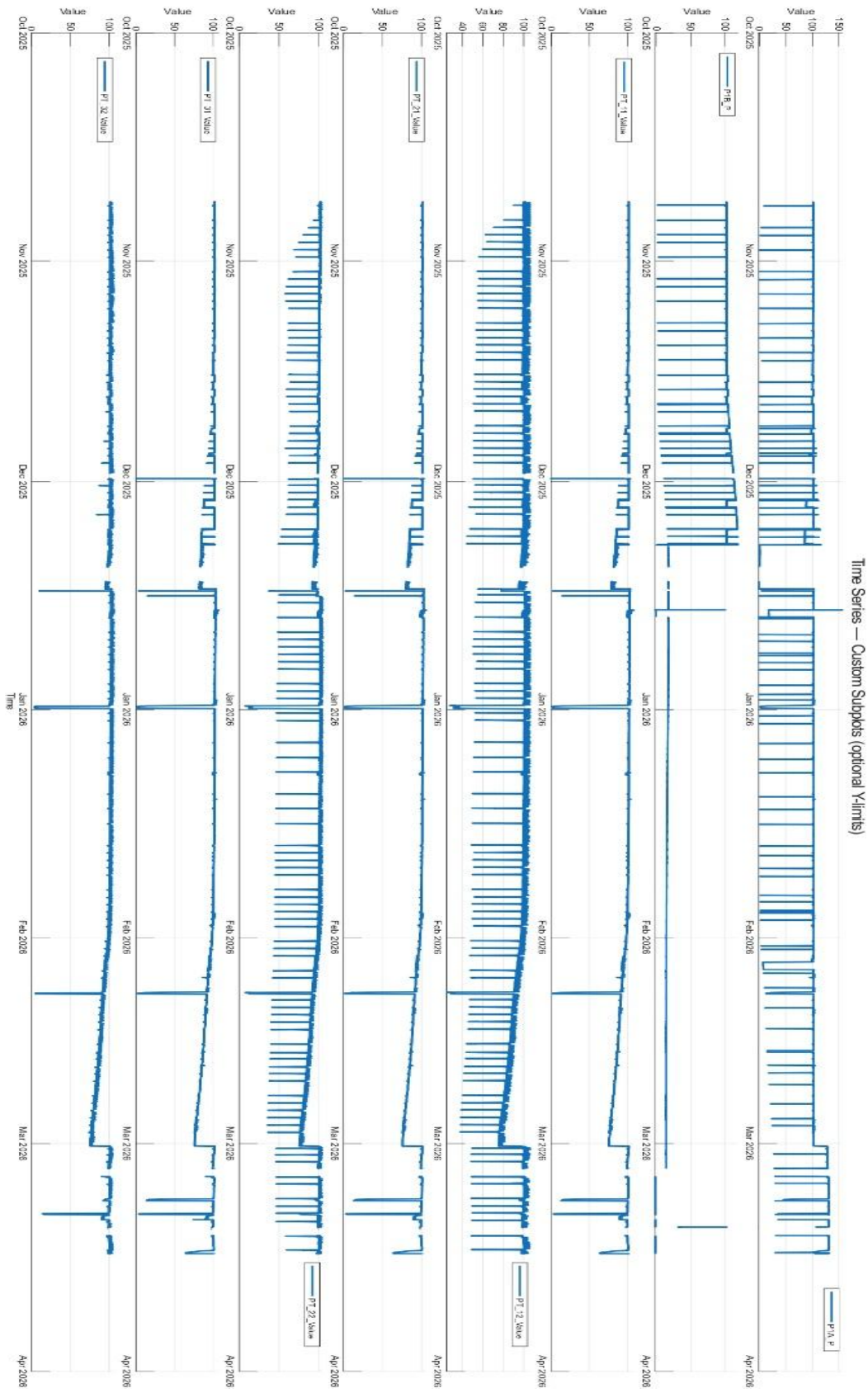

Figure 33. Incubation parameters: pressure in pump cylinders and sandpacks

Flow (Q)

Flow rates for both pump cylinders are presented in Fig. 34. P1A_Q represents the flow rate in cylinder A, while P1B_Q represents the flow rate in cylinder B. As observed in the data, flow from cylinder B ceased in mid-December, corresponding to its mechanical failure.

Negative flow values are observed in the plots, which indicate the direction of flow towards the sandpacks. This sign convention reflects the operational setup of the system rather than an actual reversal of flow.

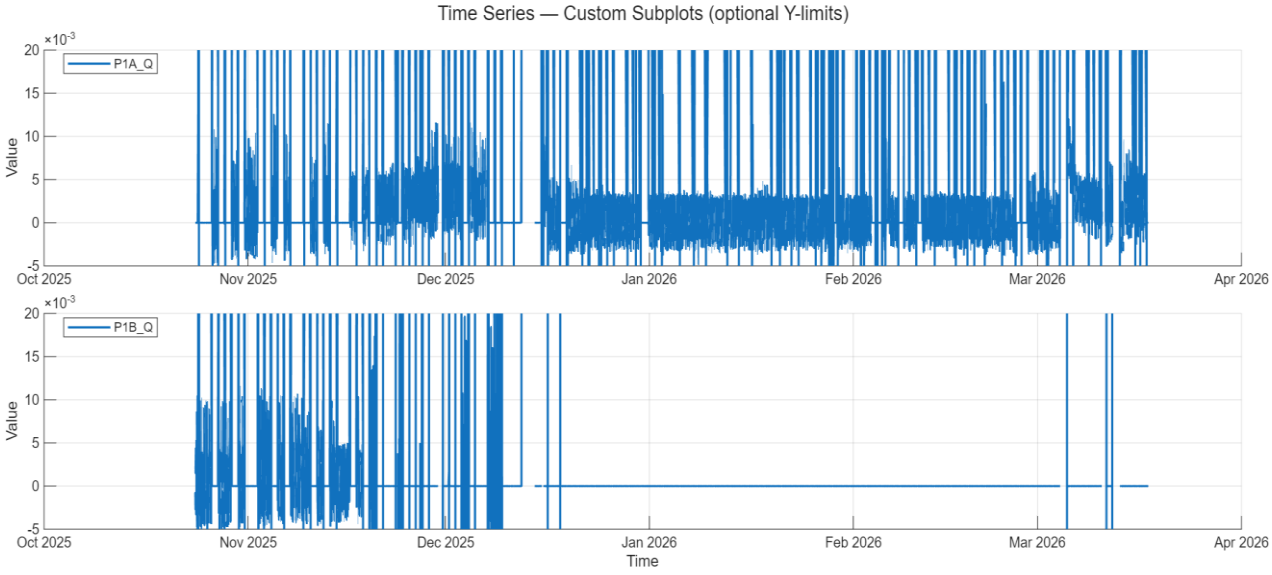

Figure 34. Incubation parameters: flow rates in pump cylinders A and B

Temperature (T)

Temperature measurements for all sandpacks are shown in Fig. 35. Throughout the experiment, temperatures were generally maintained within a range of approximately 5 to 8 $°C$, indicating relatively stable thermal conditions.

Each incubator is equipped with multiple temperature sensors. For example, TE_13 corresponds to the temperature of the visual cell within the system. The presence of multiple sensors allows for the monitoring of temperature variations across different components of the setup.

The minimum temperature was slightly higher at the beginning of the experiment and was later reduced as part of an intentional adjustment to the experimental conditions

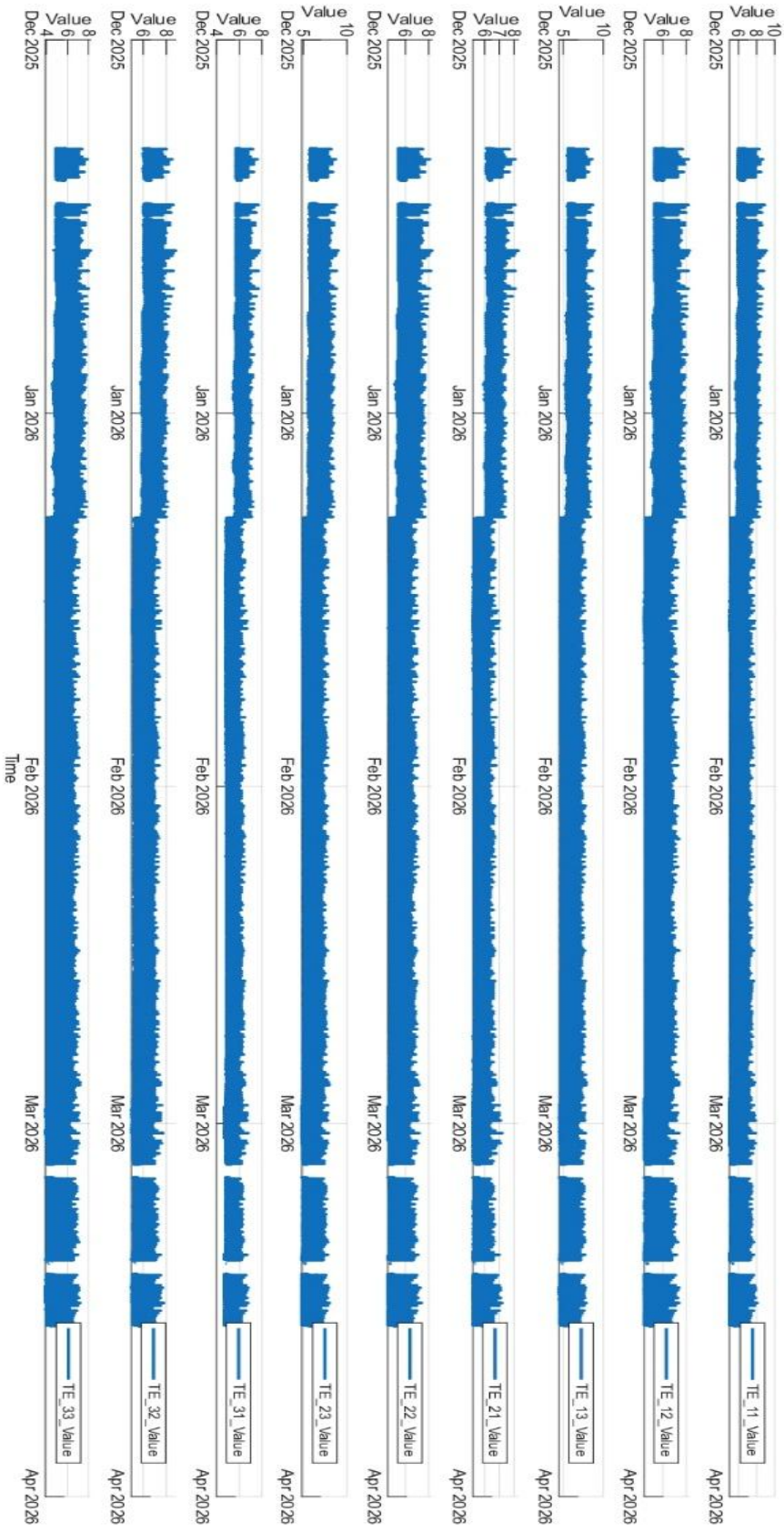

Figure 35. Incubation parameters: temperature in all incubators

Anions and Cations

This section presents the temporal and spatial evolution of major dissolved ions (Cl^-, SO_4^{2-}, Na^+, K^+, Mg^{2+}, and Ca^{2+}) measured throughout the incubation experiment using ion chromatography. In total, 576 samples were analyzed across 19 IC batches for their major anion and cation concentrations. The analysis includes both absolute concentrations and normalized ion ratios to better distinguish between physical transport effects (eg, dilution and flow variations) and geochemical processes occurring within the sandpacks. Particular emphasis is placed on chloride-normalized ratios (eg, Ca/Cl), as Cl^- behaves conservatively and provides a reliable reference for interpreting relative changes in solute composition. The results are evaluated across different sandpack positions and experimental phases, including changes in inlet fluid pH, to assess processes such as mineral dissolution and the overall geochemical response of the system under controlled acidification scenarios.

Concentrations Over the Experiment Period

Most ions showed an overall decreasing trend throughout the experiment. This decline is particularly pronounced in the early stages and gradually stabilizes during the first acidification scenario. In the second acidification scenario, beginning around day 116, most ions, including Cl^-, SO_4^{2-}, Na^+, and Mg^{2+}, show a renewed decline. This pattern is less evident for Ca^{2+} and K^+ due to irregular fluctuations and disturbances in their trends.

Certain anions, such as bromide (Br^- and NO_3^-), were not detected in all batches due to the high dilution factor.

Concentrations for Each Position Over the Experiment Period

Fig. 36 presents a comparison of the major anions (Cl^-, SO_4^{2-}) and cations (Na^+, K^+, Mg^{2+}, Ca^{2+}) across all sandpacks over time.

Overall, all ions illustrate a decreasing concentration trend in each sandpack. The decline is initially steep (showing flushing out of salts), followed by a more gradual decrease (first acidification scenario), and then a secondary increase in slope towards the end of the experiment (second acidification scenario). This latter change coincides with the reduction of inlet IAPSO pH from 7.4 to 6, indicating a strong geochemical response to acidification. Moreover, sediment-containing sandpacks show lower concentrations of most ions than control sandpacks, which is a sign of fluid-sediment interaction happening.

In addition, compared to other cations and even anions, K^+ and Ca^{2+} show unusual behavior, with irregular and hard-to-explain fluctuations. This may be due to limitations of the IC device in accurately measuring these ions.

The original (unrefined) version of Fig. 36 is provided in the *supplementary materials*. Short-term sharp drops observed across all ions and positions correspond to brief periods of unstable pump performance, which temporarily affected flow conditions and sampling consistency.

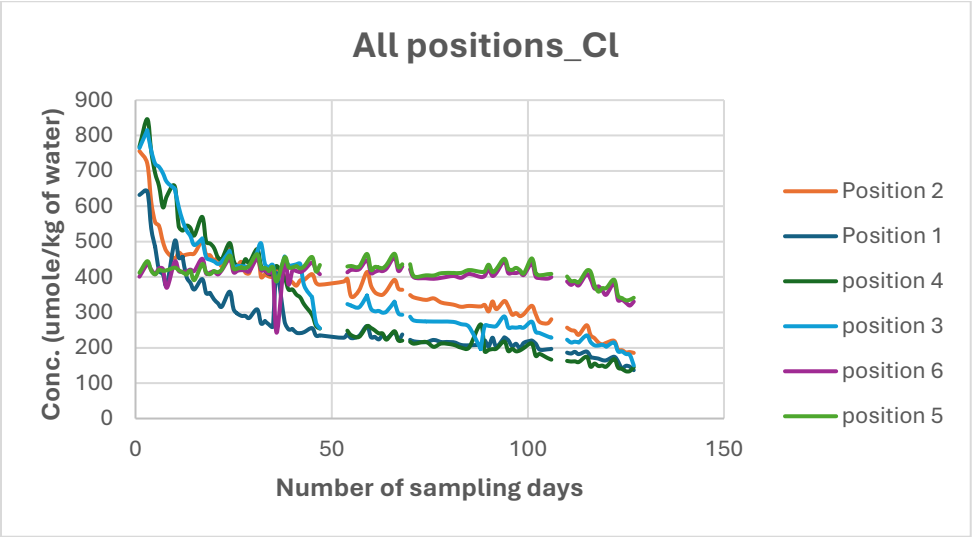

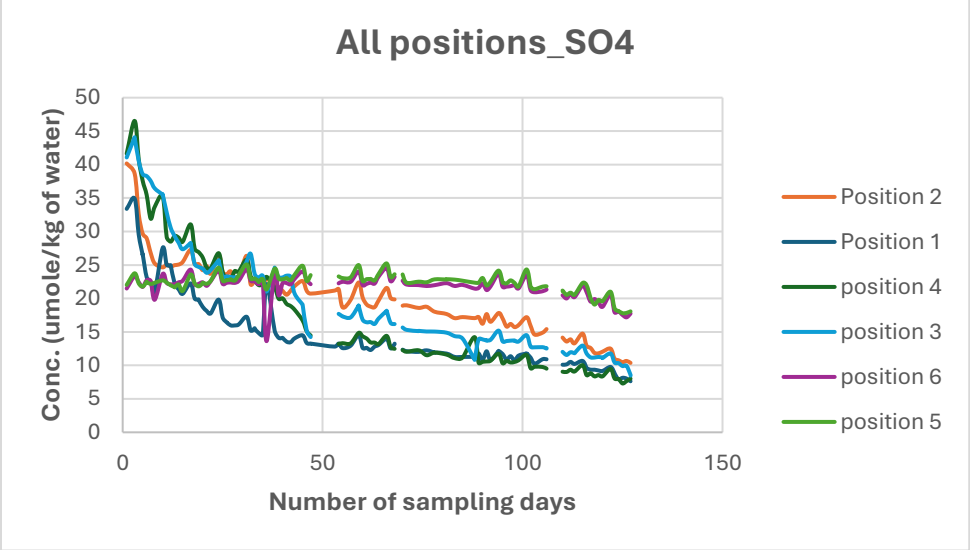

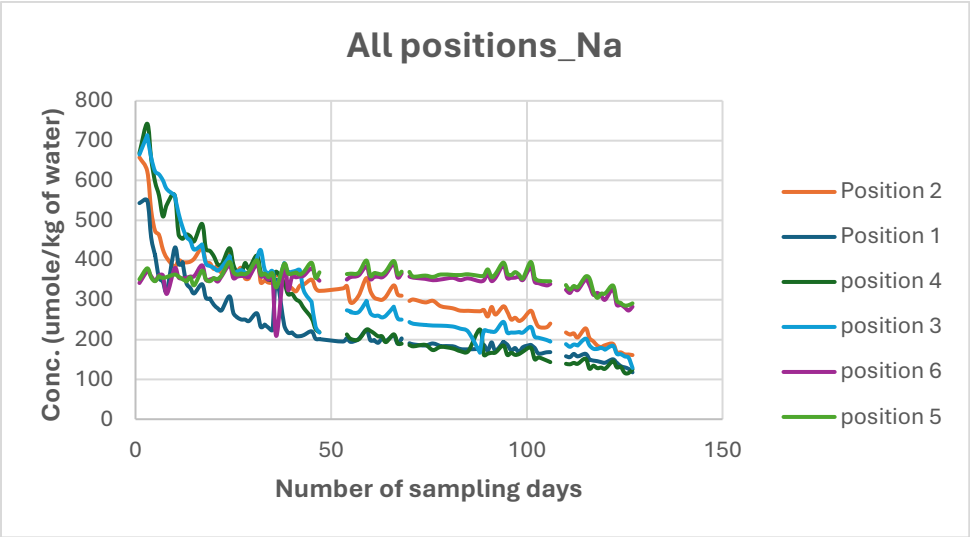
All positions_Na
Conc. (umole/kg of water)
800
700
600
500
400
300
200
100
0
0
50
100
150
Number of sampling days
Position 2
Position 1
position 4
position 3
position 6
position 5

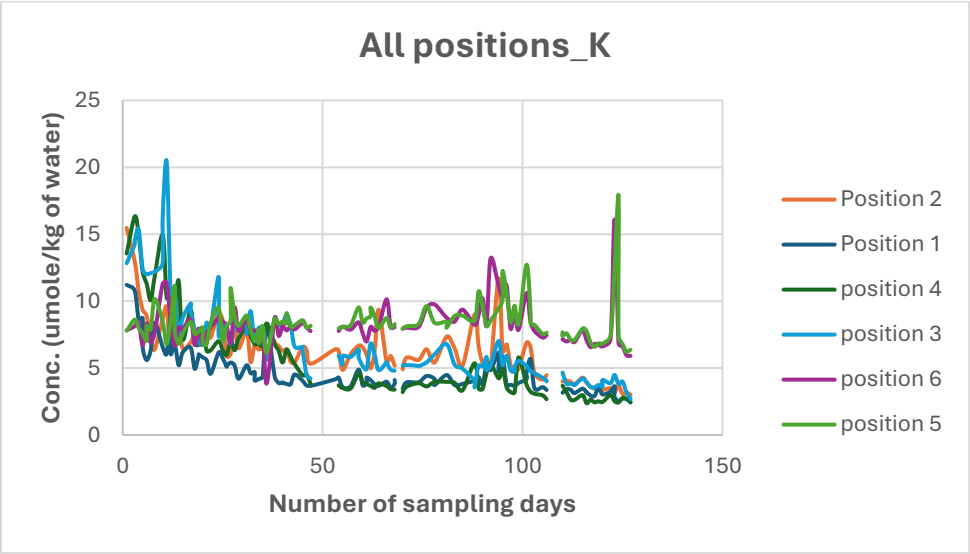
All positions_K
Conc. (umole/kg of water)
25
20
15
10
5
0
0
50
100
150
Number of sampling days
Position 2
Position 1
position 4
position 3
position 6
position 5

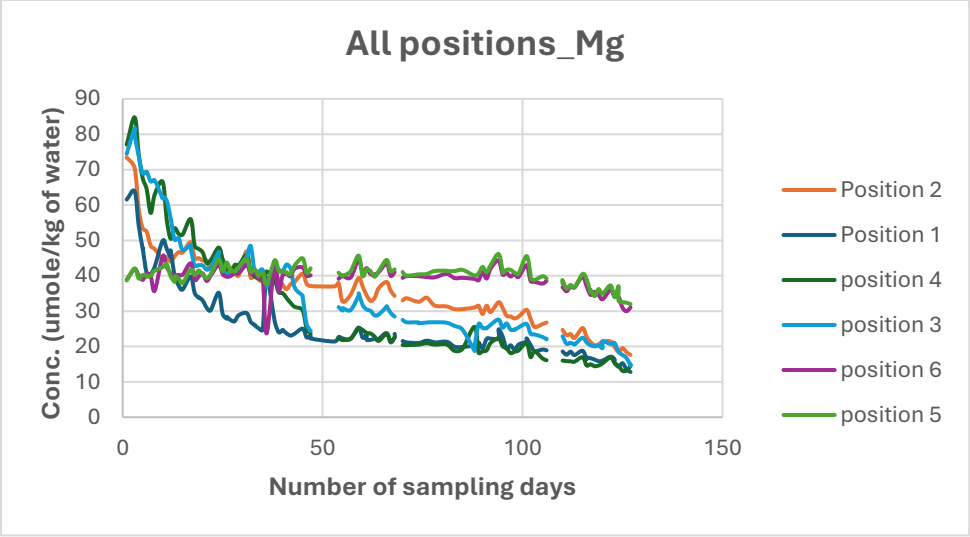
All positions_Mg
Conc. (umole/kg of water)
90
80
70
60
50
40
30
20
10
0
0
50
100
150
Number of sampling days
Position 2
Position 1
position 4
position 3
position 6
position 5

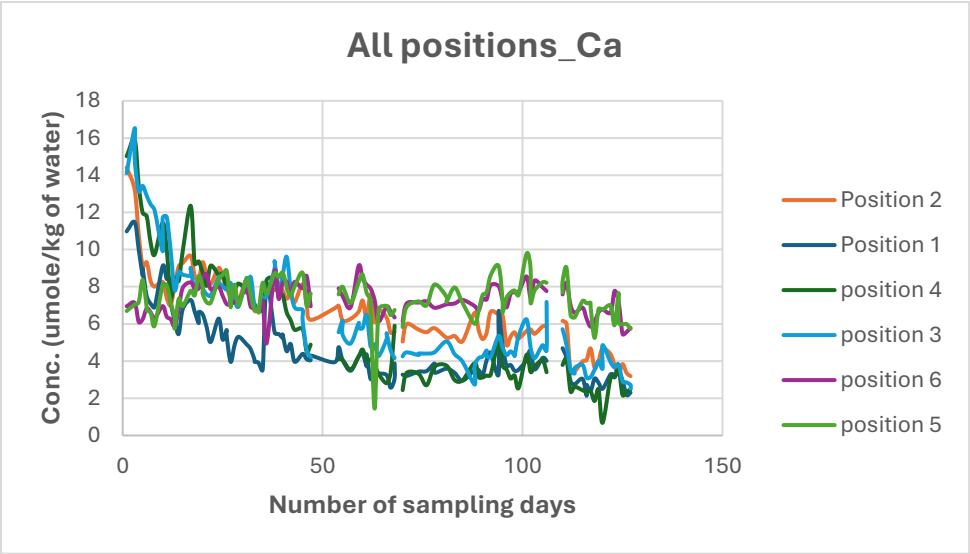

Figure 36. Ion concentrations by position over time

Normalizing the Results with Cl

Absolute ion concentrations alone do not provide a fully reliable basis for interpretation due to dilution effects and flow variations. Therefore, normalization against a conservative (inert) tracer is required. Chloride (Cl^-) was selected for this purpose, as it behaves conservatively in the system.

By expressing ion concentrations as ratios relative to chloride (eg, Ca/Cl), variations due to dilution are erased, allowing clearer identification of geochemical processes. Initial observations showed that such normalized ratios exhibit more stable and interpretable trends compared to raw concentration data.

Ion/Cl Ratio

The ion/Cl ratios for all major ions throughout the experiment are shown below (Fig. 37).

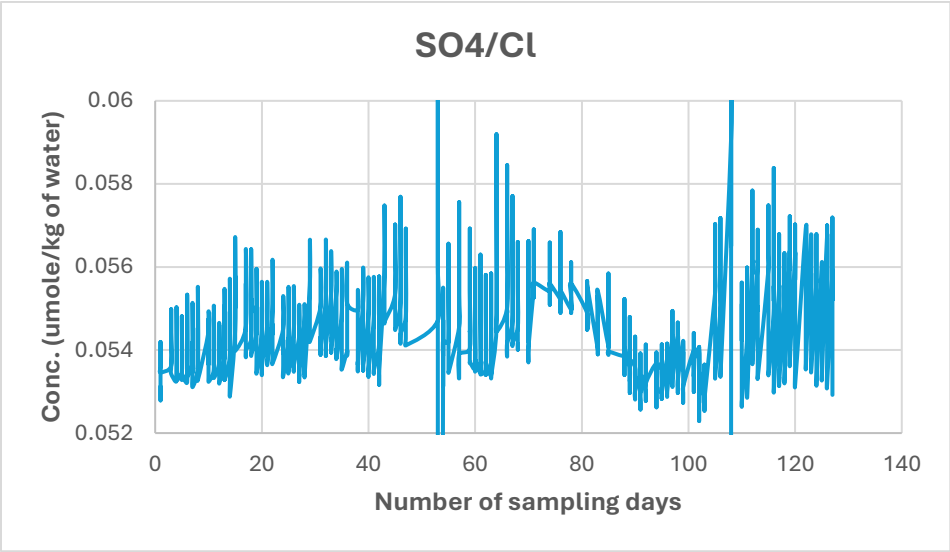
SO4/Cl
Conc. (umole/kg of water)
0.06
0.058
0.056
0.054
0.052
0
20
40
60
80
100
120
140
Number of sampling days

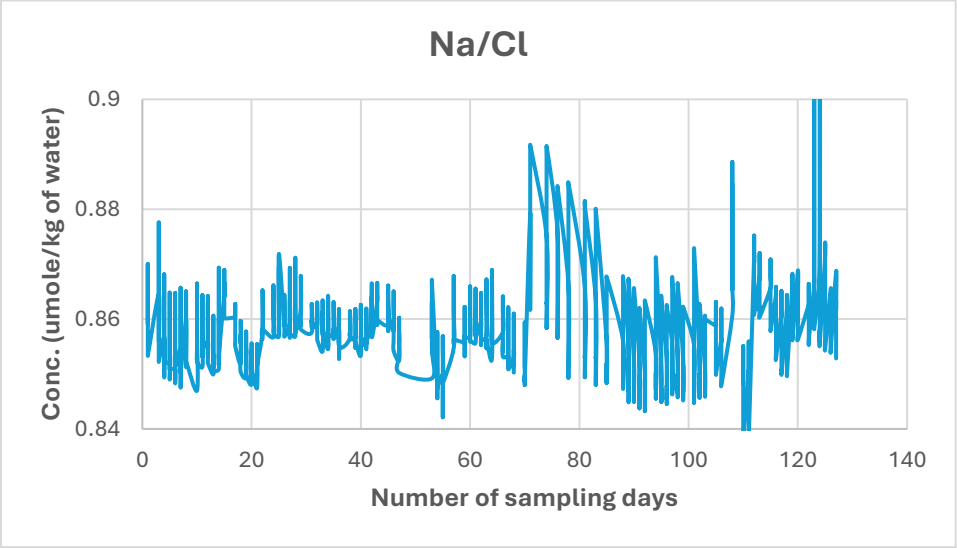
Na/Cl
Conc. (umole/kg of water)
0.9
0.88
0.86
0.84
0
20
40
60
80
100
120
140
Number of sampling days

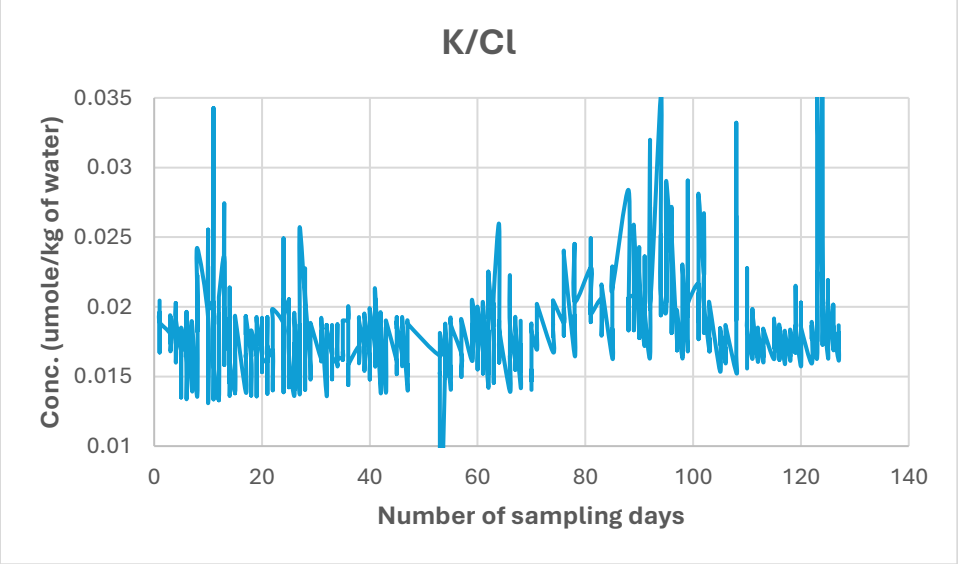
K/Cl
Conc. (umole/kg of water)
0.035
0.03
0.025
0.02
0.015
0.01
0
20
40
60
80
100
120
140
Number of sampling days

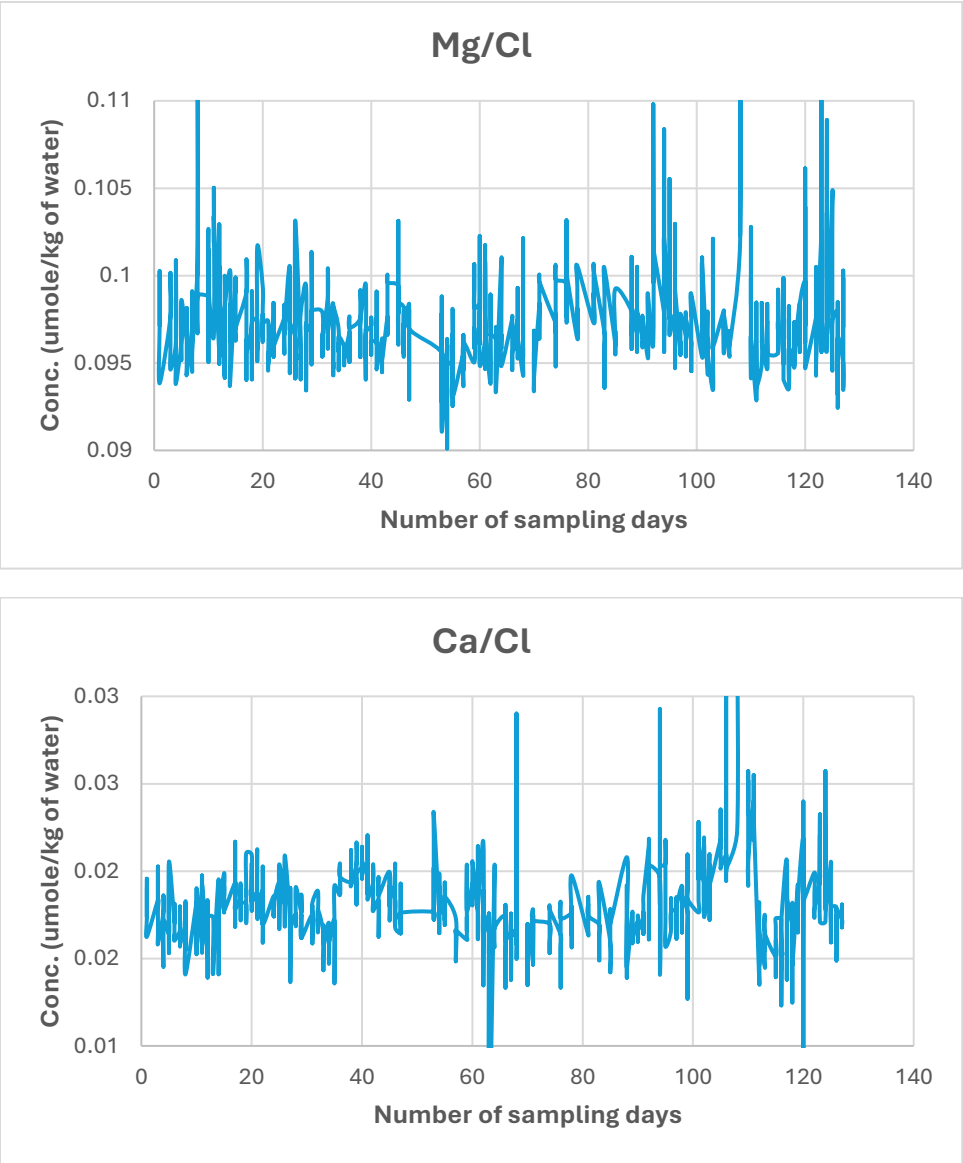

Figure 37. Ion/Cl^- ratios over the experimental period

Ca/Cl Ratio for Each Position

The Ca/Cl ratio is used as a key indicator of geochemical processes, particularly carbonate dissolution. Since Cl^- is assumed to be conservative, variations in the Ca/Cl ratio directly reflect changes in calcium concentration.

In the figures below (Fig. 38), sediment-containing sandpacks are compared with their corresponding seawater-filled control sandpacks to better isolate sediment-driven processes. Specifically:

- Upper sediment sandpacks (2 & 4) are compared with the upper control sandpack (6)

- Lower sediment sandpacks (1 & 3) are compared with the lower control sandpack (5)

This comparison provides a clearer understanding of system behavior than raw concentration plots alone.

The normalized results show significant fluctuations, so the overall trend is not very reliable. When a trendline is plotted for each sandpack, there seems to be a slight increase, but this cannot be trusted because the data varies so much.

There are a couple of possible reasons for this. First, the IC device may not be very precise when measuring calcium (Ca^{2+}). Second, there could be some contamination in the system, likely coming from the sandpack filters or non-acid-washed incubation sampling vials.

Another important point is that even the control sandpacks show similar fluctuations as the sediment sandpacks. This is unusual and raises the question of why Ca^{2+} concentration changes so much when there is no sediment present to interact with.

Finally, as it will be mentioned in the next section, Ca^{2+} showed one of the highest replicate errors (after K^{+}), which suggests that its measurements from the IC may not be very accurate. This also indicates that the IC is not sensitive enough to detect small changes in Ca^{2+}, whereas alkalinity measurements from the auto-titrator are more accurate and reliable.

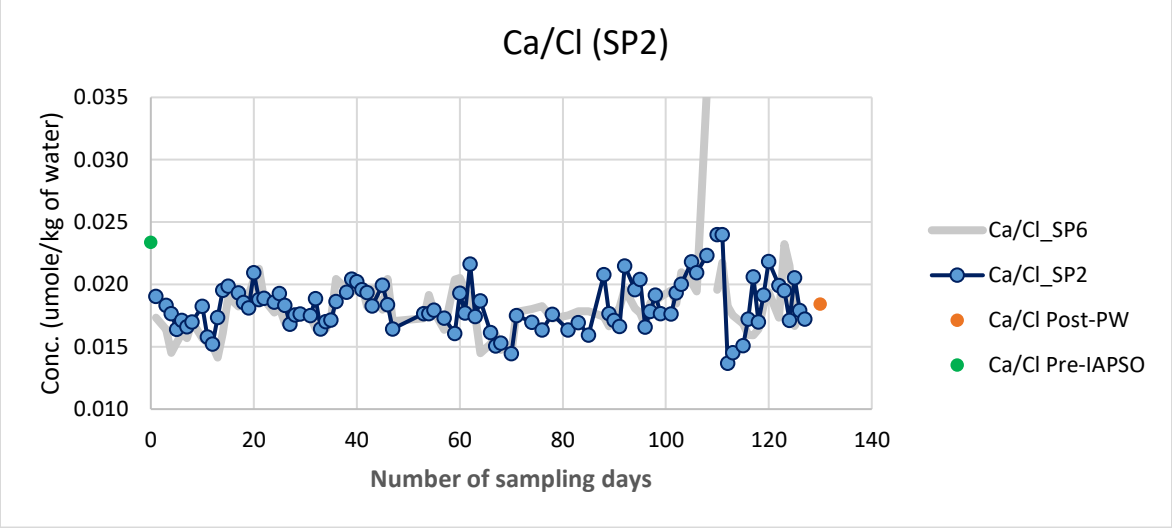

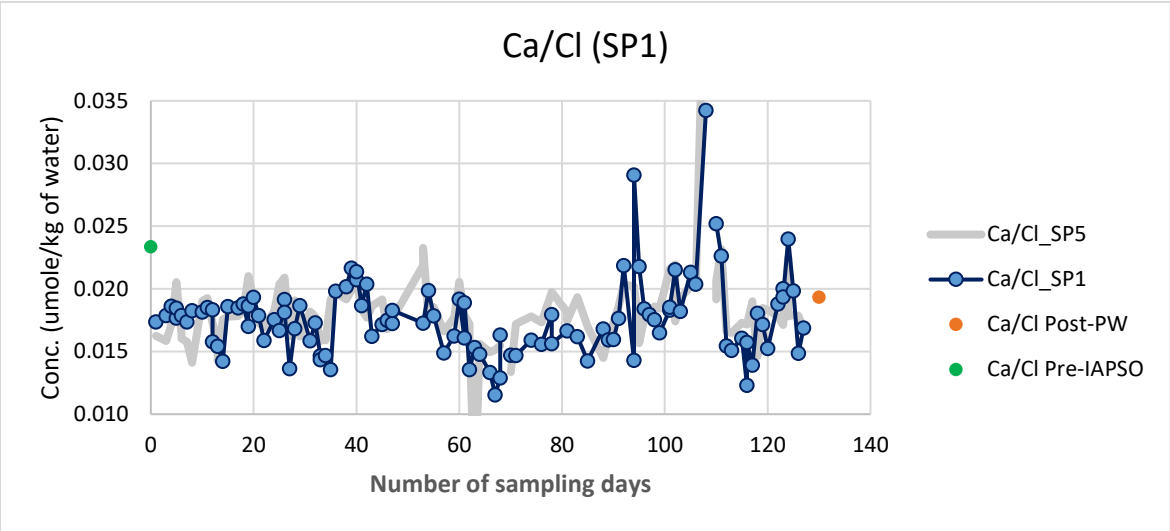

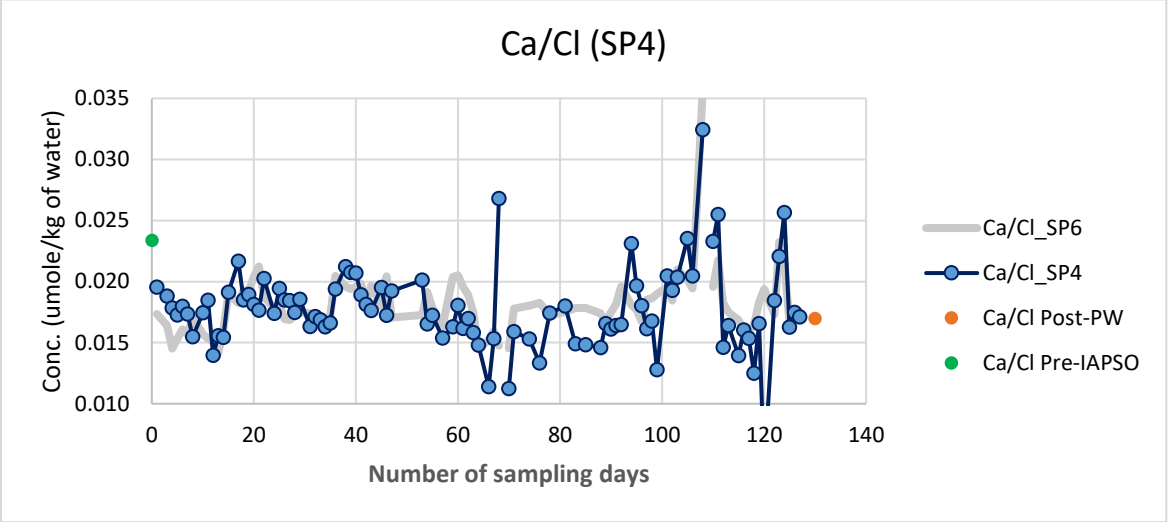

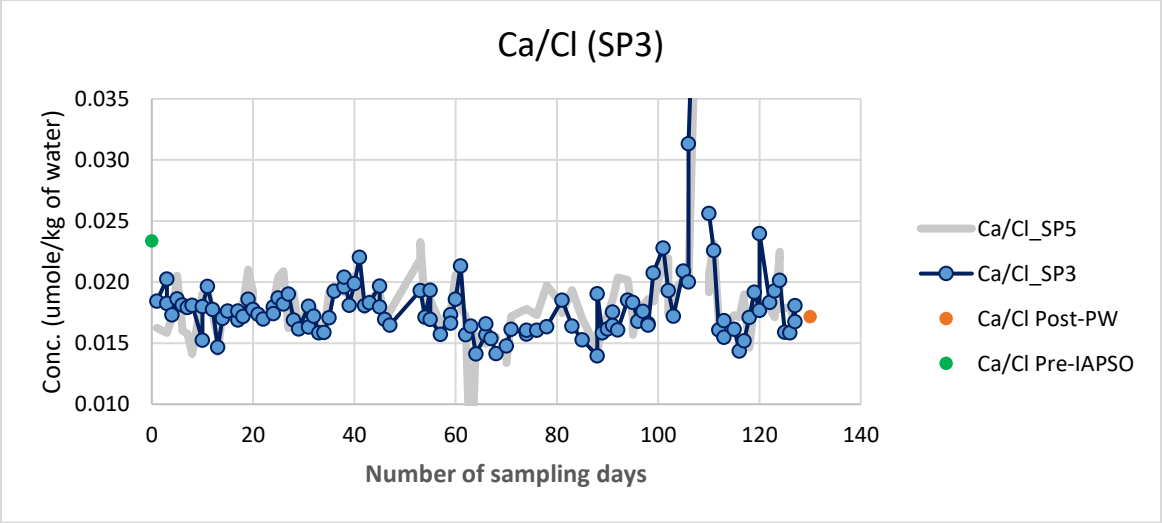

Figure 38. Ion/Cl⁻ ratios at different sampling positions throughout the experimental period, with the post-experiment porewater Ca/Cl ratio indicated by the orange point and the pre-experiment IAPSO Ca/Cl ratio shown by the green point.

IC Data Accuracy Results

As mentioned previously, replicates, control standards, and blanks were used to assess the accuracy of the analytical results.

Replicate Error

To ensure reliable concentration measurements, duplicate analyses (replicates) were performed for every 10 samples instead of a single run. For each pair of replicates, the average (Ave), standard deviation (SD), and coefficient of variation (CV) were calculated in Excel according to the following formula:

$$\text{CV (\%)} = \frac{\text{SD}}{\text{Average}} \times 100$$

The *Supplementary Materials* section contains a detailed table (Table 19) with concentrations of major anions and cations for each replicate, along with the calculated parameters (Ave, SD, CV) for each sample pair.

The CV reflects the relative dispersion of the data and provides insight into measurement precision and potential outliers. Based on the results, the majority of replicate measurements exhibited CV values below 10%, which is generally considered acceptable.

Fig. 39 illustrates the relationship between average concentration and standard deviation (SD) for each ion. Since CV is defined as the ratio of SD to the average value, these plots effectively represent the variation in CV and thus the relative dispersion of the data.

Replicates exhibiting a concentration difference greater than 0.5 $mmol/kg\ of\ water$ were reanalysed, and the updated values replaced the original data in the plots. It should be noted that this threshold is expressed in $mmol/kg\ of\ water$, with concentrations reported on a water-mass basis following an appropriate correction (dividing by 1.03, which is the density of seawater) to ensure consistency between solution and water mass units.

In total, 42 replicate pairs were analyzed across 19 batches. Among these:

- **Potassium (K):** 7 replicates exhibited CV values greater than 10% (i.e., 16.7% of replicates)
- **Calcium (Ca):** 4 replicates exceeded the 10% CV threshold (i.e., 9.5% of replicates)

These samples were subsequently remeasured. The results indicate that potassium measurements show relatively high uncertainty, while calcium measurements are somewhat variable and require careful handling.

To improve accuracy, calcium may be reanalyzed using an alternative method, such as ICP or with an adjusted dilution factor in IC. However, potassium data appear unreliable under the current conditions and should be interpreted with caution.

Apart from K (and to a lesser extent Ca), all other anion and cation measurements demonstrated good precision and can be considered reliable.

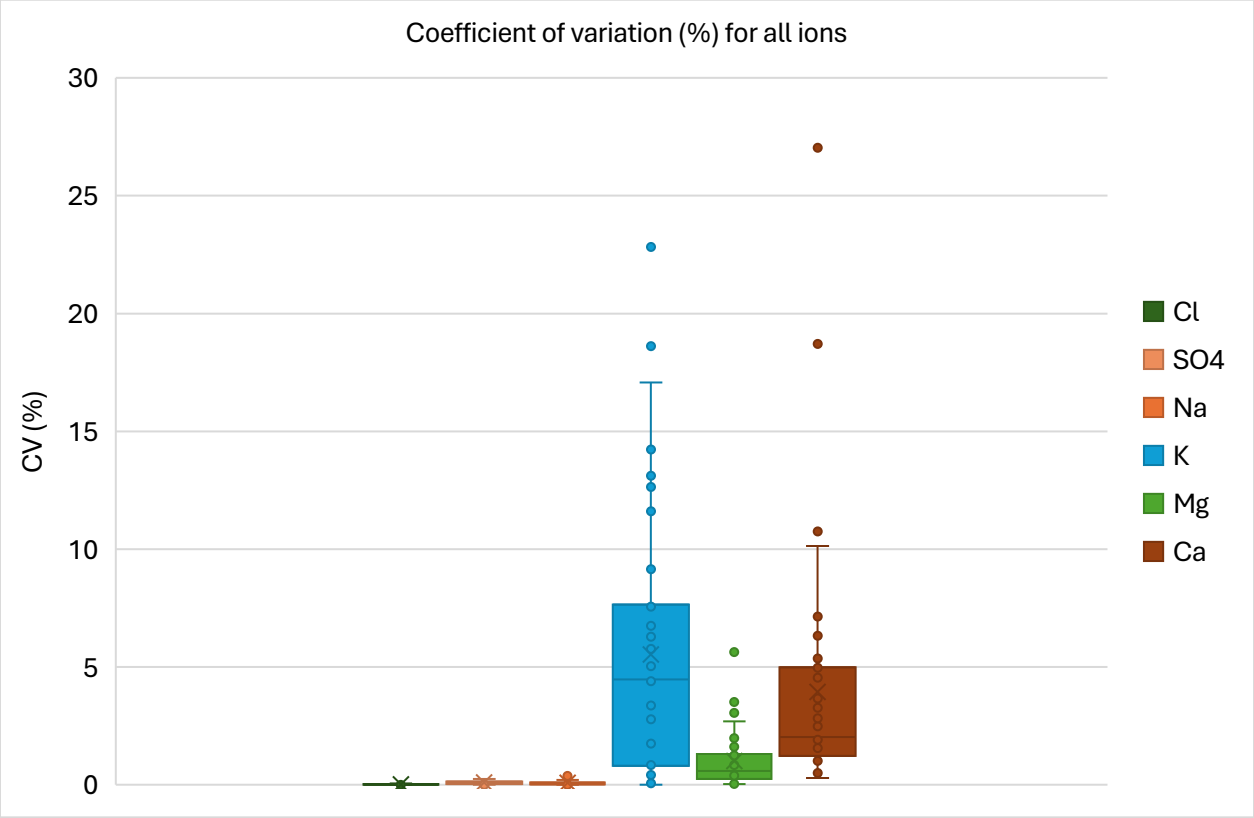

Figure 39. Coefficient of variation (CV) for each ion, indicating replicate error. Cl, SO_4, and Na have a CV<1%.

Control Standard Error

A thousand times dilution of the IAPSO standard was used as a control in every batch. Table 14 presents the concentrations of major cations and anions in each batch for IAPSOX1000, calculated using both linear and quadratic calibration methods. As is evident, the concentrations obtained from linear and quadratic calibrations are very similar, with only minor differences.

	Batch No.	Calibration	F	Cl	NO2	Br	NO3	PO4	SO4	Na	K	Mg	Ca
IAPSO (X1000)	1	Linear	0	552.599	0	0	0	0	28.662	468.11	10.751	53.033	12.484
		Quadratic	0	546.236	0	0	0	0	29.212	468.067	10.995	53.45	12.004
	2	Linear	0	552.656	0	0	0	0	28.628	468.251	13.433	53.435	13.338
		Quadratic	0	546.234	0	0	0	0	29.147	468.568	13.197	53.081	12.394
	3	Linear	0	545.567	0	0	0	0	28.691	468.244	10.357	52.795	12.237
		Quadratic	0	540.088	0	0	0	0	29.202	468.845	10.432	52.393	11.569
	4	Linear	0	549.998	0	0	0	0	28.658	468.863	10.72	52.403	13.428
		Quadratic	0	544.05	0	0	0	0	29.126	469.545	10.783	52.245	12.695
	5	Linear	0	549.482	0	0	0	0	28.87	469.889	11.194	53.23	13.298
		Quadratic	0	543.424	0	0	0	0	29.367	470.365	11.285	53.16	12.582
	6	Linear	0	550.618	0	0	0	0	28.73	469.725	10.66	52.294	12.587
		Quadratic	0	544.567	0	0	0	0	29.221	470.217	10.817	52.412	11.82
	7 & 8	Linear	0	547.593	0	0	1.241	0	28.9	470.407	10.398	53.312	12.523
		Quadratic	0	541.776	0	0	1.298	0	29.568	471.053	10.433	53.088	11.76
	9	Linear	0	552.125	0	0	1.258	0	28.78	469.101	10.608	52.119	12.646
		Quadratic	0	545.763	0	0	1.312	0	29.428	469.84	10.677	51.947	11.525
	10	Linear	0	548.033	0	0	1.247	0	28.888	470.525	10.41	51.989	12.625
		Quadratic	0	542.225	0	0	1.302	0	29.573	470.401	10.681	52.236	11.804
	11 & 12	Linear	0.736	547.787	0	0	0	0	28.958	469.817	10.212	52.516	12.276
		Quadratic	0.789	541.762	0	0	0	0	29.654	470.429	10.29	51.735	11.406
	13	Linear	0.707	551.81	0	0	1.117	0	28.817	465.617	10.456	52.137	12.784
		Quadratic	0.75	546.091	0	0	1.156	0	29.161	465.603	10.561	51.752	12.339
	14	Linear	0.741	552.721	0	0	0	0	28.2	464.195	10.441	52.104	12.605
		Quadratic	0.785	546.989	0	0	0	0	28.584	464.323	10.512	52.304	11.964
	15	Linear	0.674	552.154	0	0	0	0	28.477	464.944	10.933	51.806	12.936
		Quadratic	0.714	546.459	0	0	0	0	28.79	464.981	11.039	51.897	12.397
	16	Linear	0	547.879	0	0	1.4	0	28.39	464.849	10.237	52.275	12.632
		Quadratic	0	542.663	0	0	1.453	0	28.799	464.93	10.163	52.702	12.061
	17	Linear	0	547.033	0	0	1.363	0	28.4	469.827	10.145	51.983	12.854
		Quadratic	0	541.353	0	0	1.42	0	28.988	470.299	10.391	52.18	12.348
	18	Linear	0	551.076	0	0	1.347	0	28.561	470.437	12.552	52.42	12.314
		Quadratic	0	544.678	0	0	1.404	0	29.165	470.888	12.72	52.186	11.721
	19	Linear	0	551.787	0	0	1.368	0	28.614	469.638	10.242	52.205	12.52
		Quadratic	0	545.456	0	0	1.421	0	29.168	470.117	10.34	51.385	11.926

Table 14. Measured ion concentrations in the IAPSO (X1000) control standard across IC batches

The summary of the IAPSO measurements across all 19 batches, including average, standard deviation (SD), and coefficient of variation (CV), is presented in Table 15. For the calculation of these parameters, linear calibration results were used for cations, and quadratic calibration results were used for anions.

Parameter	F	Cl	NO3	SO4	Na	K	Mg	Ca
Average	0.938	576.251	1.346	30.879	495.728	11.452	55.521	13.472
SD	0.030	2.068	0.092	0.279	2.073	0.854	0.489	0.349
CV (%)	3.234	0.359	6.821	0.903	0.418	7.458	0.881	2.589

Table 15. Statistical parameters calculated for the IAPSO (X1000) control standard

The results indicate that CV values are very good for all ions. Notably:

- Potassium (K^+), like the sample replicates, shows relatively higher variability, suggesting that IC measurements of K are less precise.
- Nitrite (NO_2), Bromide (Br^-), and Phosphate ($PO4^{3-}$) are absent in IAPSO, so no meaningful CV can be calculated for them.
- Fluoride (F^-) and nitrate (${NO_3}^{2-}$) concentrations are negligible in all batches; therefore, their CV values are not reliable.
- Important anions consistently present across all batches are chloride (Cl^-) and sulfate (${SO_4}^{2-}$).

A CV below 5% is considered excellent, while a CV below 10% is acceptable. Based on the data:

- **Excellent CV (<5%)**: Cl (0.4%), SO4 (0.9%), Na (0.4%), Mg (0.9%), Ca (2.6%)
- **Good CV (<10%)**: K (7.5%)

Overall, the IAPSO control standard demonstrates excellent reproducibility for most major ions, with K^+ being the only ion showing moderate variability.

Blank Error

In each batch, two blanks were run, one at the beginning of the first set of standards and one at the beginning of the second set. Since the blanks consisted of Milli-Q water, no ions were expected to be present. However, a small calcium (Ca) peak was consistently observed in all blank chromatograms. To account for this, the measured blank Ca concentration was subtracted from the Ca concentrations in all samples to obtain the true Ca values.

The other ions did not show observable peaks in the blanks; however, magnesium (Mg) and Sodium (Na) occasionally exhibited a negligible signal that was too small to be considered in the calculations. For Mg, the blank error was < 0.3 mmol/kg of water, while for Na it was < 0.7 mmol/kg of water.

As linear calibration performed better for cations in the post-run analysis, since the second set of standards was used for calibration, the Ca concentration from the blank in the

second standard set (linear calibration) was subtracted from all Ca measurements in the incubation samples. The table below (Table 16) summarizes the blank Ca concentrations for each batch.

Batch No.	Calibration	Ca concentration in the blank (2nd set of standards) (mmol/kg of water)
1	Linear	2.343
	Quadratic	2.249
2	Linear	3.383
	Quadratic	3.134
3	Linear	2.141
	Quadratic	2.019
4	Linear	2.302
	Quadratic	2.17
5	Linear	2.22
	Quadratic	2.094
6	Linear	0.947
	Quadratic	0.886
7 & 8	Linear	1.756
	Quadratic	1.644
9	Linear	2.034
	Quadratic	1.846
10	Linear	1.708
	Quadratic	1.623
11 & 12	Linear	2.743
	Quadratic	2.54
13	Linear	2.819
	Quadratic	2.717
14	Linear	2.596
	Quadratic	2.458
15	Linear	2.247
	Quadratic	2.149
16	Linear	1.103
	Quadratic	1.05
17	Linear	2.247
	Quadratic	2.149
18	Linear	1.65
	Quadratic	1.567
19	Linear	1.708
	Quadratic	1.623

Table 16. Blank calcium (Ca) concentrations measured for each IC batch

Monitoring Milli-Q blanks allowed us to identify potential sources of contamination. Subsequent investigations indicated that the primary source of blank Ca was contamination from the IC vials, with approximately half of the observed Ca originating from factory-manufactured IC vials. Nevertheless, blank subtraction was applied to all samples regardless of the source of contamination.

Following this discovery, additional IC tests were performed to evaluate potential contamination from all containers and tools involved in sample handling, including incubation vials, IC vials, Falcon tubes, transfer pipettes, and standards, essentially all items that came into contact with the diluted samples. These tests further indicated that factory-manufactured Falcon tubes contributed measurable contamination, primarily from Ca and, to a lesser extent, NO_3^- and K. Therefore, Falcon tubes must be pre-treated prior to use, either by overnight rinsing with Milli-Q water or by acid washing, to minimize contamination during sample preparation and dilution.

pH and Total Alkalinity (TA)

pH and TA are fundamental parameters for understanding geochemical processes in aquatic systems, particularly in studies of ocean acidification and sediment–water interactions. While pH reflects the instantaneous acidity of the system, TA represents its buffering capacity against acidification. In this study, both parameters were monitored to evaluate how carbonate-rich sediments respond to controlled decreases in pH and how effectively they buffer the system over time.

To achieve this, continuous pH monitoring was combined with discrete TA measurements from samples collected across all sandpacks. This dual approach allows for a comprehensive assessment of both short-term chemical variability and long-term buffering processes within the incubation system.

pH Sensor Measurements

The pH sensor, embedded in the second incubator, continuously recorded pH values at 30-second intervals throughout the experiment. Prior to the start of sampling, the sensor was carefully calibrated to ensure measurement accuracy. Due to the high temporal resolution and the resulting large dataset, a customized MATLAB routine was used to process and visualize the data.

The resulting pH plot (Fig. 40) illustrates the temporal evolution of pH over the course of the experiment. It captures both the imposed acidification scenarios and the system's response.

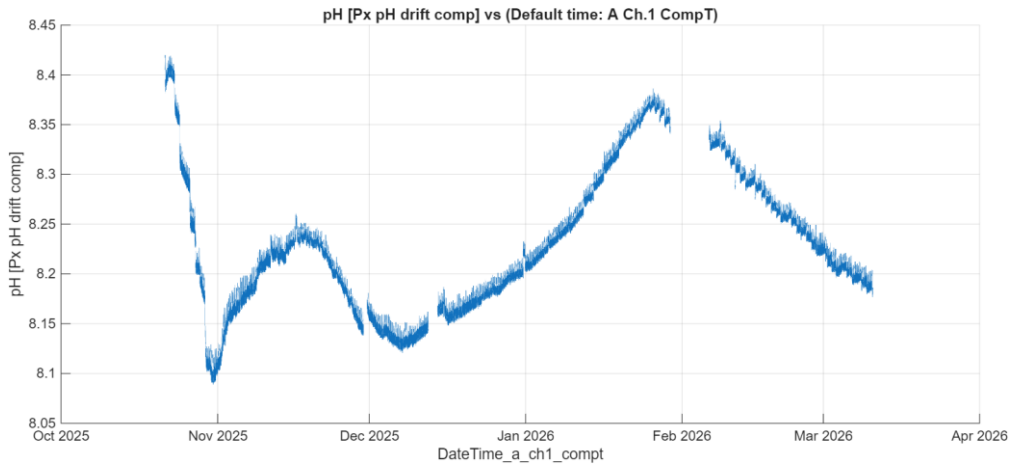

Figure 40. pH measurements over the experimental period

Auto-Titrator TA Measurements

For TA determination, some samples from each sampling position were analyzed using an auto-titrator. To ensure analytical reliability, 40 IAPSO control standards (X50 dilution) were measured at the beginning, middle, and end of batches. The average normalized alkalinity value obtained was 0.00708 meq/l, with a standard deviation of 0.0002 and a coefficient of variation (CV) of 3.1477%, indicating high precision and reproducibility.

The TA results (Fig. 41) show distinct differences between sediment-containing and control sandpacks. The sediment-containing sandpacks display a gradual increase in TA over time, whereas the control sandpacks remain comparatively stable, indicating limited geochemical interaction. This contrast highlights the role of active water–sediment interactions in driving alkalinity changes within the sediment-filled ones.

However, after approximately day 120, the trends in the control sandpacks begin to diverge, suggesting the presence of anomalies within the system. The underlying causes of these deviations remain unclear but may be linked to experimental factors such as pressure instability or other operational fluctuations. These disturbances could also explain the occurrence of outliers observed in the sediment-containing sandpacks (SP1 and SP2). A small number of outliers were identified, likely arising from sampling or instrumental variability, and were excluded from the analysis as they do not align with the overall trends. In Fig. 41, arrows mark these omitted values, with their corresponding measurements indicated.

Despite the lowered pH conditions, the continued increase in TA indicates that the system is persistently adjusting to the imposed acidic input. This response reflects ongoing geochemical buffering processes, suggesting that sediment–water interactions remain active and responsive under acidified conditions.

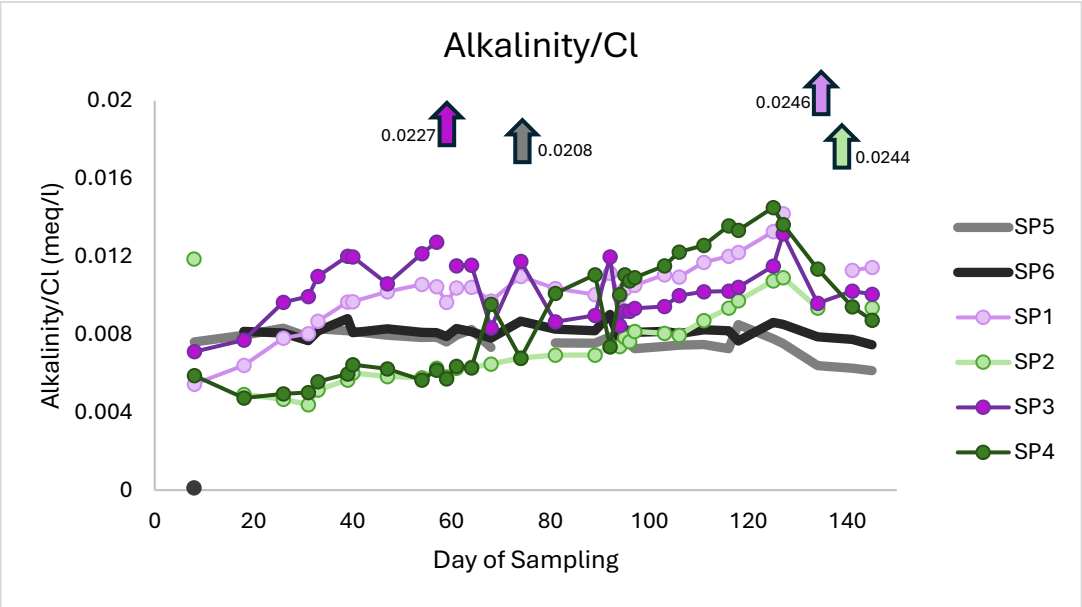

Figure 41. Total alkalinity/Chloride trends in sandpacks

Sediment Analysis Results Before and After the Incubation Experiment

Sediment samples from the three cores collected during the GEOEO2024 Expedition were analyzed to determine their geochemical composition and mineralogical characteristics prior to the incubation experiments. The analyses included carbon and nitrogen measurements, mineralogical characterization, and microscopic observations.

Pre-Experiment Sediment

Carbon and Nitrogen (C/N) Results

All three sediment cores were analyzed for their carbon-to-nitrogen (C/N) ratios. The results indicated relatively high carbon contents within the samples, suggesting the presence of substantial amounts of carbonate minerals. This observation was supported during the preparation of samples for total organic carbon (TOC) analysis, where the addition of acid produced vigorous gas release, consistent with carbonate dissolution.

Among the three investigated cores, core MC-38 exhibited the highest carbonate content according to measurements obtained using the *elemental analyzer (EA)*. Based on these results, this core was selected as the primary sediment source for the incubation experiments. The relationship between the C/N ratio and sediment depth is illustrated in Fig. 42.

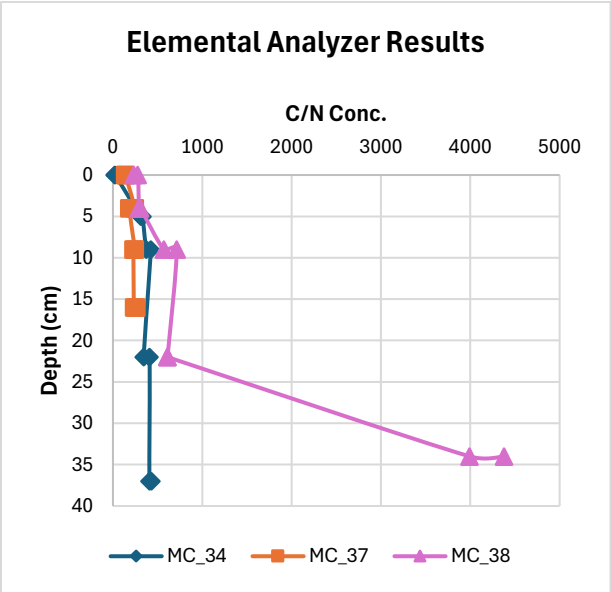

Figure 42. Carbon and nitrogen (C/N) results measured by the elemental analyzer (EA)

Total Carbon, Total Nitrogen, and Total Organic Carbon

Measurements of total carbon (TC), total nitrogen (TN), and total organic carbon (TOC) were performed using an isotope ratio mass spectrometry system. Prior to TOC analysis, carbonate removal was required to isolate the organic carbon fraction.

To remove carbonate minerals, 10 *g* of sediment was treated with 10% *Hydrochloric acid* (HCl). Under normal conditions, approximately 100µL of acid is sufficient for this procedure. However, because the sediments contained a high concentration of carbonates, the acid was added gradually in two stages to control the intense gas release that occurred during the reaction.

The procedure involved the following steps:

1. Addition of 50µL of 10% HCl to the sample.
2. Drying of the sample in an oven for approximately 1 hour.
3. Addition of another 50µL of acid.
4. Overnight drying in the oven to ensure complete removal of carbonates.

After the acid treatment and drying steps were completed, the samples were analyzed for TOC using the analytical instrument (IRMS). Results are shown in Fig. 43.

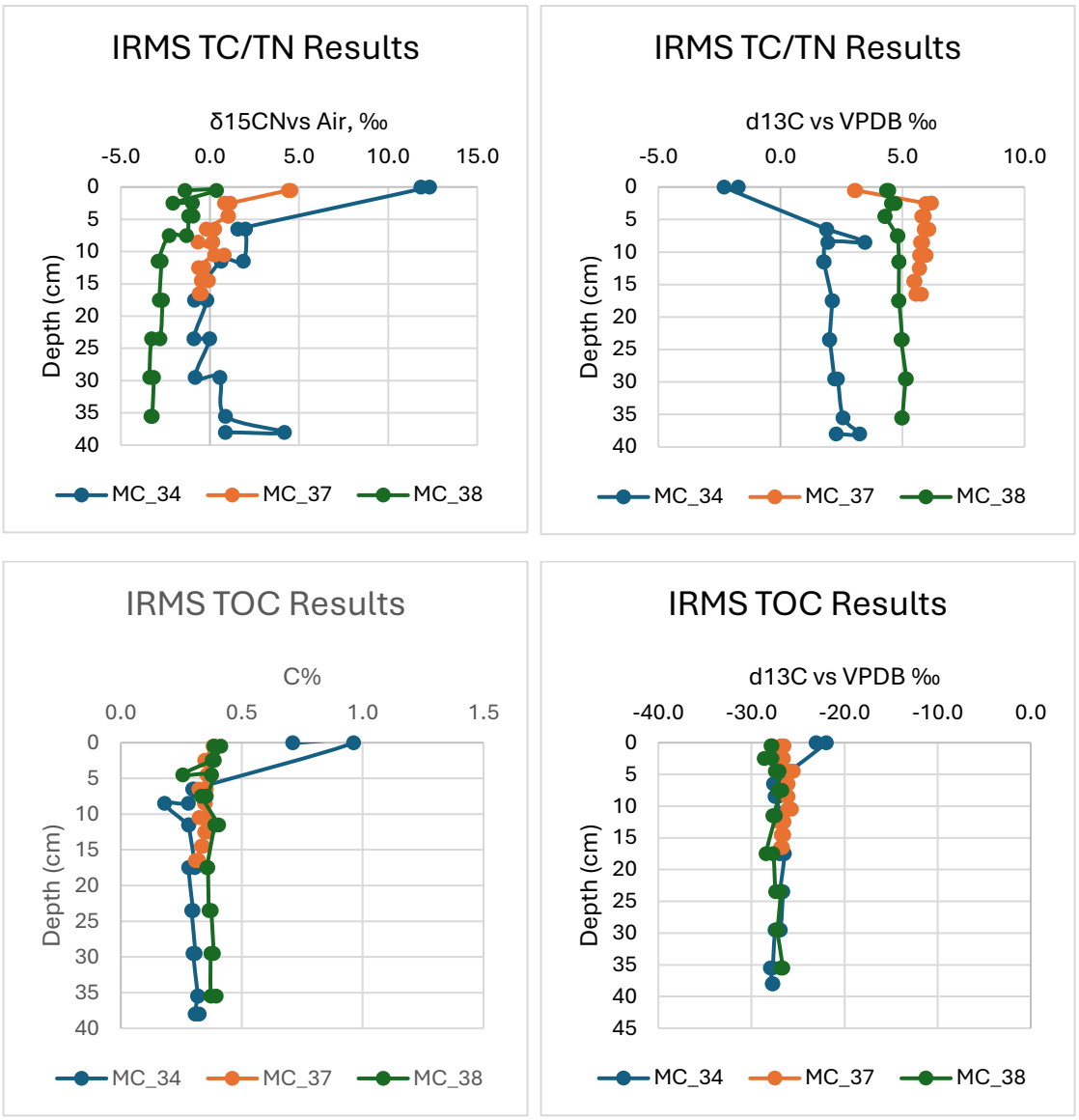

Figure 43. Total carbon, total nitrogen, and total organic carbon results measured by IRMS

Mineralogical Composition (XRD Results)

The mineralogical composition of core MC-38 was investigated using X-ray diffraction (XRD) at two depth intervals: the surface layer (5–6 cm) and a deeper interval (37–40 cm) (Table 17). The results indicate that the sediments comprise a mixture of silicate and carbonate minerals, including quartz, feldspars, clay minerals, amphibole, and carbonates such as calcite and dolomite.

Calcite and dolomite were particularly abundant, consistent with the high carbonate content identified in the carbon analysis. Overall, the mineral assemblages were relatively similar between the surface and deeper layers, although some variation in carbonate abundance was observed, with slightly higher carbonate content at depth.

These results provide important insight into the buffering capacity of the sediments. Both carbonate and silicate minerals are present, but carbonate minerals (calcite and dolomite) constitute a major fraction of the sediment. In both depth intervals, calcite and dolomite together often exceed the abundance of individual silicate phases such as quartz, feldspars, and clay minerals, indicating that carbonates are the dominant reactive component.

The high abundance of calcite and dolomite suggests a strong buffering capacity against pH changes. These carbonate minerals readily dissolve under acidic conditions, releasing carbonate species that help neutralize acidity and stabilize pH. The consistent presence of these minerals throughout the core indicates that buffering potential is strong across both surface and deeper sediments, with deeper layers potentially exhibiting slightly enhanced buffering due to higher carbonate content (Bibi et al., 2026; Cetiner et al., 2025; Sulpis et al., 2021).

In contrast, the silicate minerals, quartz, feldspars, and clay minerals, contribute less to short-term buffering due to their slower weathering rates. Although present in notable amounts, silicates are distributed across multiple mineral phases rather than concentrated in a highly reactive form like carbonates. Because silica was not directly measured in this study, the role of silicate weathering is inferred from established geochemical knowledge rather than experimental observations (Brantley et al., 2023; Trapp-Müller et al., 2025).

In summary, the mineralogical composition indicates that carbonate minerals might be the primary control on sediment buffering capacity, while silicate minerals would play a secondary, longer-term role. All reported abundances are expressed as weight percentages (wt%).

Sample	Albite	Amphibole	Anorthite	Calcite	Chlorite	Dolomite	Halite	Illite	Muscovite	Orthoclase	Quartz
38MC 5-10cm (Tiwan)	9.1	10.9	6.5	17.3	6.8	19.2	3.6	1.9	1.9	8.2	14.7
38MC 15-20cm (Tiwan)	11	4.2	3.3	23.4	5.3	19.7	3.3	1.6	2.8	8.6	16.7
38MC 35-40cm (Tiwan)	6.2	10.5	10.3	24.5	2.4	24.5	2.2	0.4	3.1	2.6	13.1
GE24-38-MC a (5-6cm) (wt%) (Estonia)	8.5 (Plagioclase)	1.9	8.5 (Plagioclase)	19	4.6	19.5	3.2	12.6 (Mica+illite+illite-smectite)		15.6	14.3
GE24-38-MC b (37-40cm) (wt%) (Estonia)	7.2 (Plagioclase)	1.6	7.2 (Plagioclase)	26.9	4	22.9	1.7	10.1 (Mica+illite+illite-smectite)		12.5	12.2

Table 17. X-ray diffraction (XRD) results for the incubated sediment core MC-38 (before the experiment)

Scanning Electron Microscopy (SEM) Observations

Scanning electron microscopy was used to investigate the morphology and elemental composition of sediment particles. Observations included both terrestrial sediment samples and materials derived from the water column or sea ice (Fig. 44).

Terrestrial Sediment Samples

Several terrestrial sediment samples were examined:

T16

This sample displayed strong biogenic characteristics, suggesting the presence of biologically derived siliceous particles.

T18

The sample contained high concentrations of Si, Al, and Mg, together with smaller amounts of Fe, Ca, and Na. The dominance of Si and Al suggests a mineral assemblage rich in aluminosilicate minerals, likely associated with clay minerals or feldspars. The particles showed a crushed texture, and the overall morphology indicated a predominantly non-biogenic origin, although some elongated particles were observed.

T19

This sample contained abundant biogenic structures, including elongated silicate particles resembling diatom fragments and spherical bodies resembling spore-like particles.

T20

The sample showed high concentrations of Si and Al, with aluminum occurring at approximately twice the concentration of magnesium. This again suggests the dominance of aluminosilicate minerals, with some contribution from magnesium silicates. The particles were cohesive and fragmented, indicating possible physical weathering processes. Quartz grains were also identified, and some areas appeared cemented, indicating locally compacted material.

T23

This sample also exhibited biogenic characteristics, including elongated siliceous particles and spherical microstructures. The sediment particles appeared dispersed and fragmented.

Fjord Sediment

The fjord sediment sample contained predominantly silicate particles, with high concentrations of Si, O, and Al. Minor amounts of Ca, Mg, and K were also detected, along with trace amounts of Fe and Cl. Biogenic particles were rare or sparsely distributed.

Water Column and Ice-Associated Samples

Additional samples derived from the water column and ice environments were also analyzed.

W78 (Water Column Sample)

This sample was highly dispersed and dominated by Si and O, indicating the presence of silicate particles. Minor amounts of Na and Cl were detected, likely representing seawater salt residues. Trace levels of Mg and Al were also observed.

Sea Ice Sample

The sea ice sample contained abundant biogenic particles, including numerous spherical bodies and siliceous structures. Elemental analysis showed high concentrations of Si and O, with significant amounts of Al and Mg, and smaller amounts of K and Fe.

Dust in Ice

The dust sample displayed more fragmented and crushed particles than the sea ice sample. The elemental composition depicted high concentrations of Si and O, together with elevated Al and K. Moderate amounts of Fe were also present. Compared with the other samples, the dust particles showed a particularly high aluminum content.

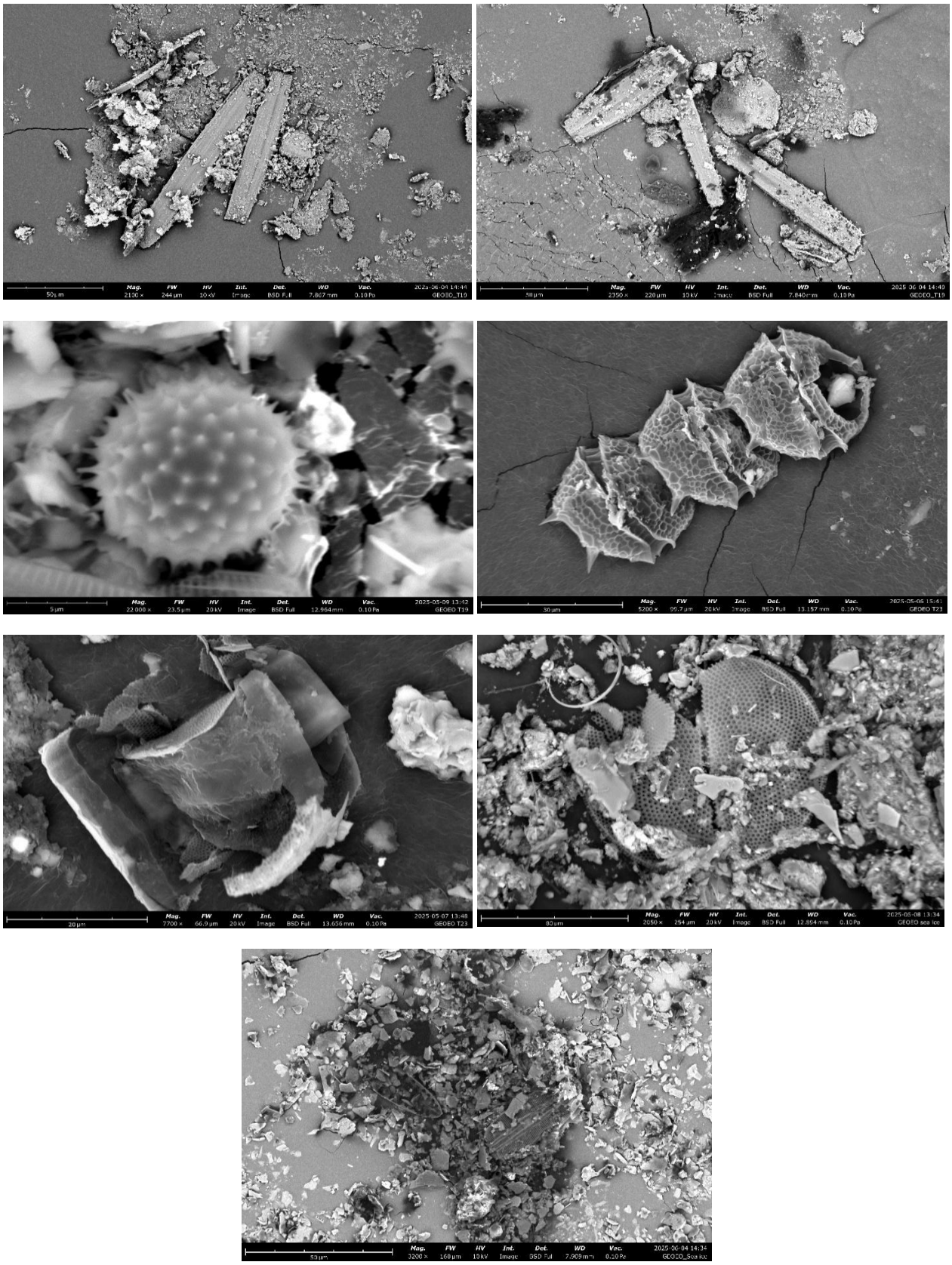

Figure 44. SEM images of terrestrial, water column, and ice-associated samples

Post-experiment sediment

Post-Sediment Pore Water Analysis

As described in Table 12 in the section *Post-Experiment Sediment Processing and Pore Water Extraction*, selected pore water (PW) samples were collected for IC analysis. The results are presented as Ca/Cl ratios for each sampling position in Fig. 38, while the ratios of the remaining ions relative to Cl are provided in the *Supplementary Materials* section.

Mineralogical Composition (XRD Results)

In the XRD analysis, LS (lower sandpack) and US (upper sandpack) represent incubated sediments from incubator 1, while MC-38 corresponds to samples of the unincubated sediment (Fig. 45). The results show no significant change in carbonate mineral content before and after the experiment, but decrease in abundance of Ca-bearing silicate minerals. Especially, *anorthite* and *amphibole* are depleted in the lower sandpack relative to both the upper sandpack and the unincubated sediment (Fig. 45 and Table 18). This pattern indicates that silicate mineral dissolution, rather than carbonates, buffers the induced acidification in this experiment.

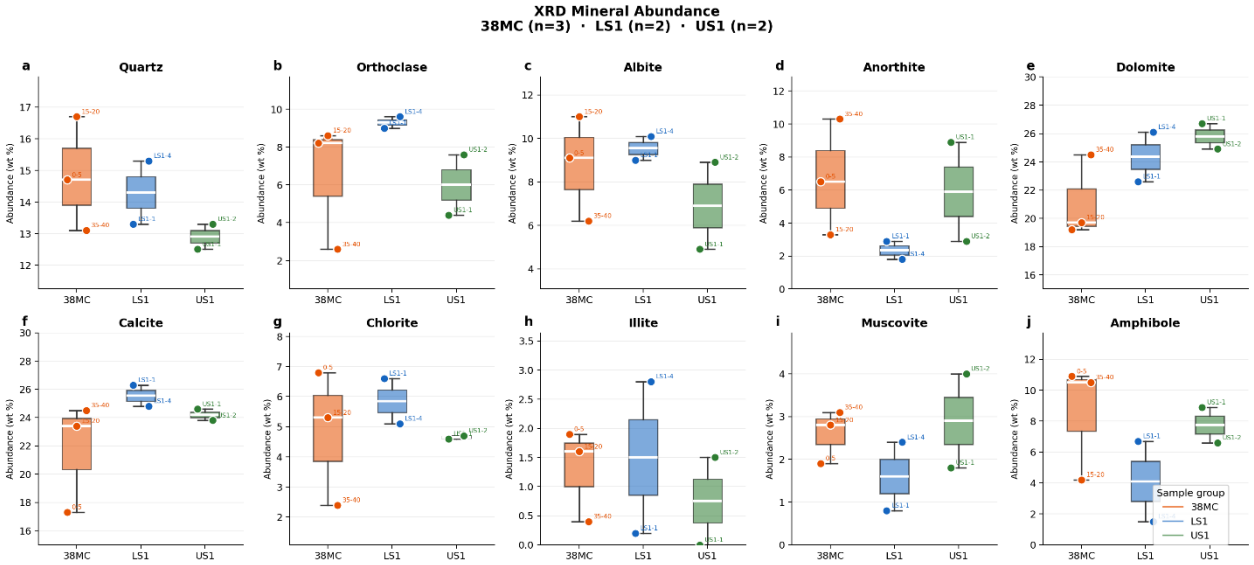

Figure 45. XRD mineral abundance (after the experiment)

Sample	Albite	Amphibole	Anorthite	Calcite	Chlorite	Dolomite	Halite	Illite	Muscovite	Orthoclase	Quartz
Sp1-1 (Tiwan)	9	6.7	2.9	26.3	6.6	22.6	2.5	0.2	0.8	9	13.3
Sp1-4 (Tiwan)	10.1	1.5	1.8	24.8	5.1	26.1	0.5	2.8	2.4	9.6	15.3
Sp2-1 (Tiwan)	4.9	8.9	8.9	24.6	4.6	26.7	2.7	0	1.8	4.4	12.5
Sp2-2 (Tiwan)	8.9	6.6	2.9	23.8	4.7	24.9	1.9	1.5	4	7.6	13.3
38MC 5-10cm (Tiwan)	9.1	10.9	6.5	17.3	6.8	19.2	3.6	1.9	1.9	8.2	14.7
38MC 15-20cm (Tiwan)	11	4.2	3.3	23.4	5.3	19.7	3.3	1.6	2.8	8.6	16.7
38MC 35-40cm (Tiwan)	6.2	10.5	10.3	24.5	2.4	24.5	2.2	0.4	3.1	2.6	13.1
GE24-38-MC a (5-6cm) (wt%) (Estonia)	8.5 (Plagioclase)	1.9	8.5 (Plagioclase)	19	4.6	19.5	3.2	12.6 (Mica+illite+illite-smectite)		15.6	14.3
GE24-38-MC b (37-40cm) (wt%) (Estonia)	7.2 (Plagioclase)	1.6	7.2 (Plagioclase)	26.9	4	22.9	1.7	10.1 (Mica+illite+illite-smectite)		12.5	12.2

Table 18. X-ray diffraction (XRD) results for the incubated sediment core MC-38 (after the experiment)

Discussions and Conclusion

In the thesis, I show that sediments from Petermann Fjord have high potential to buffer ocean pH even under foreseeable future ocean acidification.

pH and TA are closely linked through the carbonate system, but they represent fundamentally different aspects of aqueous chemistry. pH reflects the concentration of hydrogen ions (H^+), while alkalinity represents the system's capacity to neutralize acids, primarily controlled by carbonate species such as bicarbonate (HCO_3^-) and carbonate (CO_3^{2-}) (Middelburg et al., 2024). The buffering capacity of the system can be defined as the total quantity of cations released (not limited to Ca), expressed as:

$$\beta = \frac{dC}{d(pH)}$$

where β is the buffering capacity, dC is the amount of acid or base added, and $d(pH)$ is the resulting change in pH. This relationship shows that systems with higher alkalinity exhibit greater resistance to pH fluctuations.

Within carbonate systems, this relationship is controlled by equilibrium reactions such as (Lerman & Mackenzie, 2018):

$$CO_2 + H_2O \rightarrow H_2CO_3 \rightarrow HCO_3^- + H^+$$

$$CaCO_3 + CO_2 + H_2O \rightarrow Ca^{2+} + 2HCO_3^-$$

As CO_2 increases, pH decreases due to the formation of H^+ ions. At the same time, the dissolution of carbonate minerals such as calcite and dolomite generates bicarbonate, which increases alkalinity and enhances the buffering of the system.

In this study, controlled acidification of IAPSO seawater simulated ocean acidification conditions. The continuous pH measurements show the imposed decrease in pH, while TA data reveal the system's buffering response (van de Velde et al., 2025). This increase in TA acts as a feedback mechanism, buffering the system and moderating further pH changes (Renforth & Henderson, 2017).

The combined analysis of pH and TA demonstrates that ocean acidification conditions were successfully reproduced under controlled laboratory settings. pH served as the primary controlled variable, while TA reflected the system's geochemical response.

As is observable in Fig. 46, the highest TA values in incubator 1 were observed in the bottom sandpack (SP1), where freshly acidified fluid first enters the system. At this stage, the fluid is most chemically reactive, promoting intense carbonate/silicate dissolution and rapid alkalinity generation. As the fluid moves upwards through the system, it becomes progressively buffered, reducing its reactivity and limiting further carbonate/silicate dissolution. Consequently, the upper sandpack (SP2) exhibits lower TA values, in some cases approaching those of the control sandpacks. This demonstrates that buffering is not uniform but dynamically controlled by flow-driven reaction history (Amiri et al., 2026).

In incubator 2 (Fig. 46), the trend initially mirrors that of incubator 1 up to the midpoint of the experiment. However, a notable shift occurs afterwards: the upper and lower sandpacks appear to reverse roles, with the upper sandpack exhibiting higher TA values and the lower showing reduced TA. The underlying cause of this reversal is uncertain. It may be related to sediment heterogeneity, possibly due to fractures observed in the sandpacks upon post-experimental inspection. As this behavior is not observed in incubator 1, it is unlikely to be driven by system-wide factors such as pressure instability or other parameters common to both incubators.

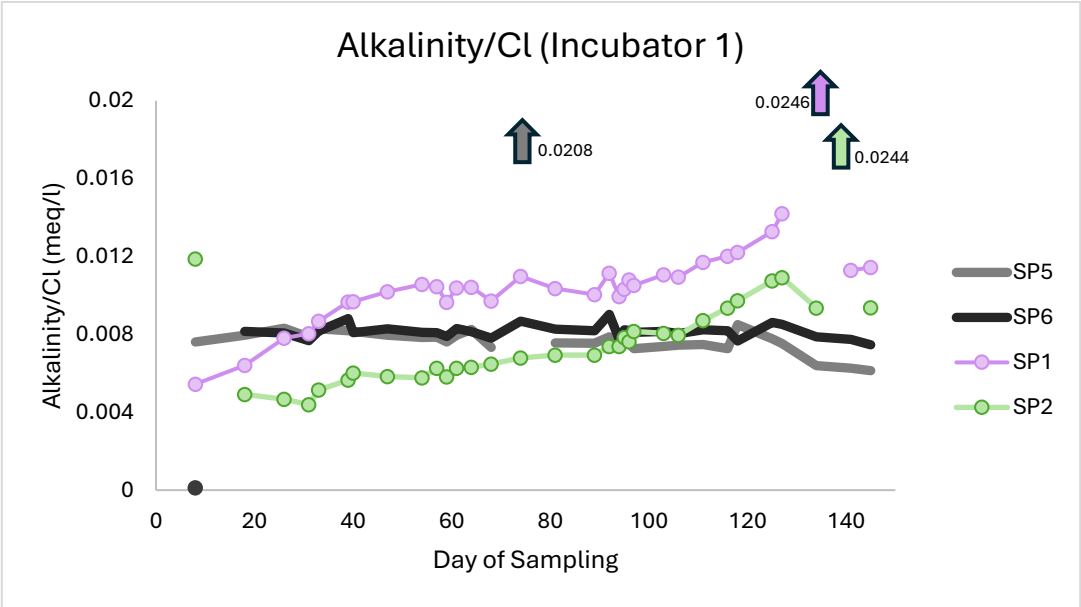

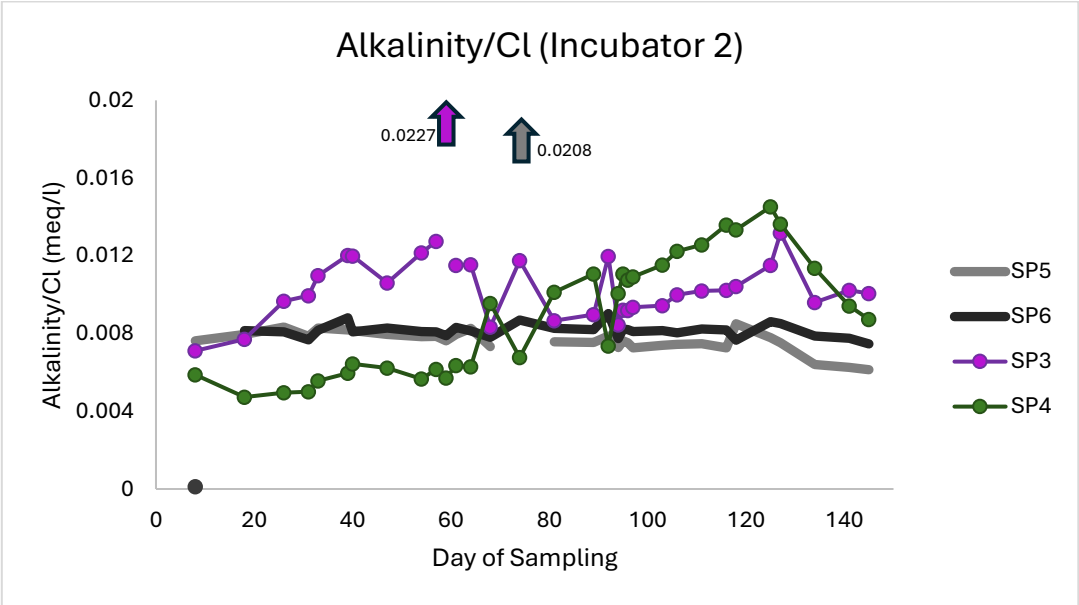

Figure 46. Alkalinity/Cl in incubators 1 and 2

But overall, disregarding this reversal, the TA plot reveals that sandpacks follow consistent trends in pairs (Fig. 47):

- Upper sandpacks: SP2 & SP4
- Bottom sandpacks: SP1 & SP3
- Control sandpacks: SP5 & SP6

This paired behavior, in sediment-containing sandpacks, reflects the influence of system configuration, particularly the upward flow direction, sampling order, and the sequence of fluid–sediment interaction.

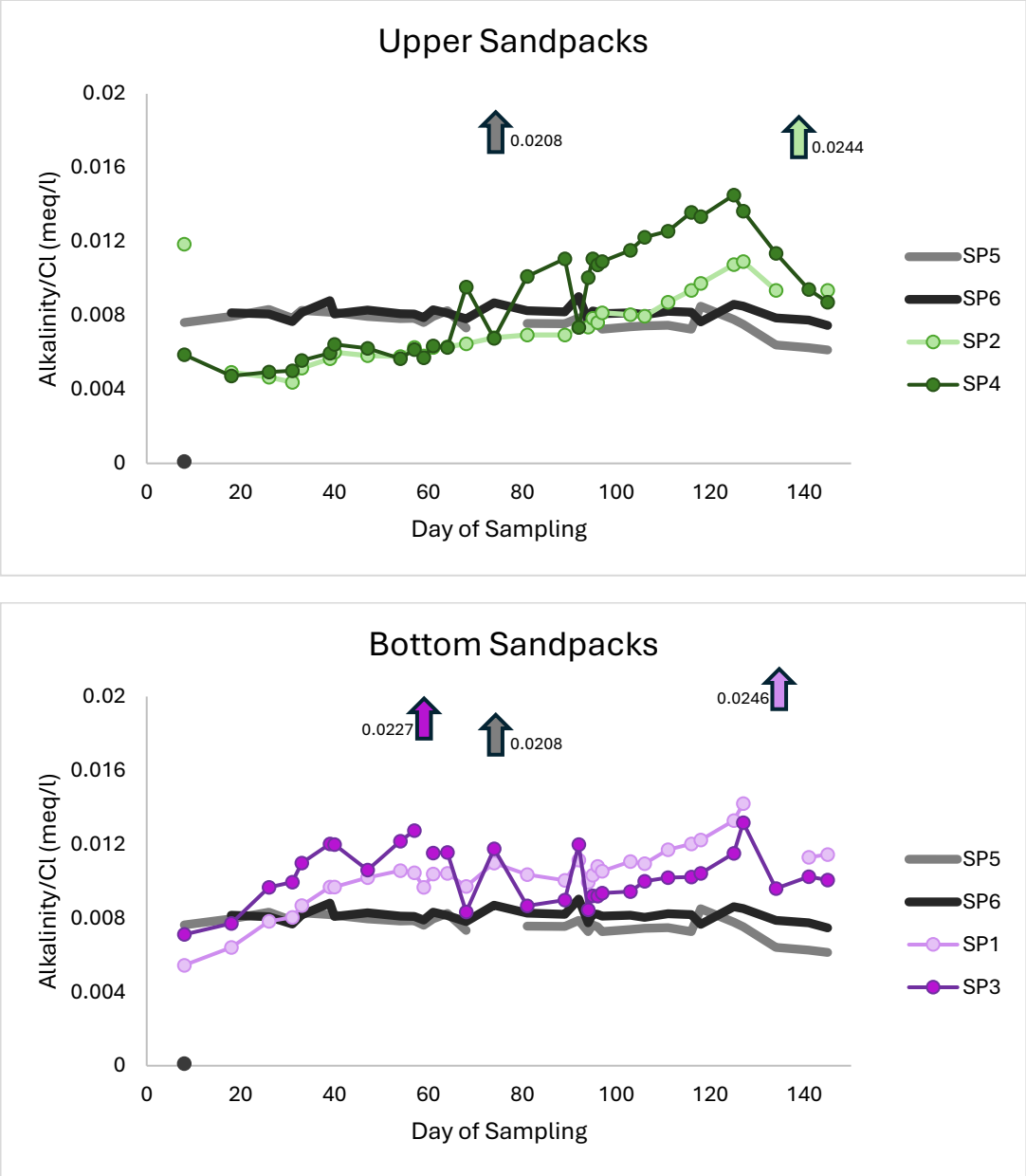

Figure 47. Alkalinity/Cl in upper and bottom sandpacks

Another thing is that although samples are collected sequentially during a sampling cycle (approximately 3.5 hours in total, with ~17 minutes per position), the numbering of samples can be misleading when interpreted in a geochemical context. For example, what is labeled “sample 1” may be perceived as the earliest or least-reacted sample; however, due to the upward-flow configuration, this is not necessarily the case. In reality, the fluid reaching

the upper sandpacks has already passed through and interacted with the lower sandpacks prior to sampling. This means that, despite being collected earlier in the sequence, these samples may represent fluid that has undergone more extensive geochemical reaction.

Therefore, the apparent order of sampling does not correspond to the reaction history of the fluid. Instead, fluid composition is primarily controlled by its pathway through the system. As acidic seawater flows upwards, it first reacts with sediments in the bottom sandpacks, where dissolution is most intense, and then continues towards the upper sandpacks in a progressively buffered state. Consequently, differences in TA and ion concentrations between sandpacks are governed by reaction progress along the flow path rather than the chronological order of sample collection within a sampling cycle.

In flow-through systems such as this, geochemical gradients naturally develop along the flow path, with reaction intensity decreasing upwards as the fluid becomes progressively buffered.

Comparing both pH and TA plot (Fig. 48) reveals that the initial fluctuation in pH (grey shaded area) is most likely caused by system adjustment as a result of seawater flushing of residual salts, as supported by a concurrent drop in Ca concentration (Fig. 36). This is followed by a partial recovery in pH, indicating that buffering processes become active, which suggests that the system is not passive.

In the first acidification scenario (inflow pH ≈ 7.4, yellow shaded area), the increase in pH following the initial drop coincides with a rise in TA, indicating active buffering, most likely driven by carbonate/silicate dissolution within the sediments. Despite the inflow being acidified, the measured pH gradually increases over time rather than decreasing. This counterintuitive behavior can only be explained by a buffering process, specifically Carbonate/silicate dissolution from the sediments, which consumes acidity, releases alkalinity, and raises pH. This provides the strongest evidence of buffering, particularly since the control sandpacks do not exhibit this behavior (ie, no corresponding increase in TA). After reaching a maximum value, pH begins to decline again, marking a transition towards steady-state conditions. At this stage, the continuous input of acid starts to exceed the reaction rates of mineral dissolution, leading to a gradual decrease in pH.

In the second acidification scenario (inflow pH ≈ 6, orange shaded area), the system is even pushed further. Carbonate/silicate dissolution continues to increase TA, but this increase is not sufficient to counterbalance the higher acidity, leading to an overall decrease in pH under sustained low-pH conditions. Although Carbonate/silicate dissolution remains active and contributes to alkalinity production, it cannot keep pace with the continuous proton input due to kinetic limitations. As a result, the system cannot fully buffer the imposed acidity at these low pH levels. Under these conditions, proton supply exceeds the rate of

mineral dissolution, and the system's behavior becomes primarily controlled by reaction kinetics rather than buffering.

Moreover, XRD analyses of the incubated core reveal no significant change in carbonate mineral content before and after the experiment, whereas a measurable decrease is observed in Ca-bearing silicate minerals. This pattern indicates that silicate mineral dissolution, rather than carbonate dissolution, is the dominant process buffering the induced acidification.

Taken together, these findings underscore the critical role of flow dynamics and sediment–water interactions in shaping geochemical gradients within the system. The results demonstrate that dissolution of Ca-bearing silicate minerals can substantially enhance total alkalinity (TA) and contribute to pH stabilization, highlighting the importance of sedimentary processes as a natural mitigation mechanism against ocean acidification.

However, the buffering capacity of the sediments is not unlimited. While effective under moderate acidification, it weakens and may ultimately be overwhelmed under more intense acidification scenarios. Nevertheless, sediments from Petermann Fjord demonstrate a clear ability to buffer and mitigate ocean acidification under the conditions tested. The observed gradual but persistent increase in TA throughout the experiment further indicates that Ca release via mineral dissolution is an ongoing process. This continuous response suggests that the system is dynamically adjusting towards a new geochemical equilibrium; however, this adjustment remains kinetically constrained, with reaction rates limiting the speed and extent of buffering.

Because the unincubated sediment was rich in carbonates, we expected carbonate weathering to occur more rapidly than silicate weathering as carbonate minerals generally exhibit faster dissolution kinetics. Previous work by Lehmann et al. (Lehmann et al., 2023) shows that carbonate weathering typically dominates solute production due to its high reactivity even in systems containing abundant silicate minerals. Based on this expectation, carbonate phases were anticipated to show earlier or more pronounced alteration than silicate minerals. However, our results do not support this assumption. No measurable alteration of carbonate minerals was detected whereas clear weathering signatures were observed in silicate phases specifically amphibole and anorthite. This suggests that, under the specific hydrochemical conditions of our experiment and the Petermann Fjord setting, silicate weathering happened earlier or was more detectable than carbonate dissolution.

This observation is consistent with findings from Liu et al. (Liu et al., 2012) who demonstrated that Ca-feldspar dissolution can represent a major source of solutes in Greenland meltwaters. Their results indicate that silicate weathering may contribute significantly to geochemical fluxes in subglacial environments and in some cases may be

comparable to or even exceed carbonate-derived solutes. This supports our interpretation that silicate minerals can undergo measurable alteration even when carbonate phases appear unreactive over similar timescales.

Urra's study (Urra A, 2019) demonstrates that chemical weathering beneath the Greenland Ice Sheet is often dominated by silicate mineral dissolution rather than carbonate weathering. Unlike smaller glacial systems where carbonate dissolution can be dominant due to its rapid kinetics the Greenland Ice Sheet is primarily underlain by carbonate-poor crystalline bedrock which promotes silicate weathering pathways. Their study also highlights that subglacial meltwaters are typically enriched in Na and K which are key indicators of silicate mineral breakdown. In contrast, contributions of Ca and Mg from carbonates are relatively limited in most catchments. In addition, longer subglacial water residence times in large ice sheet systems can enhance silicate weathering despite its slower reaction rates, allowing it to become the dominant geochemical process.

Finally, these findings support our experimental results from Petermann Fjord where silicate minerals showed detectable alteration while carbonate phases remained unchanged. This suggests that silicate weathering may play a more active or earlier role than carbonate dissolution under the conditions simulated in our study, consistent with observations from other Greenland Ice Sheet environments.

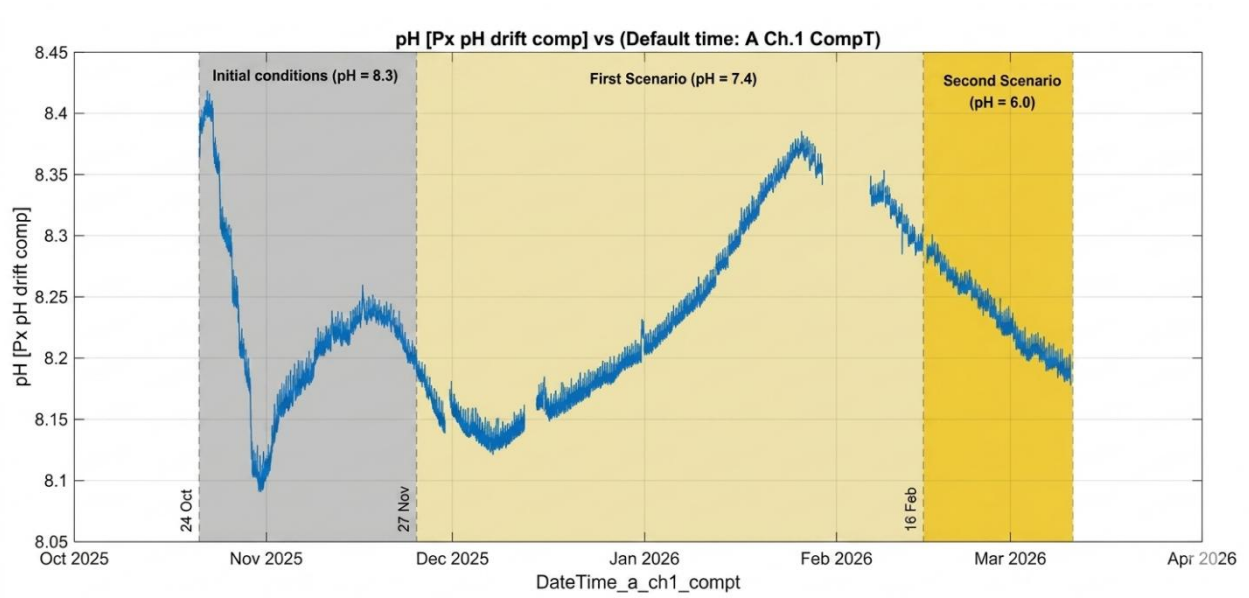

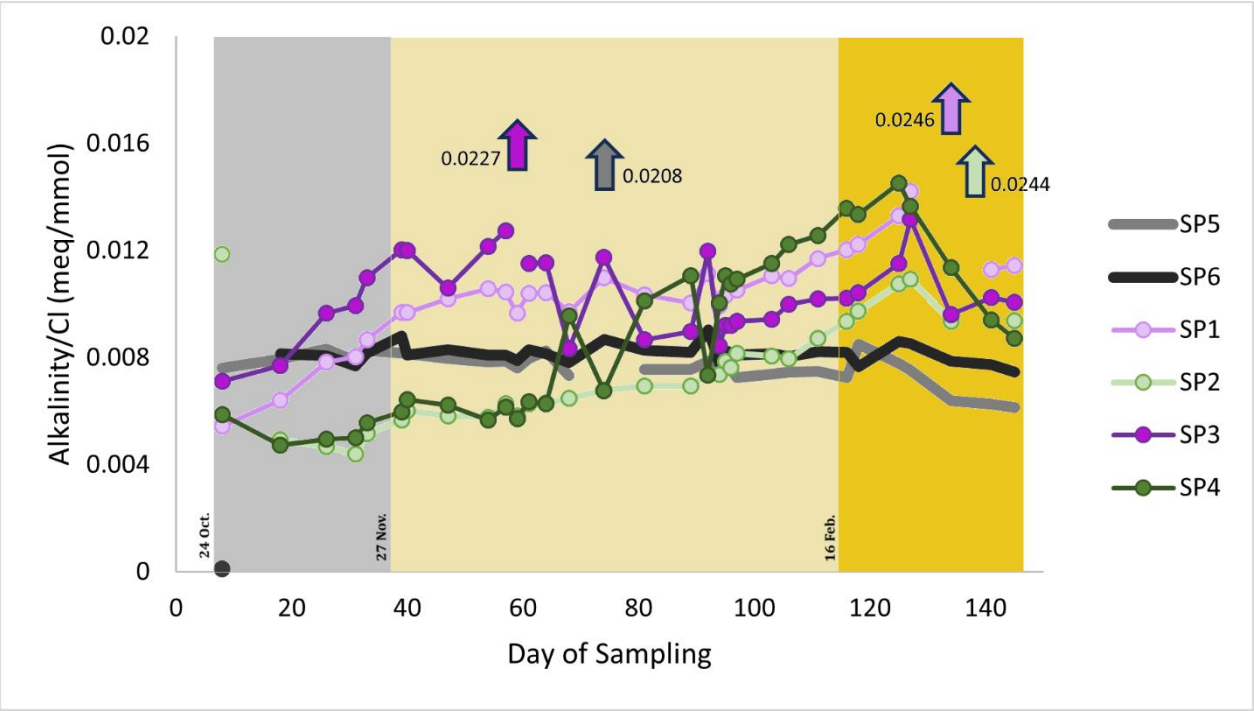

Figure 48. Comparing pH and TA

Recommendations for Future Improvements

To improve data quality and reduce contamination in future experiments, several procedural adjustments are recommended.

First, all sample containers, including IC vials, vial caps, incubation vials, and Falcon tubes, should be thoroughly cleaned prior to use. Either Milli-Q rinsing or acid washing (using nitric acid) is recommended. Experimental tests indicated that a significant portion of the calcium contamination observed in blanks originated from insufficiently cleaned IC vials as well as Falcon tubes. Initially, the contamination was attributed to potential issues with the MQ water system; however, comparative tests confirmed that the primary source was the vials and Falcon tubes themselves. Both MQ-rinsed and acid-washed vials were found to effectively reduce background contamination and improve chromatogram quality. Nevertheless, an overnight soaking step is strongly recommended to ensure thorough cleaning and minimize residual contamination.

In addition, improved pressure regulation within the sandpack system is recommended. More stable and controlled pressure conditions would enhance experimental consistency and reduce potential variability in flow and sampling, ultimately leading to more reliable results.

References

1. Aðalsteinsdóttir, S., Stockmann, G., Sturkell, E., Bali, E., Guðfinnsson, G., & Stefánsson, A. (2025). Petrological Studies and Geochemical Modelling of Water–Rock Interactions in the Grønnedal-Íka Alkaline Complex Generating Ikaite Deposition in Ikka Fjord, SW Greenland. *Minerals*. doi:https://doi.org/10.3390/min15040373

2. Aguilar-Vega, X., Fransson, A., Chierici, M., Washbourne, I., & Spyrakos, E. (2025). Carbon in an Arctic fjord: sea ice carbon transformations and CO2 linkages. *Front. Mar. Sci.* doi:https://doi.org/10.3389/fmars.2025.1688237

3. Akhoudas, C., Ulfsbo, A., Thornton, B., & et. al. (2025). Unraveling ocean pCO2 dynamics in Northwest Greenland Fjords. *Sci Rep*. doi:https://doi.org/10.1038/s41598-025-12720-1

4. Amiri, N., Hong, W.-L., O'Regan, M., Kirchner, N., & Jakobsson, M. (2026). Can seafloor carbonate weathering buffer ocean acidification in northwestern Greenland? *EGU General Assembly 2026*. Vienna, Austria. doi:https://doi.org/10.5194/egusphere-egu26-14382

5. Bibi, I., Amin, A., Haese, R., & et al. (2026). Unraveling dolomite dissolution stoichiometry in circumneutral to alkaline pH environments. *Acta Geochim, 45*. doi:https://doi.org/10.1007/s11631-025-00758-x

6. Brantley, S., Shaughnessy, A., Lebedeva, M., & Balashov, V. (2023). How temperature-dependent silicate weathering acts as Earth's geological thermostat. *Science, 379*(6630). doi:https://doi.org/10.1126/science.add2922

7. Bridier, G., Meziane, T., Grall, J., Chauvaud, L., & Sejr, M. (2019). Coastal waters freshening and extreme seasonality affect organic matter sources, quality, and transfers in a High Arctic fjord (Young Sound, Greenland). *Mar Ecol Prog Ser, 610*. doi:https://doi.org/10.3354/meps12857

8. *Buffer Reference Center*. (2026). Retrieved from Merck: https://www.sigmaaldrich.com/SE/en/technical-documents/protocol/protein-biology/protein-concentration-and-buffer-exchange/buffer-reference-center

9. Cai, C., Rignot, E., Menemenlis, D., & Nakayama, Y. (2017). Observations and modeling of ocean-induced melt beneath Petermann Glacier Ice Shelf in northwestern Greenland. *Geophys. Res. Lett., 44*(16). doi:https://doi.org/10.1002/2017GL073711

10. Cantoni, C., Hopwood, M., Clarke, J., Chiggiato, J., Achterberg, E., & Cozzi, S. (2020). Glacial Drivers of Marine Biogeochemistry Indicate a Future Shift to More Corrosive Conditions in an Arctic Fjord. *Journal of Geophysical Research: Biogeosciences, 125*(11). doi:https://doi.org/10.1029/2020JG005633Digital Object Identifier (DOI)

11. Cetiner, J., Berelson, W., & et al. (2025). Carbonate dissolution fluxes in deep-sea sediments as determined from in situ porewater profiles in a transect across the saturation horizon. *Geochimica et Cosmochimica Acta, 390*. doi:https://doi.org/10.1016/j.gca.2024.11.027

12. Chen, M., Kim, J., Choi, J., & et al. (2017). Biological early diagenesis and insolation-paced paleoproductivity signified in deep core sediment organic matter. *Sci Rep*. doi:https://doi.org/10.1038/s41598-017-01759-4

13. Cukrov, N., Cukrov, N., & Omanović, D. (2024). Early Diagenetic Processes in the Sediments of the Krka River Estuary. *J. Mar. Sci. Eng.* doi:https://doi.org/10.3390/jmse12030466

14. Detlef, H., Reilly, B., Jennings, A., Mørk Jensen, M., O'Regan, M., Glasius, M., . . . Pearce, C. (2021). Holocene sea-ice dynamics in Petermann Fjord in relation to ice tongue stability and Nares Strait ice arch formation. *The Cryosphere, 15*(9). doi:https://doi.org/10.5194/tc-15-4357-2021

15. Dillan, B., Lee, J., Ryu, J.-S., Chen, N.-C., Kavil, S., Hietbrink, S., . . . Hong, W.-L. (2025). Signs of Clay Formation in the Surficial Sediments of Victoria and Petermann Fjords, Northern Greenland. *Goldschmidt 2025 Abstract*. doi:https://doi.org/10.7185/gold2025.30455

16. Fransson, A., Chierici, M., Nomura, D., & et al. (2020). Influence of glacial water and carbonate minerals on wintertime sea-ice biogeochemistry and the CO2 system in an Arctic fjord in Svalbard. *Annals of Glaciology*. doi:https://doi.org/10.1017/aog.2020.52

17. Gadi, R., Rignot, E., & Menemenlis, D. (2023). Modeling Ice Melt Rates From Seawater Intrusions in the Grounding Zone of Petermann Gletscher, Greenland. *Geophysical Research Letters, 50*(24). doi: https://doi.org/10.1029/2023GL105869

18. Gattuso, J.-P., Alliouane, S., & Fischer, P. (2023). High-frequency, year-round time series of the carbonate chemistry in a high-Arctic fjord (Svalbard). *Earth Syst. Sci. Data, 15*(7). doi:https://doi.org/10.5194/essd-15-2809-2023

19. Grewer , D. M. (2017). Changes to Soil and Sedimentary Organic Matter Composition with Permafrost Active Layer Detachments in a Canadian High Arctic Watershed. *PhD thesis*. Graduate Department of Chemistry University of Toronto .

20. Henson, H., Holding, J., Meire, L., Rysgaard, S., Stedmon, C., Stuart-Lee, A., . . . Sejr, M. (2023). Coastal freshening drives acidification state in Greenland fjords. *Science of The Total Environment, 855*. doi:https://doi.org/10.1016/j.scitotenv.2022.158962

21. Hogan, K., & et. al. (2020). Glacial sedimentation, fluxes and erosion rates associated with ice retreat in Petermann Fjord and Nares Strait, north-west Greenland. *The Cryosphere*. doi:https://doi.org/10.5194/tc-14-261-2020

22. Hong, W.-L., Steinbach, J., Schmitt, N., Zelikman, I., Ceric, D., & Amiri, N. (2025). A coupled apparatus of flow-through incubation and automated fluid sampling system for experimenting and monitoring marine silicate alteration under in-situ conditions.

Goldschmidt 2025 Conference, Prague, Czech Republic. GOLDSCHMIDT. doi:10.7185/gold2025.27004

23. Hong, W.-L., Sun, X., Torres, M., Huang, T.-H., & Pickering, R. (2025). The role of silicate alteration in regulating marine carbon cycling. *Chemical Geology, 684*. doi:https://doi.org/10.1016/j.chemgeo.2025.122769

24. Jakobsson, M., Mayer, L., Farrell, J., & et. al. (2019). *Ryder Glacier Expedition 2019*. Stockholm University, Geological Sciences. Hämtat från https://www.su.se/english/research/research-catalogue/research-projects/7/ryder-glacier-expedition-2019

25. Johnson, H., Münchow, A., Falkner, K., & Melli, H. (2011). Ocean circulation and properties in Petermann Fjord, Greenland. *J. Geophys. Res., 116*(C1). doi:https://doi.org/10.1029/2010JC006519

26. Karlsson, E., Brüchert, V., Tesi, T., Charkin, A., Dudarev, O., Semiletov, I., & Gustafsson, Ö. (2015). Contrasting regimes for organic matter degradation in the East Siberian Sea and the Laptev Sea assessed through microbial incubations and molecular markers. *Marine Chemistry, 170*. doi:https://doi.org/10.1016/j.marchem.2014.12.005

27. Kim, D., Kim, J.-H., Ahn, Y., Forwick, M., & Nam, S.-I. (2025). Sedimentary organic carbon dynamics in a glaciated Arctic fjord: tracing contributions of terrestrial and marine sources in the context of Atlantification over recent centuries. *Biogeosciences, 22*(16). doi:https://doi.org/10.5194/bg-22-4087-2025

28. Knies, J., Ahn, Y., Ebner, B., & et al. (2025). Arctic fjord ecosystem adaptation to cryosphere meltdown over the past 14,000 years. *Commun Earth Environ*. doi:https://doi.org/10.1038/s43247-025-02251-y

29. Legge, O., Bakker, D., Meredith, M., Venables, H., Brown, P., Jones, E., & Johnson, M. (2017). The seasonal cycle of carbonate system processes in Ryder Bay, West Antarctic Peninsula. *Deep Sea Research Part II: Topical Studies in Oceanography, 139*. doi:https://doi.org/10.1016/j.dsr2.2016.11.006

30. Lehmann, N., & Bach, L. (2025). Global carbonate chemistry gradients reveal a negative feedback on ocean alkalinity enhancement. *Nat. Geosci*. doi:https://doi.org/10.1038/s41561-025-01644-0

31. Lehmann, N., Lantuit, H., Böttcher, M., Hartmann, J., Eulenburg, A., & Thomas, H. (2023). Alkalinity generation from carbonate weathering in a silicate-dominated headwater catchment at Iskorasfjellet, northern Norway. *Biogeosciences*. doi:https://doi.org/10.5194/bg-20-3459-2023

32. Lerman, A., & Mackenzie, F. (2018). Carbonate Minerals and the CO2-Carbonic Acid System. In *Encyclopedia of Geochemistry*. Springer, Cham. doi:https://doi.org/10.1007/978-3-319-39312-4_84

33. Limoges, A., Ribeiro, S., Weckström, K., Heikkilä, M., Zamelczyk, K., & et. al. (2018). Linking the Modern Distribution of Biogenic Proxies in High Arctic Greenland Shelf Sediments to Sea Ice, Primary Production, and Arctic-Atlantic Inflow. *Journal of Geophysical Research: Biogeosciences, 123*(3). doi:https://doi.org/10.1002/2017JG003840

34. Liu, L., Sletten, R. S., Hagedorn, B., Choquette, K., Cameron, K. A., Dieser, M., . . . Junge, K. (2012). Understanding of Silicate Weathering in Subglacial Environment by Inverse Modeling of West Greenland Glacial Meltwater. *American Geophysical Union*.

35. Meinhardt, A.-K., März, C., Schuth, S., Lettmann, K., Schnetger, B., Wolff, J.-O., & Brumsack, H.-J. (2016). Diagenetic regimes in Arctic Ocean sediments: Implications for sediment geochemistry and core correlation. *Geochimica et Cosmochimica Acta, 188*. doi:https://doi.org/10.1016/j.gca.2016.05.032

36. Mejía, L., Bernasconi, S., Fernandez, A., & et al. (2025). Coccolith clumped isotopes reveal modest rather than extreme northern high latitude amplification during the Miocene. *Nat Commun*. doi:https://doi.org/10.1038/s41467-025-65954-y

37. Middelburg, J. (2024). Acid-Base Equilibria. In *Thermodynamics and Equilibria in Earth System Sciences: An Introduction*. SpringerBriefs in Earth System Sciences. doi:https://doi.org/10.1007/978-3-031-53407-2_6

38. Middelburg, J., Soetaert, K., & Hagens, M. (2020). Ocean Alkalinity, Buffering and Biogeochemical Processes. *Reviews of Geophysics*. doi:https://doi.org/10.1029/2019RG000681

39. Munhoven, G. (2021). Model of Early Diagenesis in the Upper Sediment with Adaptable complexity – MEDUSA (v. 2): a time-dependent biogeochemical sediment module for Earth system models, process analysis and teaching. *Geosci. Model Dev.* doi:https://doi.org/10.5194/gmd-14-3603-2021, 2021

40. Prakash, A., Zhou, Q., Hattermann, T., & et al. (2025). Enhanced subglacial discharge amplifies Petermann Ice Shelf melting when ocean thermal forcing saturates. *Nat Commun, 16*(4213). doi:https://doi.org/10.1038/s41467-025-59469-9

41. Renforth, P., & Henderson, G. (2017). Assessing ocean alkalinity for carbon sequestration. *Rev. Geophys., 55*(3). doi:https://doi.org/10.1002/2016RG000533

42. Ribeiro, S., Sejr, M., Limoges, A., & et al. (2017). Sea ice and primary production proxies in surface sediments from a High Arctic Greenland fjord: Spatial distribution and implications for palaeoenvironmental studies. *Ambio, 46*. doi:https://doi.org/10.1007/s13280-016-0894-2

43. Scholz, F., Börker, J., Vogt, C., & et al. (2025). Natural ocean alkalinization through erosion of glacial till and weathering at the seafloor. *Commun Earth Environ*. doi:https://doi.org/10.1038/s43247-025-03009-2

44. Sheward, R. M., Herrle, J., Fuchs, J., Gibbs, S., Bown, P., & Eibes, P. (2024). Biogeochemical Traits of a High Latitude South Pacific Ocean Calcareous Nannoplankton Community During the Oligocene. *Paleoceanography and Paleoclimatology, 39*(12). doi:https://doi.org/10.1029/2024PA004946

45. Stranne, C., Nilsson, J., & Ulfsbo, A. (2021). The climate sensitivity of northern Greenland fjords is amplified through sea-ice damming. *Commun Earth Environ, 2*(70). doi:https://doi.org/10.1038/s43247-021-00140-8

46. Sulpis, O., Jeansson, E., Dinauer, A., & et al. . (2021). Calcium carbonate dissolution patterns in the ocean. *Nat. Geosci., 14*. doi:https://doi.org/10.1038/s41561-021-00743-y

47. The GEOEO Shipboard Scientific Party. (2024). *GEOEO North of Greenland 2024 Expedition*. Stockholm University, Geological Sciences. Polarforskningssekretariatet 2024.

48. Trapp-Müller, G., Caves Rugenstein, J., Conley, D., & et al. (2025). Earth's silicate weathering continuum. *Nat. Geosci., 18*. doi:https://doi.org/10.1038/s41561-025-01743-y

49. Urra A, W. J. (2019). Weathering Dynamics Under Contrasting Greenland Ice Sheet Catchments. . *Front. Earth Sci.* doi:https://doi.org/10.3389/feart.2019.00299

50. van de Velde, S., Hylén, A., & Meysman, F. (2025). Ocean alkalinity destruction by anthropogenic seafloor disturbances generates a hidden CO2 emission. *Sci. Adv., 11*(13). doi:https://doi.org/10.1126/sciadv.adp9112

51. Wang, Y., Gélinas, Y., de Vernal, A., & et al. . (2024). High rates of marine organic carbon burial on the southwest Greenland margin induced by Neoglacial advances. *Commun Earth Environ*. doi:https://doi.org/10.1038/s43247-024-01508-2

Supplementary Materials

The following pages provide supplementary materials that complement and provide additional context to the analyses presented in this thesis.

IC dual analysis anions/cations – Checklist before run

[1] Wake up instrument /turn on oven (if necessary) • If the status lights on the autosampler and pump are orange, press the *SLEEP* button on both parts • Check in the *RealtimeAnalysis* software if the oven is turned on (=yellow) and set to 40C. If not, turn on the oven on via the *Oven On* button in the software.	 
[2] Check that the suppressor is on. • On the conductivity detector, press the *back* button twice until *SUP 1 ON/OFF* appears on the screen and check that it says *ON*. • If not, press 1 and confirm with *enter*	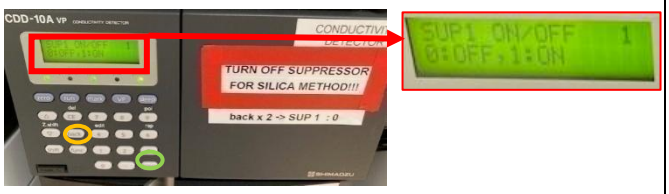
[3] Empty waste container (if necessary) • Anion/cation eluent can be emptied into the sink.	
[4] Prepare and install eluent • Never top off eluent, always make a new one. • Use respective holder bottle for eluent cap during change, wear gloves when touching tubes/filters. • **Eluent bottles and dilution plasticware are color-coded: red for cations, blue for anions. Don't mix!** • **Dilute concentrate from R322 fridge: 1800ml MilliQ water + 200ml concentrate (plastic measuring cylinder) directly in the reservoir** • **reset eluent level in software** • click the mobile phase icon, and reset the level for Pump A and B in the respective tab of the opening window	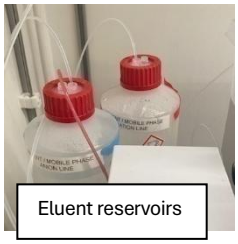   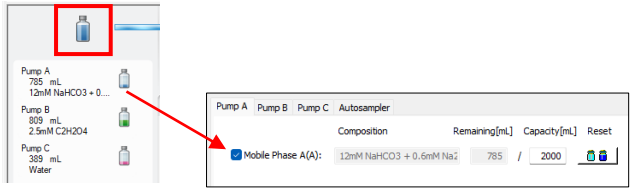
[5] Change rinse water for autosampler (MilliQ)	

• Make sure to fill the bottle sufficiently	
[6] Prime & start pumps • On pump A and B: Open pump waste valve, press *purge* button on pump. *PURGING LINE* will show on the screen. • Close valve (hand-tight) when purging is done. • Start pumps in software and check if pressure is 50-52 bar for pump A and 35-37 for pump B. (check sample log for recent values for your method)	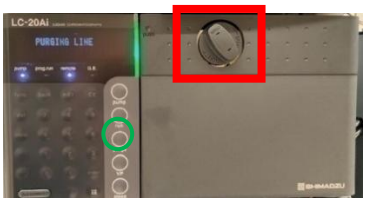 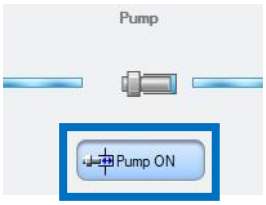
[7] Purge autosampler • Press purge button in the software	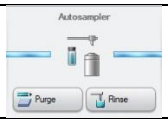
[8] Let system stabilize for at least one hour.	

IC dual anion/cation analysis – setting up a batch

In *Realtime Analysis,* click the *QuickBatch Icon* in the left taskbar or in the middle of the window.	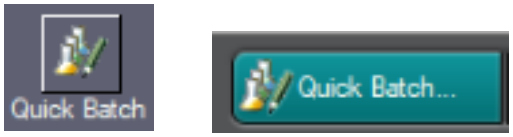
To do a standard run with a calibration curve with appropriate levels for anions and cations in seawater/marine sediment, choose *From template* and *SA2_anions_cations_cal_12_levels*.	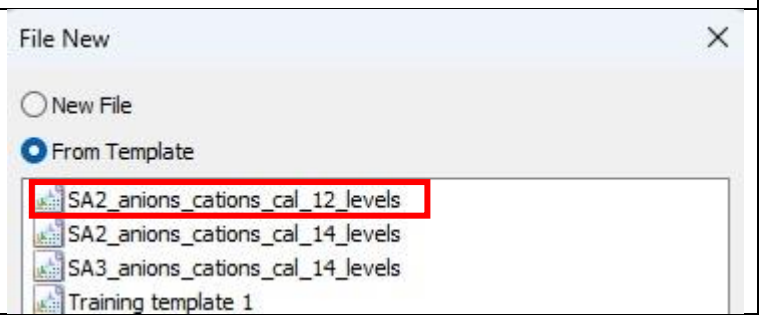

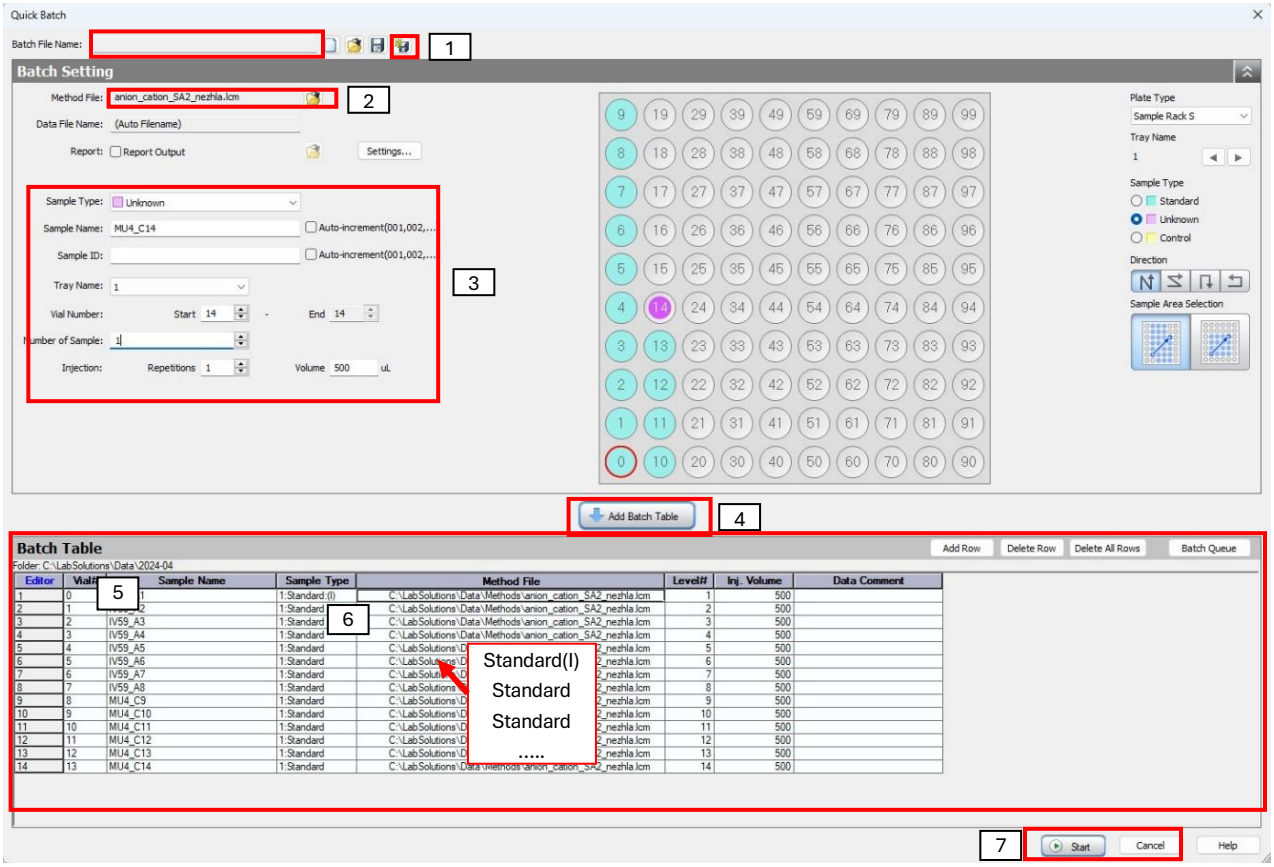

[1]	Click on the *Save a.* on and save the batch in the current month's folder (*YYYYY-MM*), using the name format *YYYYMMDD_operator_analysistype_sampleset*, e.g. *202503011_Julia_an_cat_Baltic_porewater*.

[2]	Check settings for the run: *Method File* – make sure it is an anion/cation method and for the right type of vials (matching the rack shown in the quick batch), the current standard method is *anion_cation_SA2-nezhla.lcm; Data File Name – (AutoFilename)*
[3]	Now write for each sample after each other • ***Sample type:*** *Unknown* (=sample), *Standard (*standard used for calibration), *control* (blank or working standard, not used for calibration) • ***Sample name:*** use a short but still identifiable name (check autoincrement if you add several samples at once, e.g. S_001, S_002,…) • Note: The automatic filename will be created from the batch name plus *SampleName* plus the running number of the sample in the current batch run e.g. *20250311_Julia_an_cat_Baltic_porewater_S1_01*. • ***Sample Tray***: 1 (no need to change) • ***Vial Number:*** note that the vial counting starts with 0. The vial number on the (physical) sample rack is located on the bottom left of the vial. The software automatically moves on to the next free vial, the overview on the right shows you the samples/standards that you already entered in the color of the respective type (Unknown, Standard, Control). ○ ***Number of samples***: usually 1, unless you enter several ones at the same time and use autoincrement for names ○ ***Repetitions*****:** you can choose to do replicate measurements of your samples from the same vial (2 for 1.5ml vials, more for 4ml, depending on filling height), but consider to rather spread out replicates (e.g. run S1,S2,S3, S1, S2,S3, S1,S2,S3 instead of S1,S1,S1,S2,S2,S2,S3,S3,S3 to avoid any bias due to potential instrument drift etc. during the run. ○ ***Volume*****:** ***500µl*** is the standard injection.
[4]	After entering all information for the current sample, click ***Add to Batch Table*** [4] and one line (or several lines in case of repetitions) will show up in the Batch Table [5]. You can also make edits or add/delete rows in the Batch Table after adding your sample.
[6]	One edit you have to make when using the calibration curve template is **adding more standards sets**: The template has one set of the calibration curve at the beginning, **add one set at the end and one in the middle of your run.** Note that the *Sample Type* of the first standard has to be *Standard(I)* [=initialize calibration curve], all other standards are *Sample Type Standard* [=add calibration level]. Anions and cations are one calibration curve, so only the first anion standard is *Standard(I),* all cation standards are type *Add standard*. You can either do that here in the *QuickBatch* or change to the *RealtimeBatch* view (see point 8). Right-click on the row where you want to place the standards, choose *InsertRow* and repeat until you have enough rows. Mark the standard rows, right-click and choose *CopyRow* and then *PasteRow* in the new empty lines.
[7]	After adding all your samples and making necessary edits, **save**  **batch** with and either click ***Start*** **to start directly** or ***Cancel*** **to start the batch at a later time**.

[8]	**(Optional) To make edits and start the batch from the RealTimeBatch mode:** go to *RealtimeBatch*, either by double-clicking on the icon in the left taskbar or by changing to the tab below the instrument status.  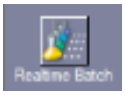
[8b]	In the Re*altimeBatch* view, open your batch using *File* → *Open* in the top taskbar. Make any necessary edits and check if all is correct.
[8c]	Start the batch using the icon in the  bar: o the left or in the top taskbar.
[11]	Since you have several sets of standards distributed over the batch, the software will ask you ***Standard(I) is not specified. Do you specify Standard(I)?*** several times. The answer is always ***No***.
[12]	Before starting the batch, the ***Shutdown*** window will pop-up, asking you to decide on the instrument state after the end of the run. Choose - *Degassing Unit Off* - ***LC Pump Off*** *(important to not run out of eluent after the run)* - *LC detector off* Confirm with *OK* to start batch. 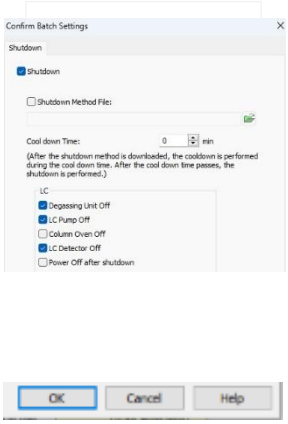
[12]	You can follow the acquisition progress and batch progress in the *DataAcquisition* tab. The function *BatchQueue* (top taskbar → *Acquisition* → *BatchQueue*) shows you the estimated time and eluent use for your run. 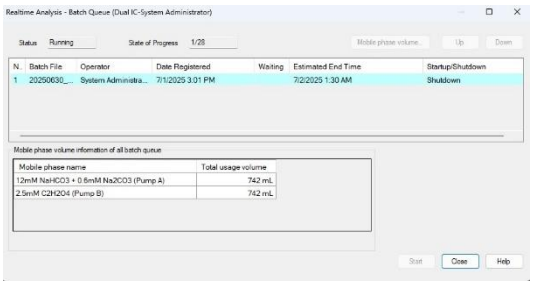
[13]	Write all relevant parameters of your run in the excel file *Sample log*

	(in folder *C://LabSolutions/_Documentation/,* should be open on-screen) and save it.

IC dual analysis anions/cations - Quantification and Calib

After your analysis run, open the *PostRun* part of *LabSolutions*:

➔ Go to the *LabSolutions Start Window* and chose *Postrun* on the left side, and then *Postrun* in the middle of the window again.

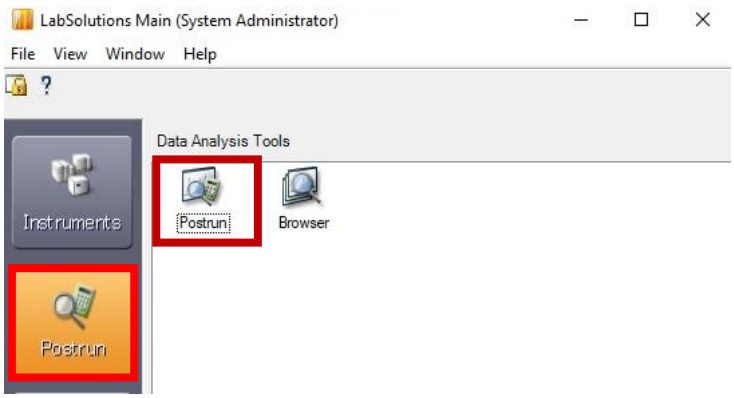

Step 1: VISUAL CHECK AND QUANTIFICATION METHOD		
[1]	Start in the tab *DataAnalysis*	 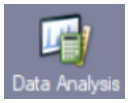
[2]	Start by looking at an anion standard (IV59): double click on the file in the *file explorer* or drag it to the data analysis window.	
	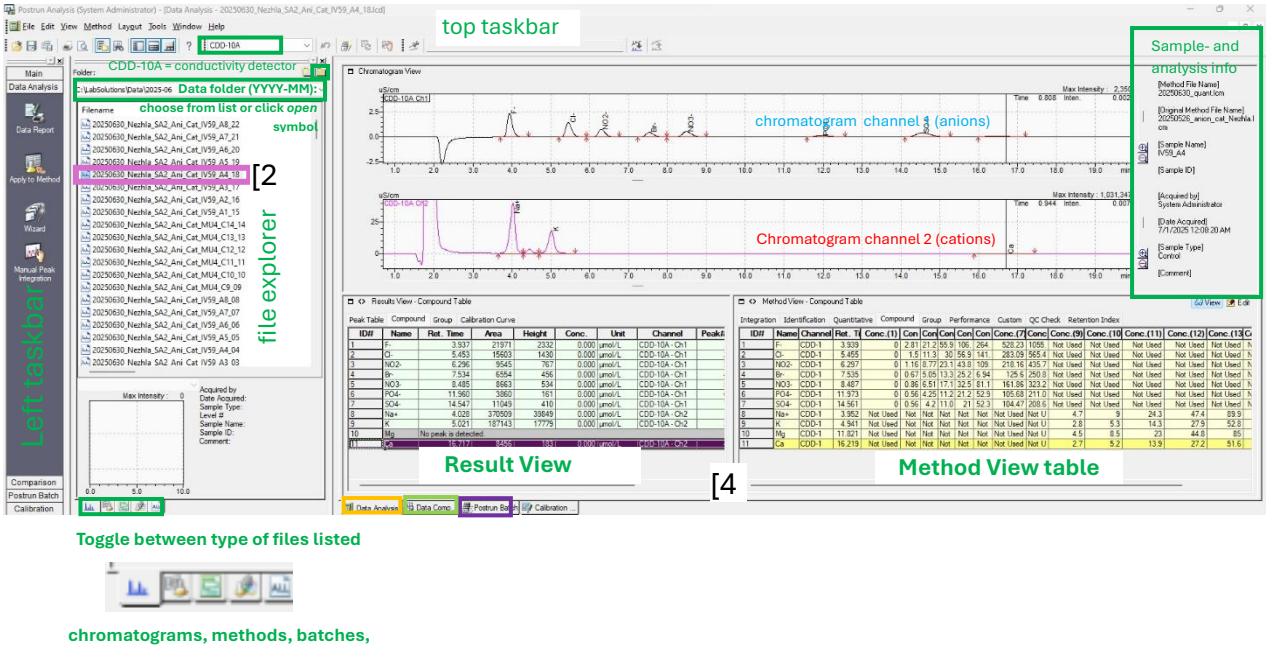	
[3]	Check if the peaks in channel 1 look comparable to those on the standard diagram.	

		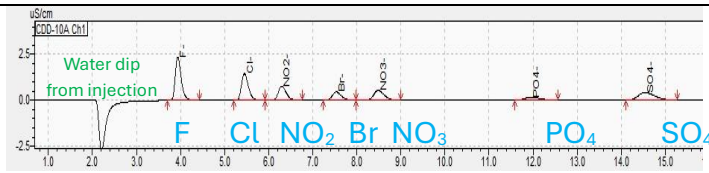
[4]	The *ResultView* table on the left shows you the retention times, areas and concentrations of the peaks in your run and as which compounds the method identified it (based on the settings in the run method), while the *MethodView* table on the right shows you the settings in the method (here tab *Compound* for both). 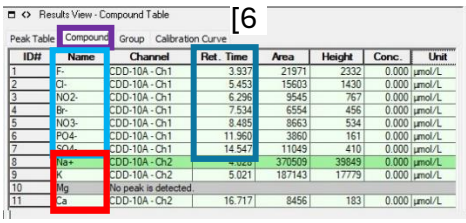 [6 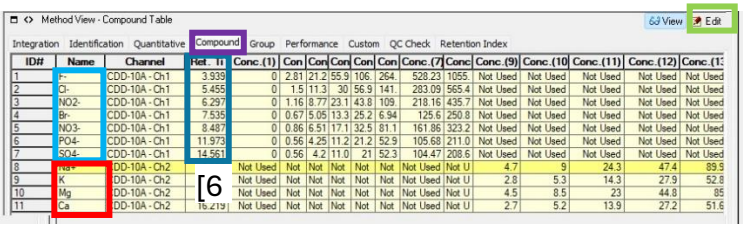 [6 [6 **Result View** **Method View table**	
[5]	Click through the *Result View* table **to check if all anion peaks are identified correctly** and peak sizes/shapes seem reasonable (ignore the cation peaks for now).	
[6]	**Update the retention times of your anion peaks** (usually there should be no large deviations from the *standard_run* times): click *Edit* on the *Method View Table* and copy the anion part of the retention time column from *Results View Table* into the *Method View Table*.	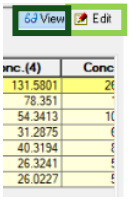
[7]	Click *View* to freeze the compound table, then save the new parameters in a quantification method: In the top taskbar, go to ***File → Save Method as*** **and save it as *YYYYMMDD_quant* in the same folder as your data**.	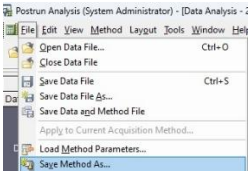
[8]	Now open a cation standard (MU4): double click on the file in the *file explorer* or drag it to the data analysis window.	

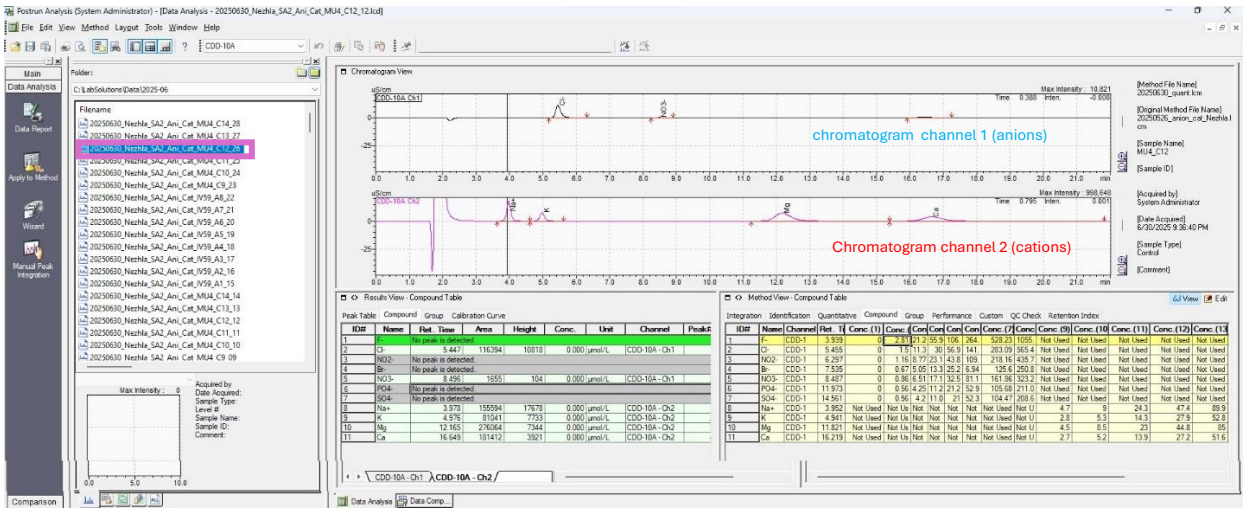

[9]	**Load the quantification method** you just made based on the anion standard: *File → Load Method Parameters (YYYYMMDD_quant)*	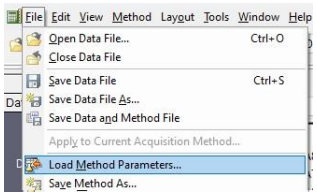
[9]	Check if the peaks in channel 2 look compa-rable to those on the standard diagram.	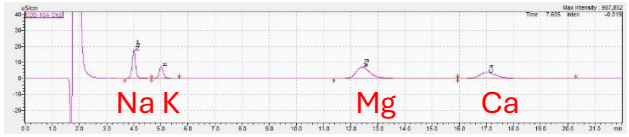
[10]	**Result View** **Method View table** 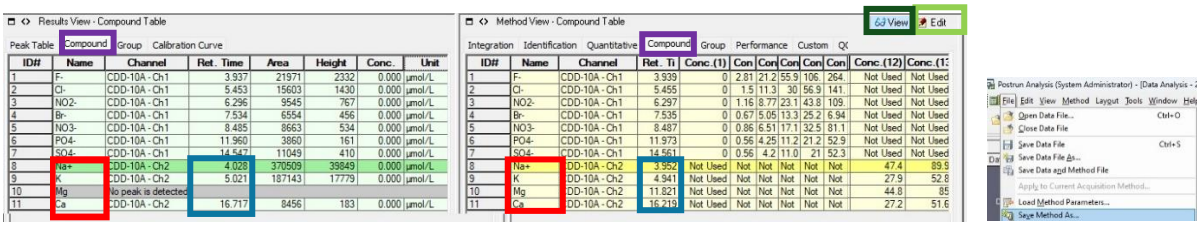 Repeat steps [4] - [7] with the cation peaks: check peak identification, copy and save retention times and save method (same name as before)	
[11]		

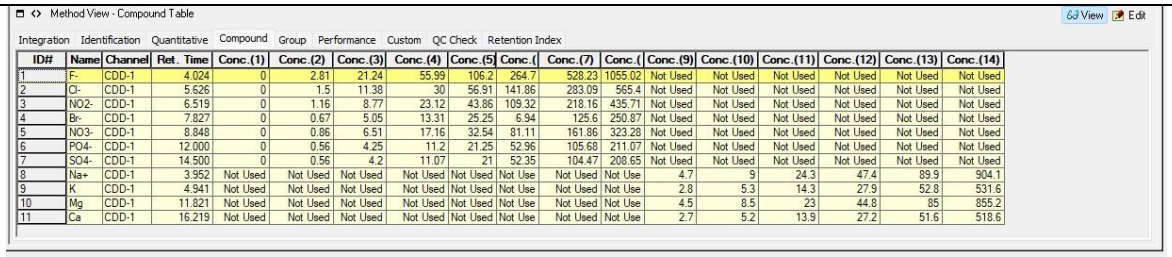

ID#	Name	Channel	Ret. Time	Conc.(1)	Conc.(2)	Conc.(3)	Conc.(4)	Conc.(5)	Conc.(6)	Conc.(7)	Conc.(8)	Conc.(9)	Conc.(10)	Conc.(11)	Conc.(12)	Conc.(13)	Conc.(14)
1	F-	CDD-1	4.024	0	2.81	21.24	55.99	106.2	264.7	528.23	1055.02	Not Used	Not Used	Not Used	Not Used	Not Used	Not Used
2	Cl-	CDD-1	5.626	0	1.5	11.38	30	56.91	141.86	283.09	565.4	Not Used	Not Used	Not Used	Not Used	Not Used	Not Used
3	NO2-	CDD-1	6.519	0	1.16	8.77	23.12	43.86	109.32	218.16	435.71	Not Used	Not Used	Not Used	Not Used	Not Used	Not Used
4	Br-	CDD-1	7.827	0	0.67	5.05	13.31	25.25	6.94	125.6	250.87	Not Used	Not Used	Not Used	Not Used	Not Used	Not Used
5	NO3-	CDD-1	8.848	0	0.86	6.51	17.16	32.54	81.11	161.86	323.28	Not Used	Not Used	Not Used	Not Used	Not Used	Not Used
6	PO4-	CDD-1	12.000	0	0.56	4.25	11.2	21.25	52.96	105.68	211.07	Not Used	Not Used	Not Used	Not Used	Not Used	Not Used
7	SO4-	CDD-1	14.500	0	0.56	4.2	11.07	21	52.35	104.47	208.65	Not Used	Not Used	Not Used	Not Used	Not Used	Not Used
8	Na+	CDD-1	3.952	Not Used	Not Used	Not Used	Not Used	Not Used	Not Use	Not Used	Not Use	4.7	9	24.3	47.4	89.9	904.1
9	K	CDD-1	4.941	Not Used	Not Used	Not Used	Not Used	Not Used	Not Use	Not Used	Not Use	2.8	5.3	14.3	27.9	52.8	531.6
10	Mg	CDD-1	11.821	Not Used	Not Used	Not Used	Not Used	Not Used	Not Use	Not Used	Not Use	4.5	8.5	23	44.8	85	855.2
11	Ca	CDD-1	16.219	Not Used	Not Used	Not Used	Not Used	Not Used	Not Use	Not Used	Not Use	2.7	5.2	13.9	27.2	51.6	518.6

Note that the concentration in the method view table are based on the dilutions of the standards as specified in the notes for *Standard preparation*. If you have used different dilutions or want to adjust the concentration of the standards based on your individual dilutions (e.g. weighing check), do that here in the Method View table. Remember to save the method after that!!

[12]

Normally you do not have to change any other method parameters. However**, if your salt level in the samples is high**, you might get in the range where the Na/Cl-calibration curve gets non-linear (peak areas >300 000, ca 300µM Cl). In this case create a **second quantification method be used for Na/Cl concentration.**

After all other adjustments to the method **and saving it**, go to tab *Quantification* in the *MethodView* table, click *Edit* and change the **Curve Fit Type from *Linear* to *Quadratic*.** Click *View* and save the (2nd) method as *(YYYYMMDD_quant_2)*.

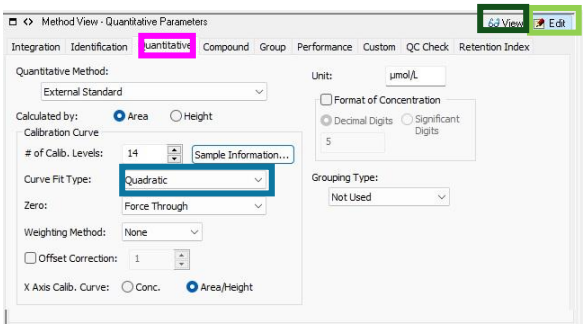

Step 2: POSTRUN BATCH

[1]

Once you have saved your quantification method, proceed to the *Postrun Batch* tab (via tab or taskbar) to apply these changes to all files in the run. 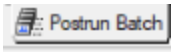

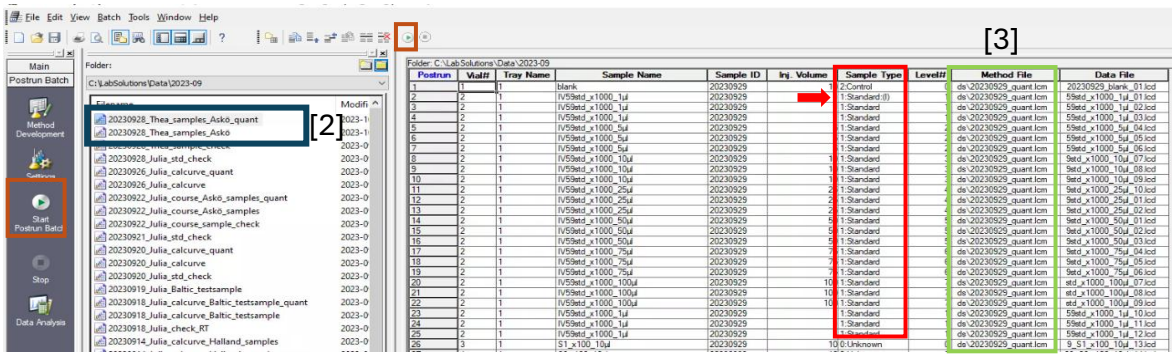

[2]

	Open the batch from your run (doubleclick in file explorer) and save it as *batchname_quant* in the same folder.
[3]	Replace the run method by your quantification method (*YYYYMMDD_quant*)
[4]	Check your standards in the batch: all standards to be used for calibration should have Sample Type *Standard,* and only the first standard should have sample type *Standard(I)* [= initialize calibration curve] (only first standard in batch, no matter if anion/cation)
[5]	Start the batch run (maybe you will have to close some open file in the *Data Analysis* tab – if you get software message *"The file is read closed"*.)
[6]	If you get the question (several times) "Do you specify Standard(I)?", answer with no.
[7]	If you created a 2nd method for high Na/Cl concentrations, you will have to run the batch a second time with this method. In this case, it is best to create a second batch file *(_quant2)*. When exporting results (step 4), make sure the batch creating the correct results has been run last (parameters applied to same data files)

Step 3: CALIBRATION	
[1]	To check the calibration curves for your run, go to tab *Calibration Curve* (via tab or taskbar) 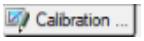 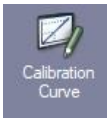
[2]	Open your quantification method *YYYYMMDD_quant* (from the file explorer, tab  *thod*)
[3]	The method contains one calibration curve per anion/cation: ID 1-7 are anions (F, Cl, NO2, Br, NO_3, PO_4, SO_4) and ID 8-11 are cations (Na, K, Mg, Ca). The table below the curve shows only the levels used for the respective compound.

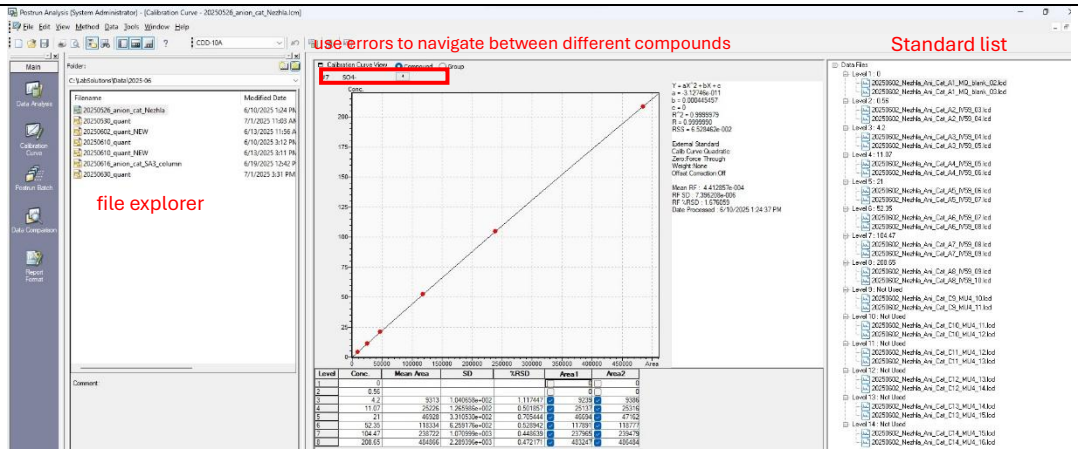

Check the quality of your calibration curve

- It should be linear, with an $R^2 > 0.99$
- RSD for each level should be <3 % (lowest level plus PO4 can be a bit higher)

[4] In case the salt levels of your samples are in a range the Cl/Na calibration is non-linear and you have created a second quantification method in step 2 *(YYYYMMDD_quant*)and run the postrun batch (step 3), your calibration curve for Cl will look like that. The same quality criteria as for the linear curve apply, but the quadratic fit will not work as well for the other compounds, so feel free to ignore the remaining curves.

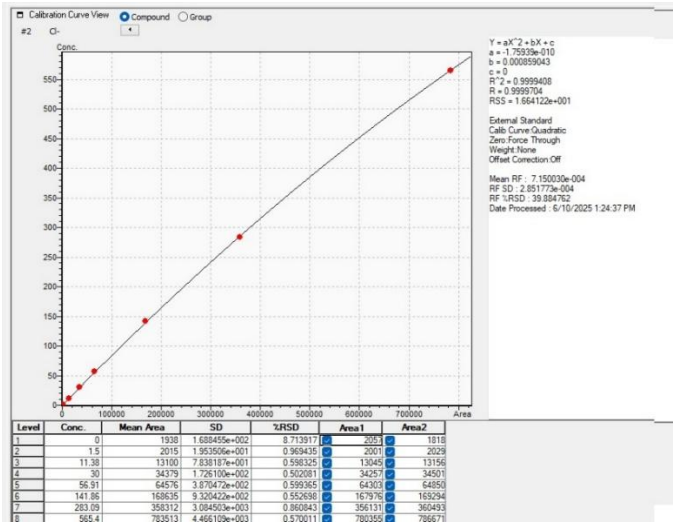

Step 4: EXPORT DATA

[1] ➔ Switch to *LabSolutions Browser:*

Go to the *LabSolutions* start window and chose *Postrun* on the left side, and then *Browser* in the middle of the window.

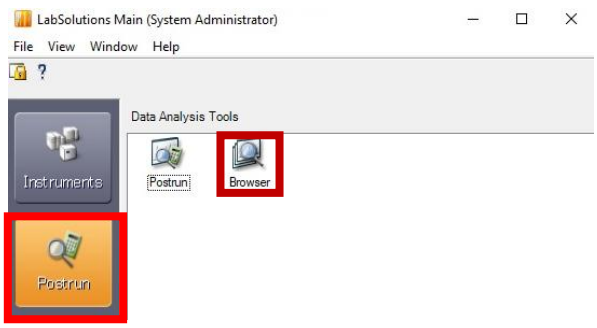

[2] In the left taskbar, chose *QuantBrowser.*

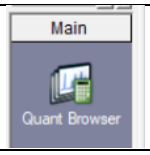

[3]

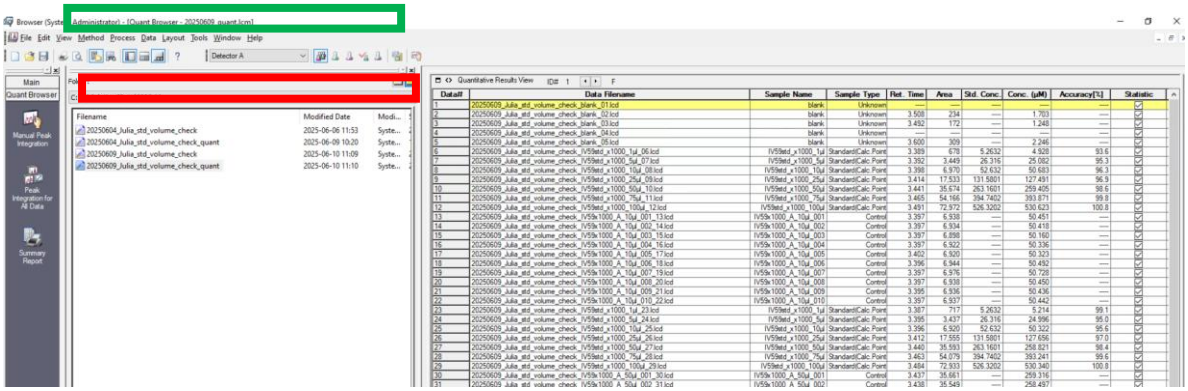

Go to the correct data folder, double-click on your postrun batch to open it in the browser (you might need to close the batch or individual files in *Postrun*)

[4] Right-click on the table and click on DataType from the menu to chose what to display and export (samples, standards, all data)

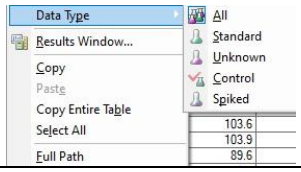

[4] To export your data to excel, go to *File* ➔ *Export Quantitative Results* in the taskbar

		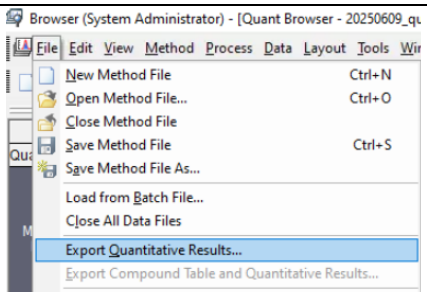
[5]	In the menu that opens, chose the following settings:	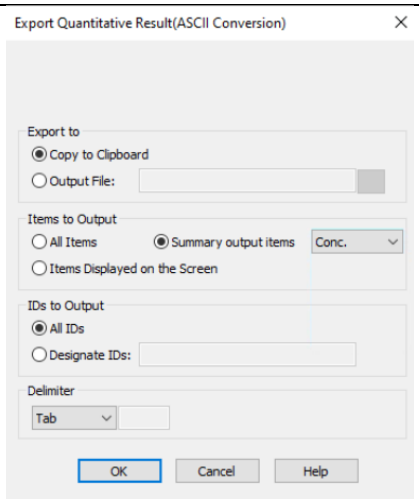
[6]	Open an excel file in the export folder, paste in the results and save it as *YYYYMMDD_yourname_batchname_identfier*.	
[7]	Remember to multiply your results with the dilution factor used and consider saving relevant metadata (calibration data, comments on the run etc) in the excel file. Never blindly trust the numbers in the exported file, always take your time to take a look at the chromatograms as well and double-check if peaks are correctly identified and well-integrated, that peak shapes are good and results seems reasonable with respect to the visual peak size.	

Fig. 36. Ion concentrations by position over time with outliers

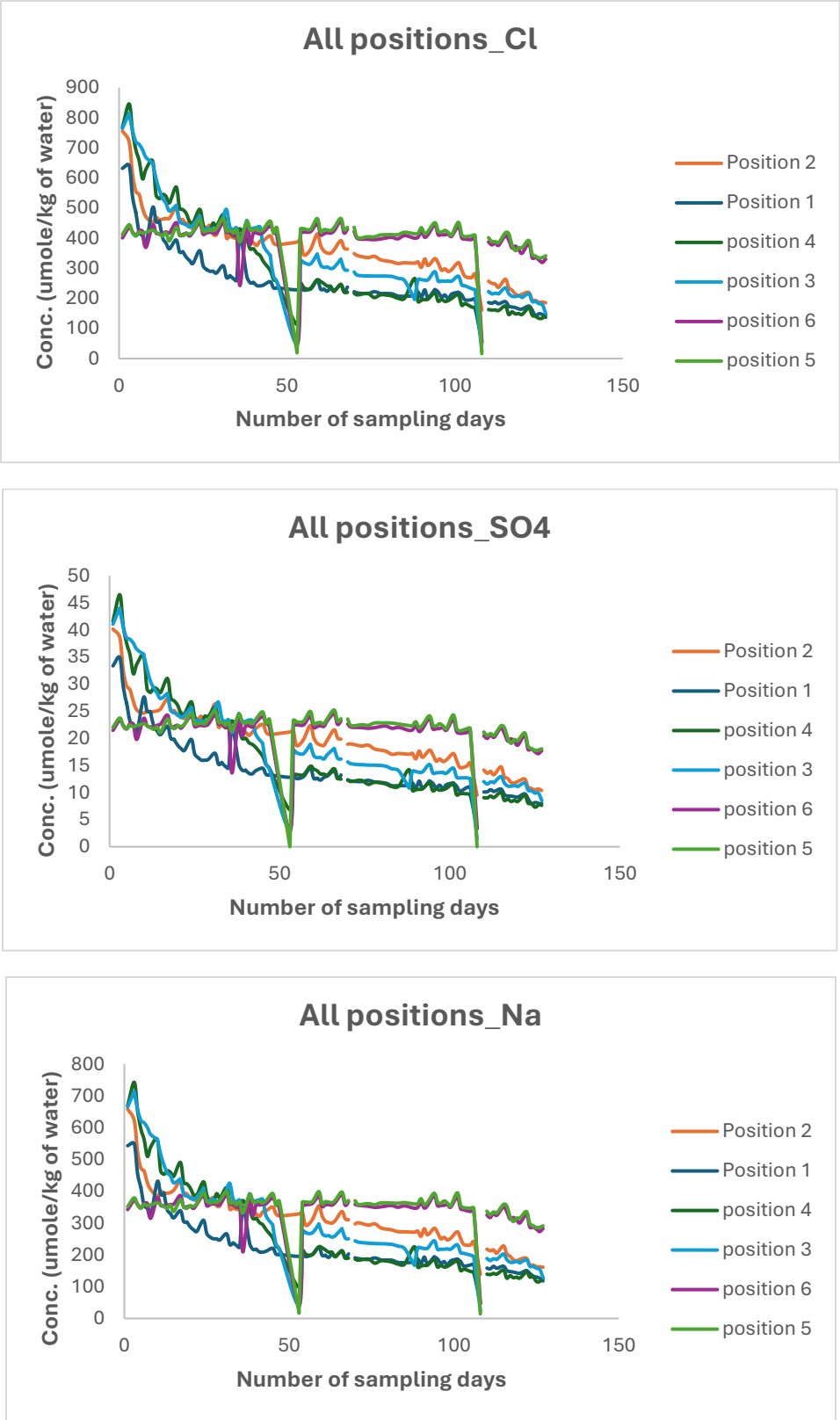

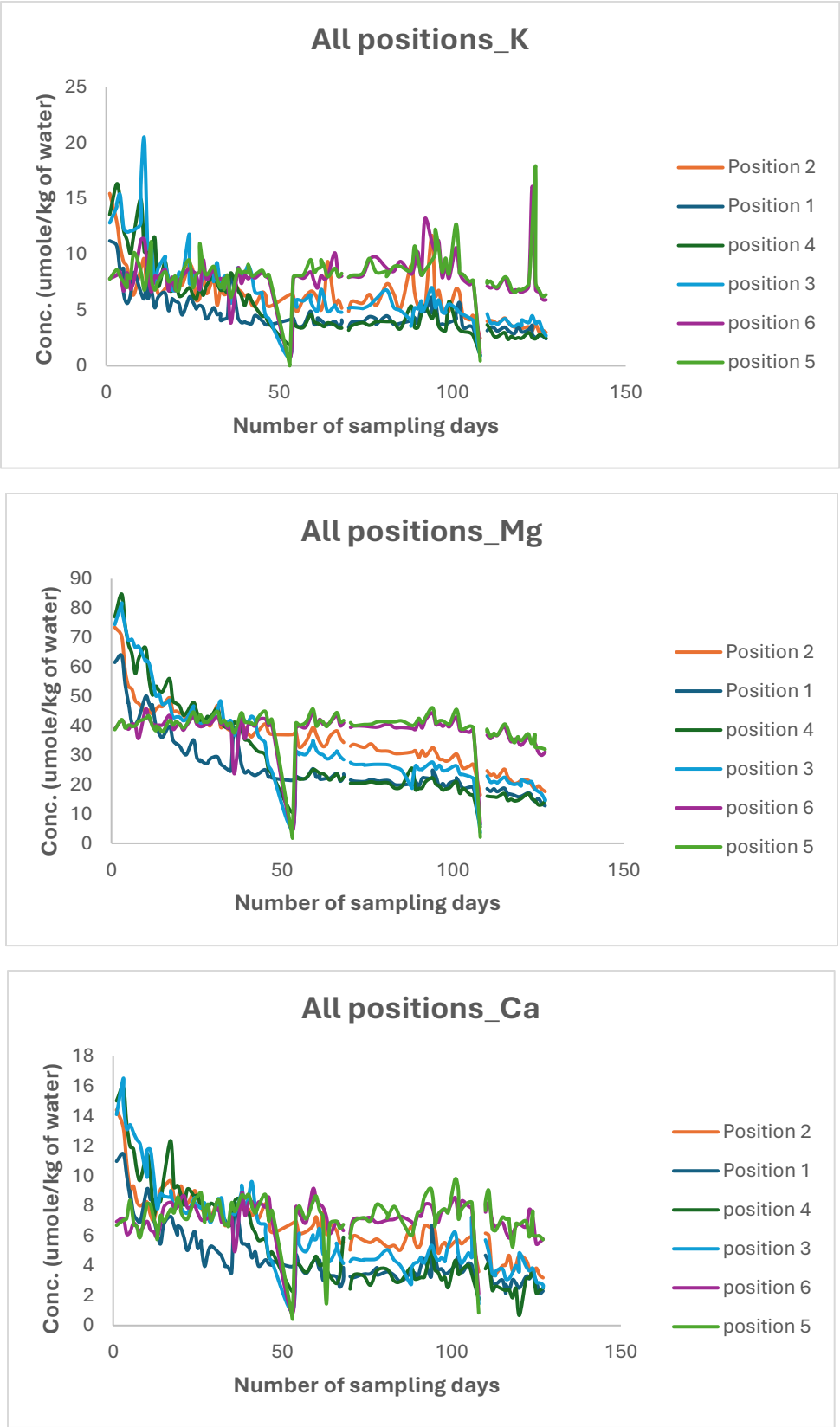

Figure 36. Ion concentrations by position over time

Fig. 38. The Ion/Cl ratios for all major ions at different positions

1- Sulfate (SO_4^{2-})

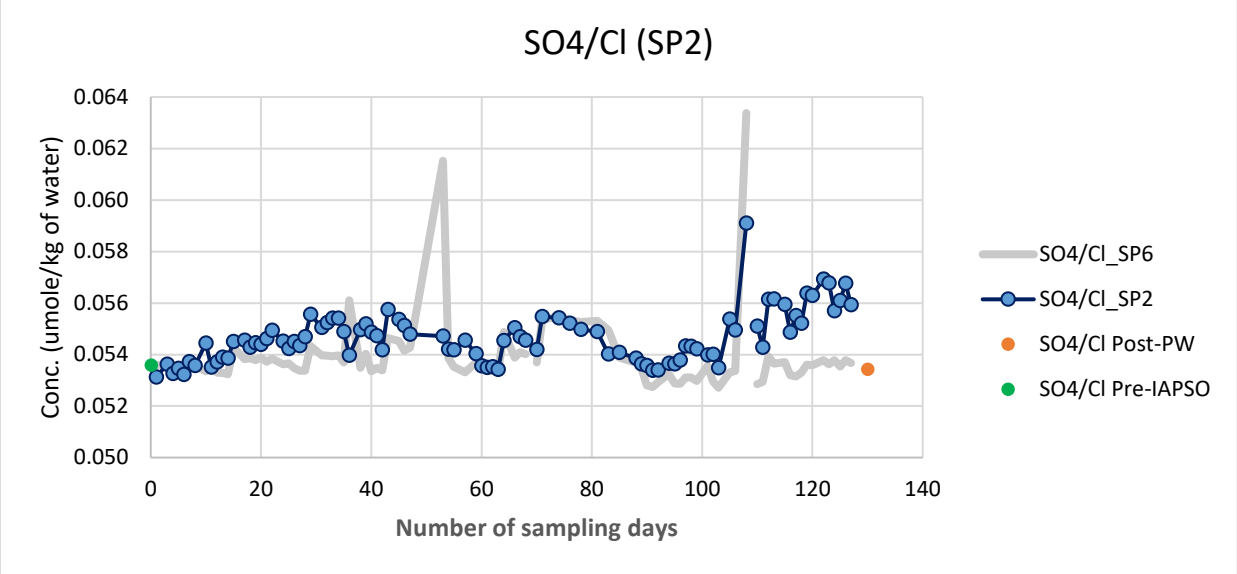

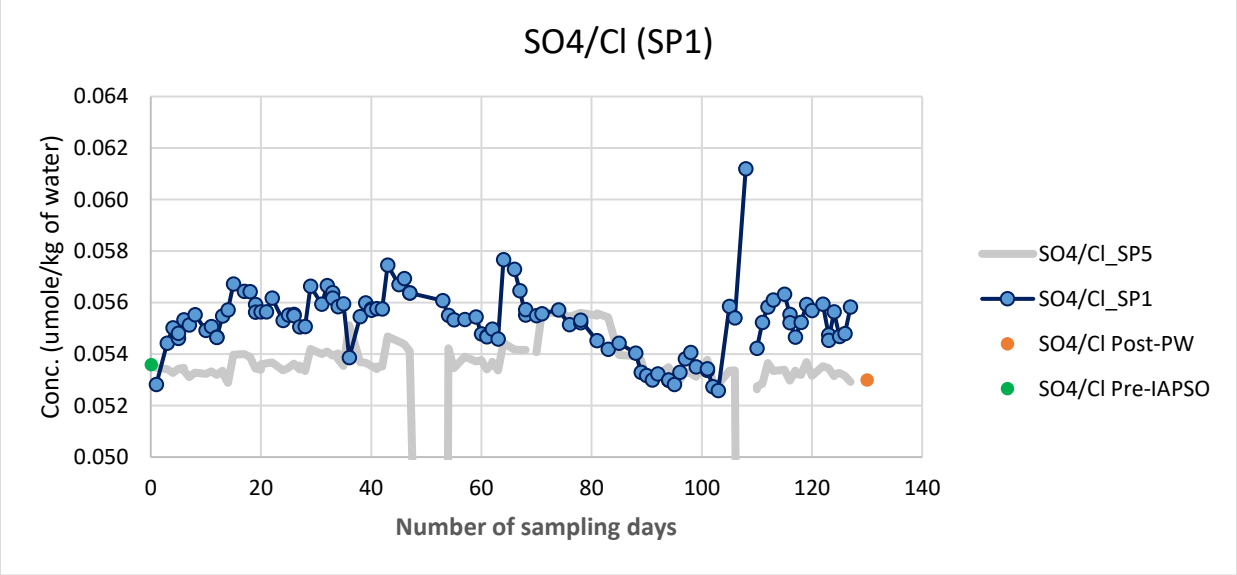

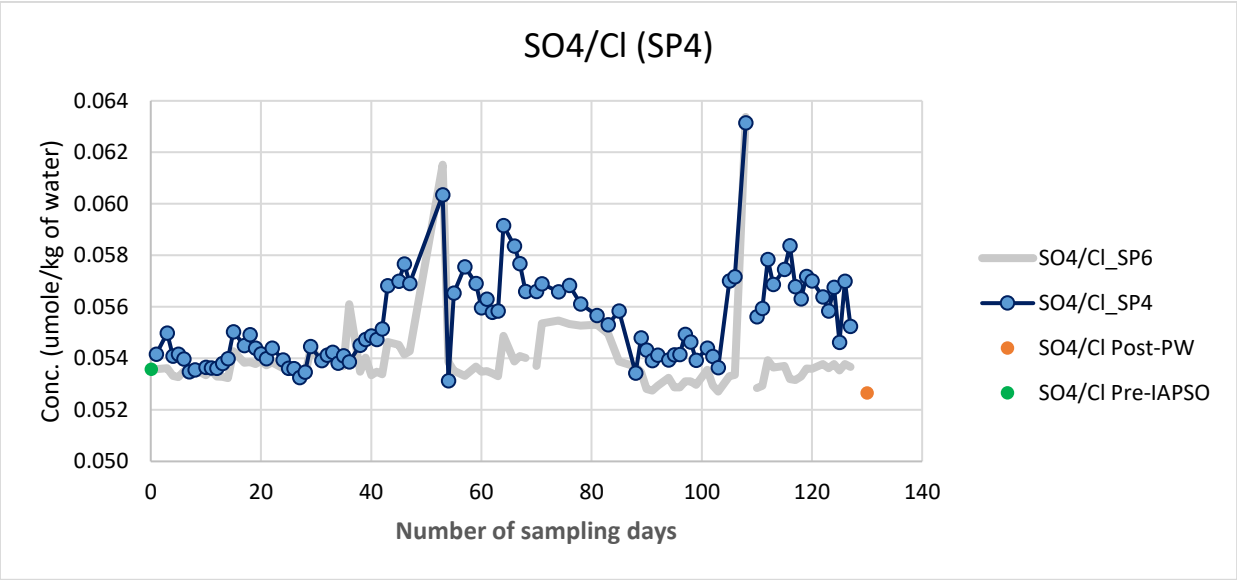
SO4/Cl (SP4)
Conc. (umole/kg of water)
0.064
0.062
0.060
0.058
0.056
0.054
0.052
0.050
0
20
40
60
80
100
120
140
Number of sampling days
SO4/Cl_SP6
SO4/Cl_SP4
SO4/Cl Post-PW
SO4/Cl Pre-IAPSO

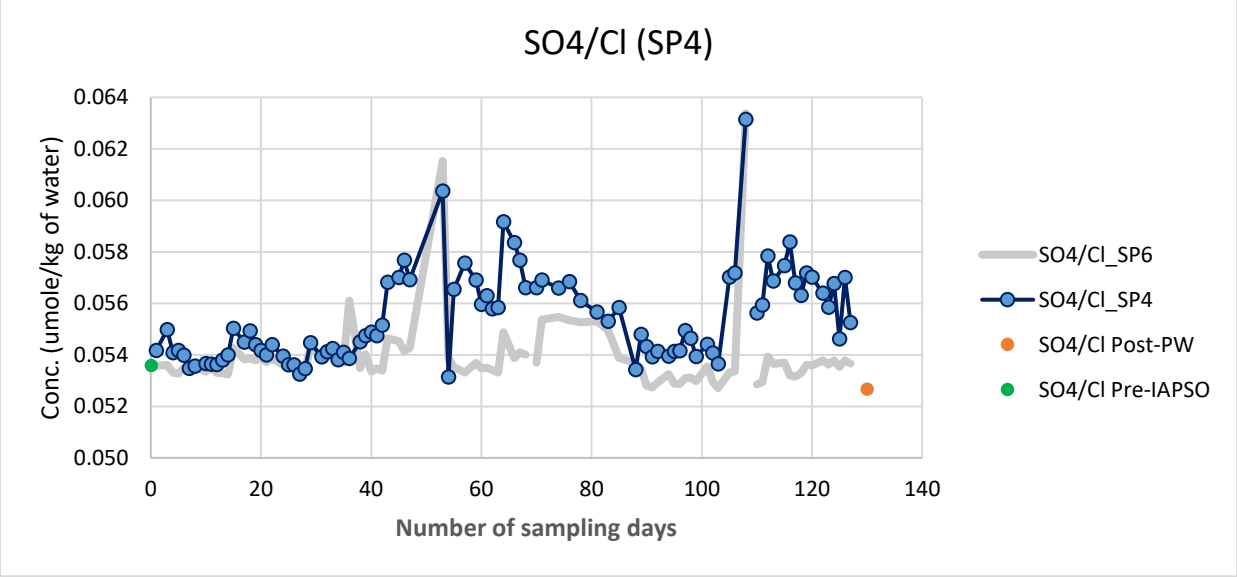
SO4/Cl (SP4)
Conc. (umole/kg of water)
0.064
0.062
0.060
0.058
0.056
0.054
0.052
0.050
0
20
40
60
80
100
120
140
Number of sampling days
SO4/Cl_SP6
SO4/Cl_SP4
SO4/Cl Post-PW
SO4/Cl Pre-IAPSO

2- Sodium (Na^+)

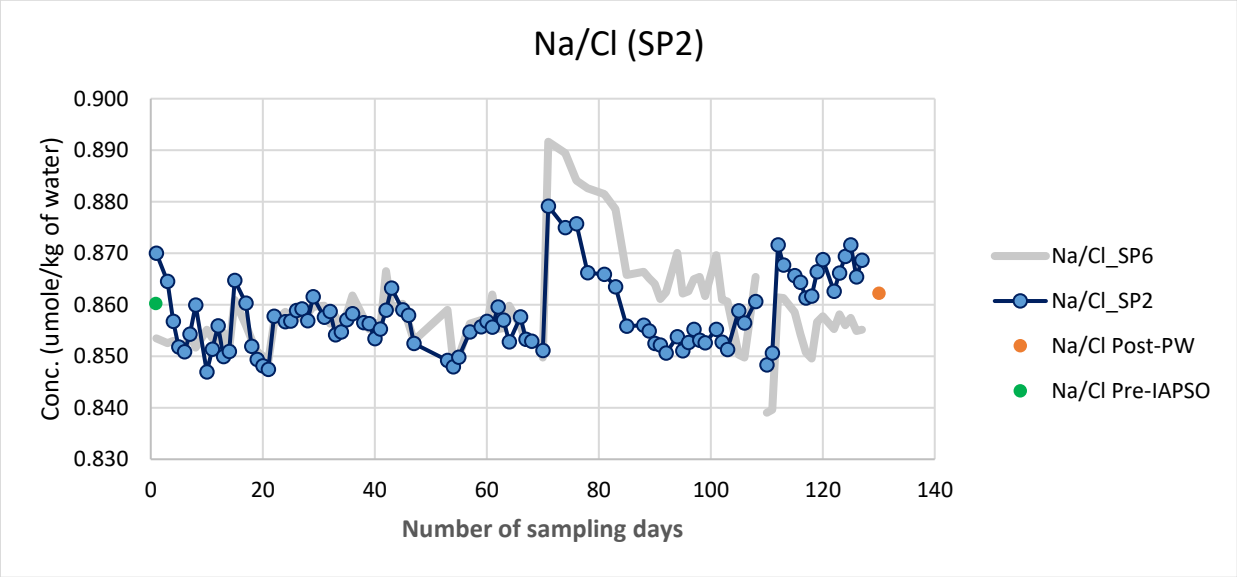
Na/Cl (SP2)
Conc. (umole/kg of water)
0.900
0.890
0.880
0.870
0.860
0.850
0.840
0.830
0
20
40
60
80
100
120
140
Number of sampling days
Na/Cl_SP6
Na/Cl_SP2
Na/Cl Post-PW
Na/Cl Pre-IAPSO

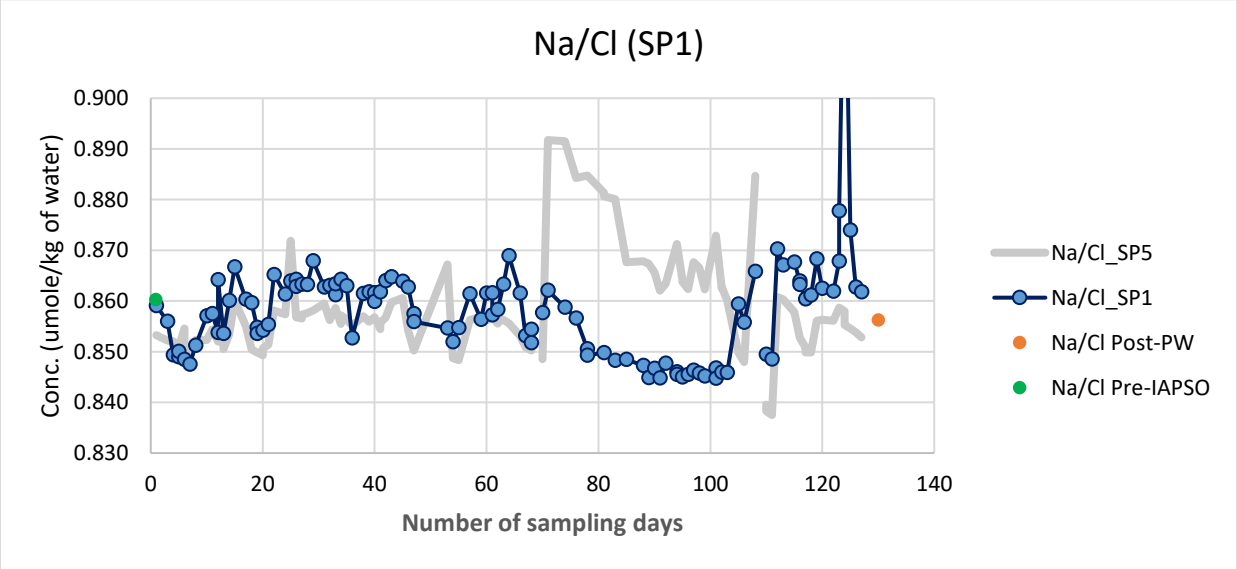
Na/Cl (SP1)
Conc. (umole/kg of water)
0.900
0.890
0.880
0.870
0.860
0.850
0.840
0.830
0
20
40
60
80
100
120
140
Number of sampling days
Na/Cl_SP5
Na/Cl_SP1
Na/Cl Post-PW
Na/Cl Pre-IAPSO

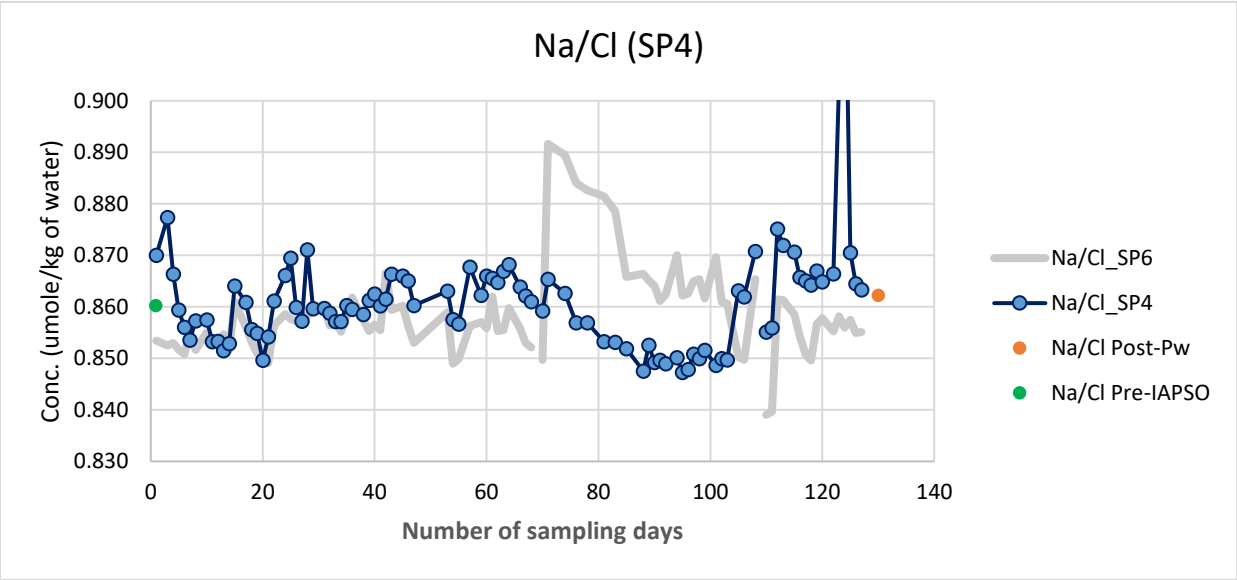
Na/Cl (SP4)
Conc. (umole/kg of water)
0.900
0.890
0.880
0.870
0.860
0.850
0.840
0.830
0
20
40
60
80
100
120
140
Number of sampling days
Na/Cl_SP6
Na/Cl_SP4
Na/Cl Post-Pw
Na/Cl Pre-IAPSO

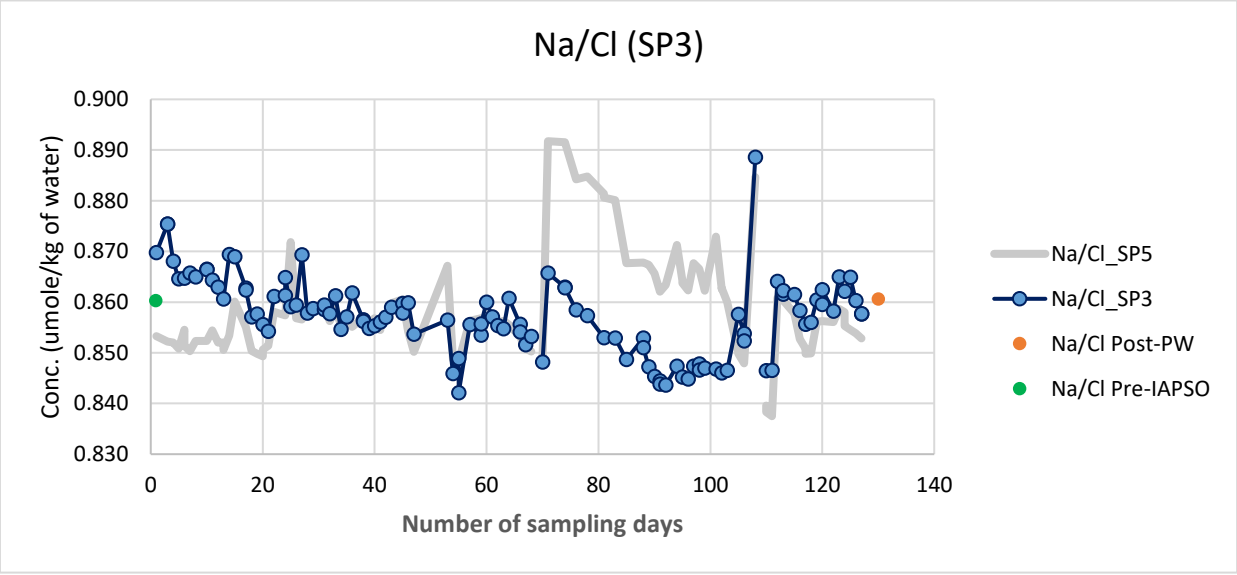
Na/Cl (SP3)
Conc. (umole/kg of water)
0.900
0.890
0.880
0.870
0.860
0.850
0.840
0.830
0
20
40
60
80
100
120
140
Number of sampling days
Na/Cl_SP5
Na/Cl_SP3
Na/Cl Post-PW
Na/Cl Pre-IAPSO

3- Potassium (K^+)

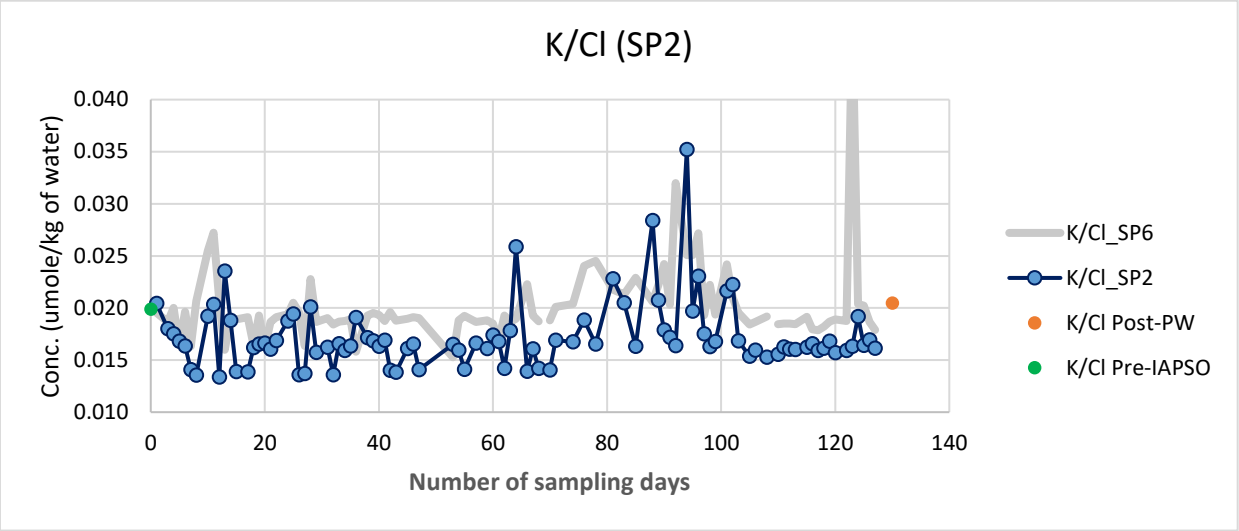

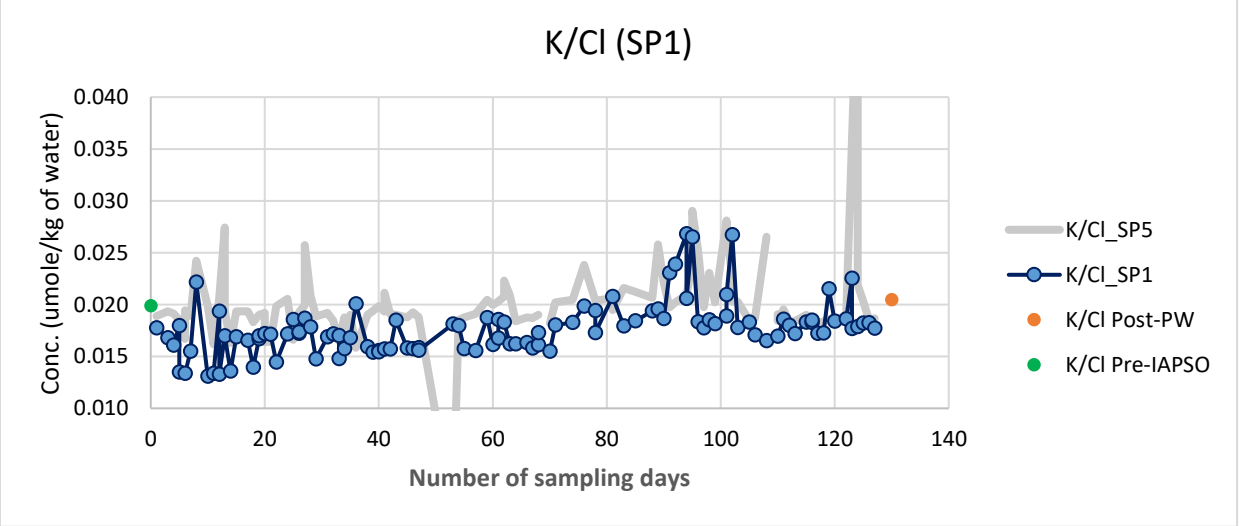

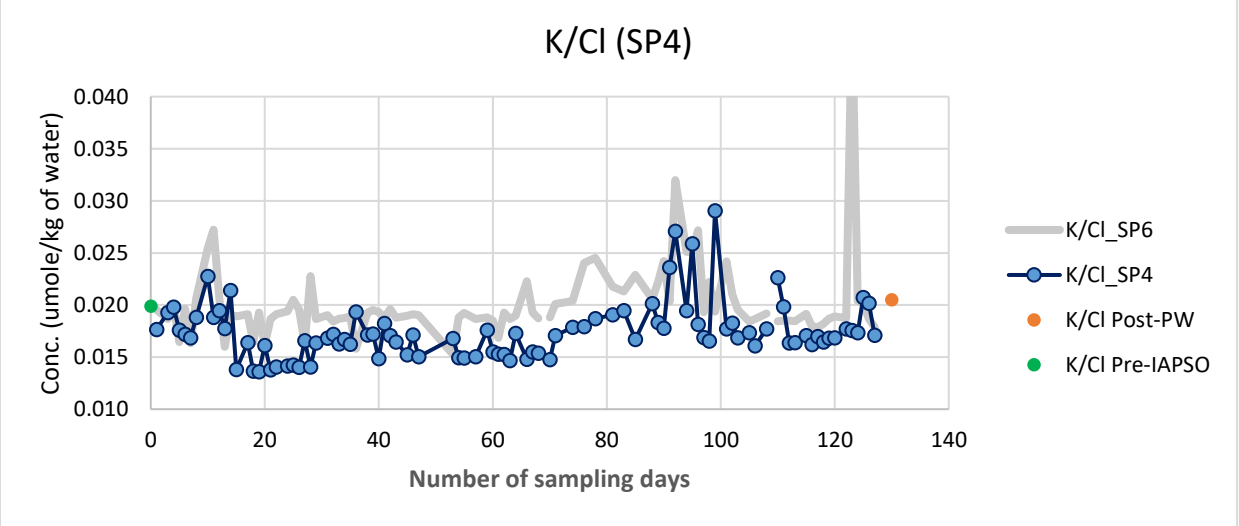

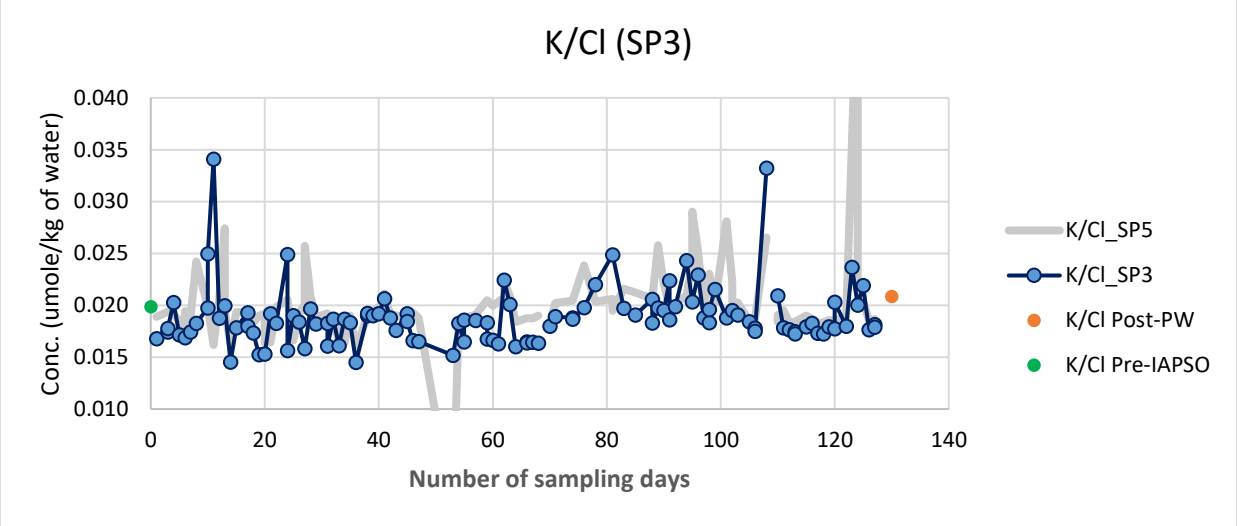

4- Magnesium (Mg^{2-})

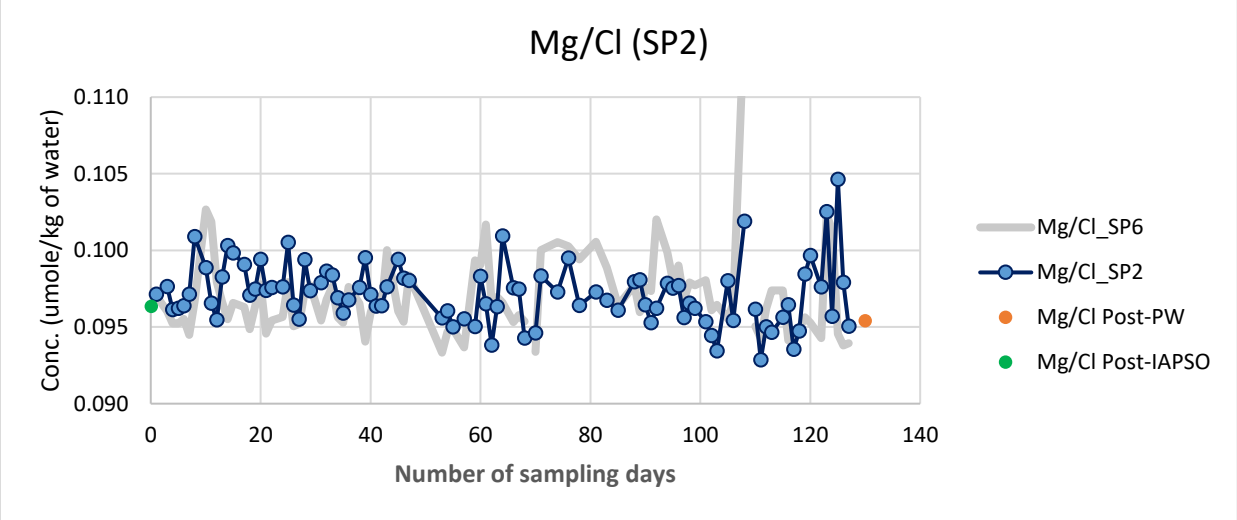

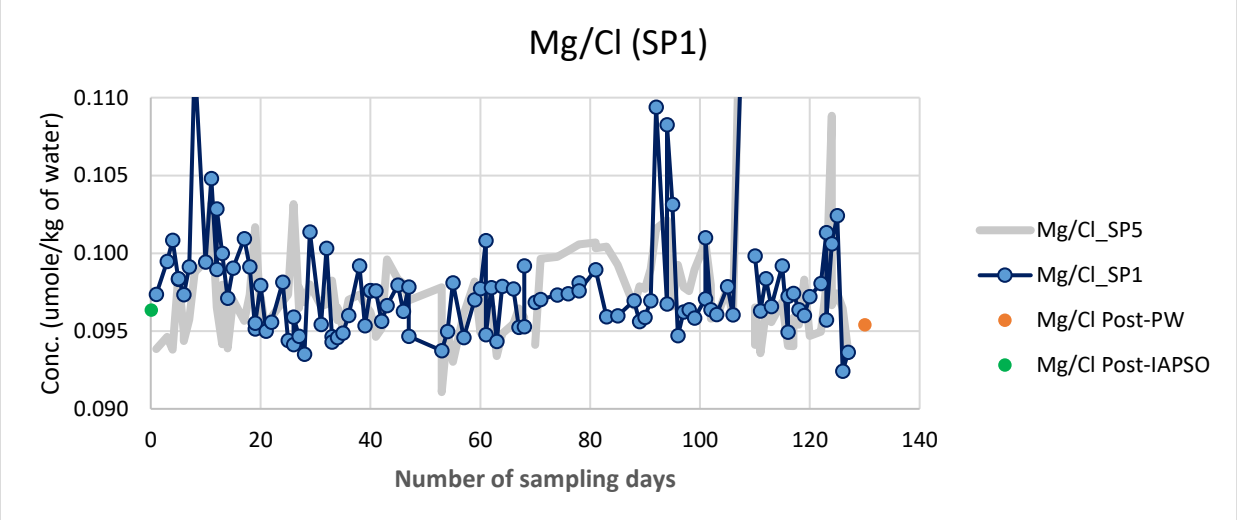

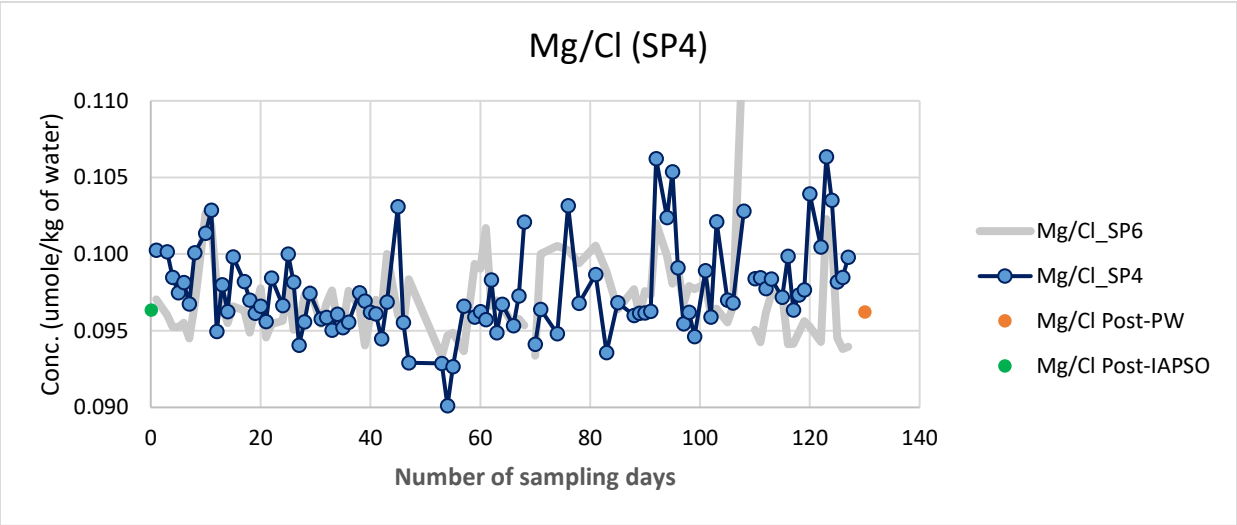
Mg/Cl (SP4)
Conc. (umole/kg of water)
0.110
0.105
0.100
0.095
0.090
0
20
40
60
80
100
120
140
Number of sampling days
Mg/Cl_SP6
Mg/Cl_SP4
Mg/Cl Post-PW
Mg/Cl Post-IAPSO

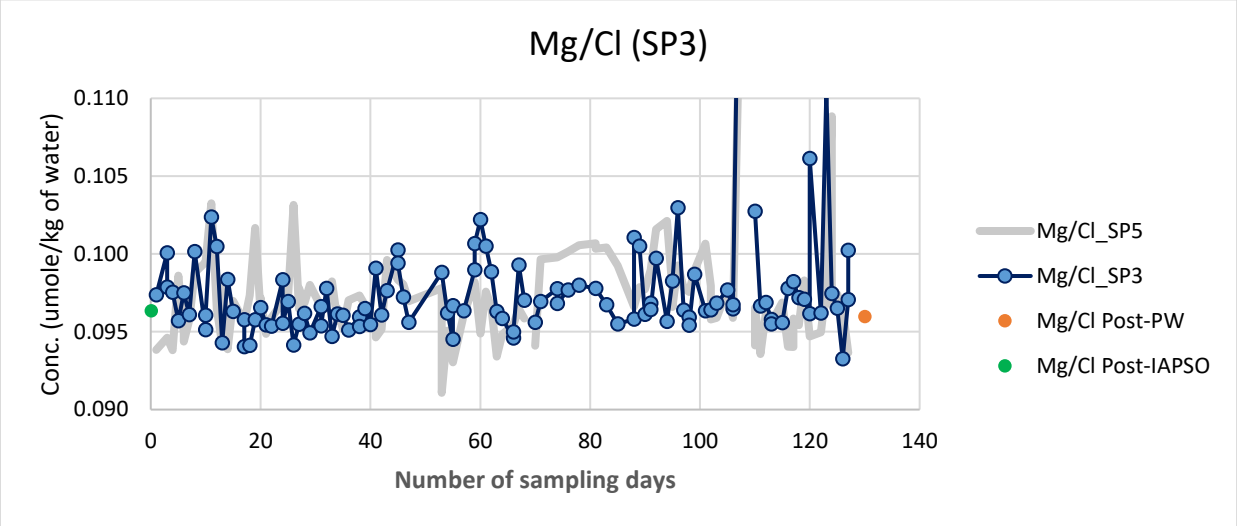
Mg/Cl (SP3)
Conc. (umole/kg of water)
0.110
0.105
0.100
0.095
0.090
0
20
40
60
80
100
120
140
Number of sampling days
Mg/Cl_SP5
Mg/Cl_SP3
Mg/Cl Post-PW
Mg/Cl Post-IAPSO

Table 19. Replicate measurement error

		Cl		SO4		Na		K		Mg		Ca		Cl			SO4			Na			K			Mg			Ca		
		Linear	Quadratic	Linear	Quadratic	Linear	Quadratic	Linear	Quadratic	Linear	Quadratic	Linear	Quadratic	Ave	SD	CV	Ave	SD	CV	Ave	SD	CV	Ave	SD	CV	Ave	SD	CV	Ave	SD	CV
Batch 1 (X1000)	Inc_10	890.951	815.492	43.34	44.092	713.845	713.473	14.221	14.539	81.605	82.194	18.868	18.162	815.359	0.133	0.016	44.080	0.012	0.028	713.728	0.117	0.016	14.357	0.136	0.947	80.692	0.913	1.132	18.048	0.820	4.543
	Inc_10	890.583	815.226	43.316	44.067	713.611	713.24	14.493	14.816	79.778	80.357	17.228	16.578																		
	Inc_20	483.832	485.456	26.004	26.511	412.148	412.154	8.722	8.922	47.733	48.114	10.929	10.506	485.527	0.070	0.015	26.564	0.053	0.200	412.466	0.317	0.077	7.636	1.087	14.230	47.753	0.020	0.041	11.121	0.192	1.722
	Inc_20	483.989	485.597	26.107	26.617	412.783	412.788	6.549	6.7	47.772	48.154	11.312	10.875																		
	Inc_30	413.215	420.913	22.063	22.505	359.701	359.739	7.029	7.191	39.947	40.273	9.229	8.869	420.851	0.063	0.015	22.478	0.027	0.122	358.978	0.724	0.002	7.604	0.575	7.562	39.827	0.121	0.303	9.157	0.072	0.792
	Inc_30	413.08	420.788	22.009	22.45	358.254	358.293	8.179	8.366	39.706	40.03	9.084	8.729																		
Batch 2 (X1000)	Inc_46	675.898	649.836	34.916	35.523	563.067	564.16	12.826	13.078	61.821	61.421	13.286	12.351	649.857	0.020	0.003	35.546	0.023	0.065	563.057	0.010	0.002	14.511	1.685	11.609	62.123	0.302	0.486	14.183	0.897	6.321
	Inc_46	675.948	649.877	34.961	35.569	563.047	564.139	16.195	16.509	62.425	62.023	15.079	14.025																		
	Inc_56	452.345	457.007	24.52	24.977	390.117	390.029	8.839	9.015	45.227	44.92	11.763	10.929	457.001	0.006	0.001	24.976	0.001	0.004	392.554	2.284	0.607	7.452	1.387	18.612	46.116	0.889	1.928	11.177	0.586	5.243
	Inc_56	452.331	456.994	24.519	24.975	394.938	394.82	6.065	6.188	47.005	46.687	10.591	9.836																		
	Inc_66	397.653	406.505	21.284	21.689	346.362	346.035	11.142	11.362	38.276	38.011	9.706	9.012	406.481	0.024	0.006	21.672	0.018	0.081	346.040	0.323	0.093	9.518	1.624	17.069	39.052	0.775	1.986	9.439	0.267	2.829
	Inc_66	397.601	406.457	21.25	21.654	345.717	345.387	7.893	8.051	39.827	39.553	9.172	8.515																		
Batch 3 (X1000)	Inc_82	510.341	509.026	27.8	28.299	439.169	439.407	9.815	9.886	48.749	48.373	10.743	10.152	509.238	0.212	0.042	28.301	0.002	0.007	439.250	0.081	0.018	9.494	0.321	3.381	48.329	0.421	0.870	10.939	0.196	1.787
	Inc_82	510.818	509.45	27.805	28.303	439.331	439.571	9.173	9.239	47.908	47.537	11.134	10.524																		
	Inc_92	343.796	355.045	19.489	19.857	303.478	302.594	5.928	5.972	33.78	33.508	8.183	7.728	355.234	0.189	0.053	19.814	0.043	0.217	303.426	0.052	0.017	5.980	0.052	0.870	33.863	0.083	0.245	8.478	0.295	3.480
	Inc_92	344.19	355.423	19.404	19.771	303.374	302.49	6.032	6.076	33.946	33.673	8.773	8.287																		
	Inc_102	409.235	416.95	21.855	22.262	354.107	353.532	8.011	8.07	40.108	39.791	10.137	9.579	417.046	0.096	0.023	22.312	0.050	0.222	354.475	0.368	0.104	7.425	0.587	7.900	40.326	0.218	0.541	9.947	0.191	1.915
	Inc_102	409.441	417.141	21.953	22.361	354.843	354.273	6.838	6.888	40.544	40.224	9.756	9.217																		
Batch 4 (X1000)	Inc_118	471.703	474.273	25.29	25.712	408.496	408.387	11.815	11.884	46.638	46.495	10.829	10.231	474.271	0.003	0.001	25.718	0.006	0.023	409.334	0.838	0.205	9.620	2.196	22.823	45.977	0.662	1.439	10.698	0.132	1.229
	Inc_118	471.697	474.268	25.302	25.724	410.171	410.081	7.424	7.468	45.315	45.175	10.566	9.982																		
	Inc_128	283.482	296.11	16.161	16.446	255.915	254.735	5.096	5.126	27.872	27.781	7.976	7.53	296.164	0.053	0.018	16.441	0.005	0.030	255.756	0.059	0.062	5.118	0.022	0.420	28.141	0.069	0.954	7.824	0.153	1.949
	Inc_128	283.59	296.217	16.151	16.436	255.596	254.415	5.139	5.17	28.409	28.317	7.671	7.241																		
	Inc_138	420.451	427.218	22.433	22.815	365.943	365.402	8.523	8.573	41.214	41.085	9.233	8.72	427.202	0.017	0.004	22.846	0.031	0.134	366.086	0.143	0.039	9.756	1.233	12.638	41.499	0.285	0.687	9.348	0.115	1.230
	Inc_138	420.415	427.185	22.494	22.876	366.228	365.689	10.989	11.054	41.784	41.654	9.463	8.937																		
Batch 5 (X1000)	Inc_154	466.311	469.544	25.037	25.48	403.12	403.003	8.571	8.642	45.365	45.305	10.698	10.108	469.711	0.167	0.035	25.499	0.018	0.073	403.468	0.347	0.086	8.064	0.507	6.287	45.089	0.277	0.613	10.295	0.396	3.842
	Inc_154	466.678	469.877	25.074	25.517	403.815	403.704	7.557	7.619	44.812	44.752	9.899	9.358																		

	Inc_164	262.586	275.957	15.272	15.559	237.666	236.831	4.697	4.736	26.118	26.081	6.267	5.919	275.777	0.180	0.065	15.521	0.039	0.248	237.804	0.138	0.058	4.387	0.310	7.066	26.053	0.065	0.249	6.223	0.044	0.707		
	Inc_164	262.223	275.596	15.197	15.482	237.941	237.106	4.077	4.111	25.988	25.952	6.179	5.836																				
	Inc_174	409.22	417.102	22.134	22.532	356.82	356.395	7.829	7.894	39.918	39.864	9.062	8.565	417.111	0.009	0.002	22.487	0.045	0.200	357.183	0.363	0.102	7.335	0.495	6.742	40.088	0.170	0.424	8.958	0.105	1.167		
	Inc_174	409.238	417.119	22.045	22.442	357.546	357.124	6.84	6.897	40.258	40.204	8.853	8.367																				
Batch 6 (X1000)	Inc_190	454.075	458.241	24.159	24.584	392.696	392.495	8.59	8.717	43.873	43.974	10.602	9.95	458.287	0.046	0.010	24.601	0.017	0.069	392.658	0.038	0.010	8.634	0.043	0.504	43.735	0.139	0.317	10.789	0.187	1.729		
	Inc_190	454.176	458.333	24.193	24.618	392.62	392.419	8.677	8.806	43.596	43.697	10.975	10.301																				
	Inc_200	240.244	253.177	13.855	14.115	219.024	218.142	3.878	3.936	24.646	24.707	6.614	6.2	253.295	0.118	0.046	14.116	0.001	0.007	218.907	0.117	0.053	3.867	0.012	0.297	24.660	0.013	0.055	6.704	0.090	1.335		
	Inc_200	240.478	253.412	13.857	14.117	218.79	217.909	3.855	3.913	24.673	24.733	6.793	6.368																				
	Inc_210	424.907	431.394	22.644	23.046	368.987	368.621	8.22	8.342	40.895	40.99	9.549	8.958	431.195	0.200	0.046	23.055	0.008	0.037	369.086	0.099	0.027	8.598	0.078	4.396	40.793	0.103	0.251	9.498	0.051	0.542		
	Inc_210	424.477	430.995	22.66	23.063	369.185	368.82	8.976	9.109	40.69	40.785	9.446	8.862																				
Batch 7&8 (X1000)	Inc_226	330.053	343.038	18.63	19.086	294.907	293.977	6.579	6.601	34.391	34.238	8.506	7.978	343.175	0.136	0.040	19.067	0.019	0.102	294.704	0.203	0.069	6.456	0.124	1.913	34.258	0.133	0.388	8.219	0.288	3.498		
	Inc_226	330.336	343.311	18.588	19.047	294.501	293.569	6.332	6.353	34.125	33.973	7.931	7.437																				
	Inc_236	220.745	234.972	12.917	13.247	201.482	200.361	3.724	3.737	22.986	22.881	5.808	5.444	235.034	0.061	0.026	13.251	0.003	0.026	201.349	0.133	0.066	3.693	0.031	0.839	22.621	0.065	0.161	5.932	0.124	2.082		
	Inc_236	220.867	235.095	12.924	13.254	201.215	200.093	3.662	3.674	22.256	22.154	6.055	5.676																				
	Inc_246	17.197	19.109	0	0	16.57	16.4	0	0	1.869	1.86	2.174	2.035	19.118	0.009	0.047	0.000	0.000	#DIV/0!	16.577	0.005	0.033	0.000	0.000	#DIV/0!	1.806	0.064	0.317	2.188	0.014	0.617		
	Inc_246	17.213	19.127	0	0	16.582	16.41	0	0	1.742	1.734	2.201	2.061																				
	Inc_256	305.198	318.947	16.89	17.307	270.734	269.71	5.253	5.271	30.148	30.012	7.928	7.435	319.003	0.056	0.018	17.306	0.002	0.009	269.711	1.023	0.379	5.588	0.353	5.995	30.496	0.348	1.140	7.548	0.380	5.034		
	Inc_256	305.312	319.059	16.883	17.304	268.687	267.658	5.923	5.943	30.843	30.704	7.168	6.721																				
Batch 9 (X1000)	Inc_268	335.187	347.749	18.485	18.93	296.79	295.707	6.379	6.421	34.421	34.301	8.073	7.344	347.739	0.010	0.003	18.932	0.002	0.011	297.168	0.378	0.127	6.102	0.277	4.539	34.712	0.291	0.837	7.949	0.125	1.566		
	Inc_268	335.166	347.729	18.489	18.934	297.546	296.467	5.825	5.863	35.002	34.88	7.824	7.116																				
	Inc_278	217.005	230.931	12.323	12.631	198.973	197.656	3.874	3.899	23.28	23.196	5.752	5.227	231.015	0.084	0.036	12.632	0.001	0.008	198.541	0.433	0.218	4.080	0.206	5.037	22.590	0.690	3.054	6.078	0.326	5.356		
	Inc_278	217.169	231.098	12.325	12.633	198.108	196.792	4.285	4.314	21.9	21.821	6.403	5.821																				
	Inc_288	419.248	427	22.366	22.891	365.323	364.75	8.872	8.93	41.236	41.095	9.377	8.535	427.030	0.030	0.007	22.913	0.022	0.094	365.430	0.107	0.029	9.198	0.263	3.539	41.251	0.015	0.035	9.199	0.178	1.935		
	Inc_288	419.311	427.059	22.408	22.934	365.537	364.965	9.523	9.585	41.265	41.123	9.021	8.209																				
Batch 10 (X1000)	Inc_304	317.357	330.529	17.698	18.148	282.797	282.988	5.449	5.594	31.268	31.426	7.387	6.895	330.600	0.071	0.021	18.159	0.011	0.061	282.617	0.181	0.064	5.433	0.016	0.304	31.340	0.072	0.230	7.536	0.149	1.971		
	Inc_304	317.503	330.671	17.719	18.17	282.436	282.628	5.416	5.56	31.412	31.57	7.684	7.174																				
	Inc_314	223.644	237.661	12.858	13.195	203.054	203.272	3.832	3.935	22.647	22.763	5.265	4.911	237.665	0.004	0.002	13.220	0.025	0.189	202.745	0.310	0.153	3.971	0.139	3.500	23.111	0.464	2.006	5.670	0.405	7.143		
	Inc_314	223.652	237.669	12.907	13.245	202.435	202.653	4.11	4.22	23.574	23.695	6.075	5.668																				
Batch 11&12 (X500)	Inc_340	555.894	548.711	29.525	30.232	473.519	474.178	10.308	10.387	53.645	52.85	11.392	10.581	548.864	0.152	0.028	30.274	0.042	0.139	473.617	0.098	0.021	10.283	0.026	0.248	53.398	0.247	0.463	11.477	0.085	0.736		
	Inc_340	556.251	549.016	29.607	30.316	473.715	474.377	10.257	10.336	53.151	52.362	11.561	10.739																				

	Inc_350	423.173	431.028	23.221	23.801	366.607	366.155	8.369	8.433	42.284	41.636	10.483	9.734	431.283	0.254	0.059	23.836	0.035	0.145	366.557	0.051	0.014	7.912	0.457	5.776	42.199	0.085	0.201	9.987	0.496	4.966		
	Inc_350	423.727	431.537	23.289	23.87	366.506	366.053	7.455	7.513	42.114	41.469	9.491	8.81																				
	Inc_360	911.459	822.805	44.696	45.66	725.2	730.696	16.954	17.08	82.844	81.721	17.656	16.434	823.048	0.243	0.030	45.706	0.046	0.101	725.108	0.092	0.013	16.495	0.459	2.783	82.723	0.121	0.147	17.382	0.274	1.576		
	Inc_360	912.168	823.291	44.787	45.752	725.016	730.507	16.036	16.156	82.601	81.481	17.108	15.921																				
Batch 13 (X500)	Inc_376	382.827	392.207	21.389	21.657	334.495	334.511	7.993	8.074	37.871	37.58	8.6	8.296	392.327	0.120	0.031	21.646	0.011	0.051	334.228	0.267	0.080	7.553	0.441	5.833	38.917	0.146	0.288	9.636	0.136	10.751		
	Inc_376	383.08	392.447	21.367	21.635	333.961	333.978	7.112	7.185	39.963	39.658	10.672	10.297																				
Batch 14 (X500)	Inc_394	523.329	521.004	27.023	27.393	439.956	440.017	11.652	11.731	50.449	50.643	11.743	11.144	521.015	0.011	0.002	27.437	0.043	0.159	439.797	0.160	0.036	10.675	0.978	9.157	50.343	0.107	0.212	11.458	0.285	2.487		
	Inc_394	523.355	521.026	27.109	27.48	439.637	439.696	9.697	9.763	50.236	50.431	11.173	10.602																				
	Inc_404	455.027	459.271	24	24.335	388.528	388.468	12.315	12.398	44.43	44.604	9.165	8.692	459.338	0.066	0.014	24.341	0.006	0.025	388.479	0.049	0.013	10.887	1.429	13.122	47.084	2.654	5.637	12.561	3.396	27.033		
	Inc_404	455.172	459.404	24.012	24.347	388.43	388.37	9.458	9.522	49.738	49.931	15.956	15.157																				
	Inc_414	922.312	844.02	44.283	44.822	729.456	730.758	20.293	20.425	82.44	82.729	17.027	16.179	844.027	0.007	0.001	44.766	0.056	0.126	729.260	0.197	0.027	22.404	2.111	9.420	81.982	0.458	0.559	16.425	0.603	3.668		
	Inc_414	922.33	844.033	44.171	44.709	729.063	730.363	24.514	24.671	81.524	81.81	15.822	15.03																				
Batch 15 (X500)	Inc_430	518.738	516.909	27.149	27.451	438.22	438.236	9.477	9.569	49.586	49.674	10.837	10.381	516.967	0.058	0.011	27.418	0.034	0.122	437.972	0.248	0.057	9.808	0.331	3.370	49.463	0.124	0.250	10.806	0.032	0.292		
	Inc_430	518.866	517.024	27.083	27.384	437.724	437.74	10.138	10.236	49.339	49.426	10.774	10.32																				
	Inc_440	435.75	441.561	23.299	23.564	373.901	373.875	8.348	8.429	42.861	42.938	10.334	9.898	441.556	0.005	0.001	23.579	0.015	0.064	373.449	0.452	0.121	8.803	0.454	5.163	43.731	0.870	1.989	10.386	0.051	0.496		
	Inc_440	435.738	441.55	23.329	23.594	372.997	372.971	9.257	9.348	44.601	44.682	10.437	9.997																				
	Inc_450	890.644	820.206	42.984	43.412	707.455	707.789	18.224	18.395	80.34	80.47	20.234	19.418	820.228	0.022	0.003	43.406	0.006	0.015	707.575	0.119	0.017	17.428	0.797	4.570	79.457	0.884	1.112	18.373	1.861	10.132		
	Inc_450	890.703	820.25	42.971	43.399	707.694	708.028	16.631	16.788	78.573	78.701	16.511	15.833																				
Batch 16 (X1000)	Inc_466	215.644	228.305	12.318	12.514	194.92	194.768	4.067	4.092	22.025	22.221	5.674	5.41	228.702	0.397	0.174	12.544	0.030	0.239	195.098	0.178	0.091	4.038	0.030	0.731	22.093	0.068	0.308	6.980	1.306	18.705		
	Inc_466	216.427	229.099	12.377	12.574	195.276	195.123	4.008	4.032	22.161	22.357	8.285	7.904																				
	Inc_486	392.803	401.574	20.82	21.135	337.148	337.054	7.662	7.707	37.796	38.117	8.794	8.39	401.558	0.017	0.004	21.157	0.022	0.104	336.882	0.266	0.079	7.530	0.132	1.753	38.278	0.482	1.258	9.091	0.297	3.267		
	Inc_486	392.769	401.541	20.863	21.179	336.616	336.522	7.398	7.442	38.759	39.088	9.388	8.958																				
Batch 17 (X1000)	Inc_502	201.68	214.821	11.541	11.806	185.074	184.238	3.755	3.849	20.577	20.662	5.573	5.347	214.795	0.026	0.012	11.814	0.008	0.068	185.128	0.054	0.029	3.731	0.024	0.643	20.545	0.032	0.156	5.722	0.149	2.595		
	Inc_502	201.628	214.769	11.557	11.822	185.182	184.346	3.707	3.8	20.513	20.598	5.87	5.632																				
	Inc_512	161.042	172.968	9.387	9.606	149.434	148.656	3.16	3.239	16.421	16.49	4.379	4.2	173.050	0.082	0.047	9.583	0.023	0.240	149.441	0.007	0.005	3.180	0.019	0.613	16.628	0.207	1.242	4.675	0.296	6.322		
	Inc_512	161.199	173.131	9.342	9.56	149.448	148.67	3.199	3.279	16.834	16.904	4.977	4.768																				
	Inc_522	364.767	375.523	19.605	20.034	319.492	318.883	6.867	7.037	35.309	35.449	9.387	9.012	375.540	0.016	0.004	20.014	0.021	0.102	319.326	0.167	0.052	6.863	0.005	0.066	35.653	0.344	0.965	9.292	0.095	1.022		
	Inc_522	364.802	375.556	19.564	19.993	319.159	318.549	6.858	7.027	35.997	36.14	9.197	8.829																				